textiles

MDPI

Article

A Fully 3D-Printable Pull-Off Fixture for Adhesion Testing of FDM Prints on Textile Substrates

Radu Firicel [1,2], Constantin Eugen Ailenei [1,2], Andreea Talpa [1], Emil Constantin Loghin [1,2,*], Savin Dorin Ionesi [1,2,*] and Maria Carmen Loghin [1,2]

[1] Faculty of Industrial Design and Business Management, "Gheorghe Asachi" Technical University of Iasi, 700050 Iași, Romania; radu.firicel@academic.tuiasi.ro (R.F.); constantin-eugen.ailenei@academic.tuiasi.ro (C.E.A.); andreea.talpa@academic.tuiasi.ro (A.T.); maria-carmen.loghin@academic.tuiasi.ro (M.C.L.)

[2] Centre for Research and Innovation in Textiles and Fashion Industry—SMART-Tex-IS, 700050 Iași, Romania

* Correspondence: emil-constantin.loghin@academic.tuiasi.ro (E.C.L.); savin-dorin.ionesi@academic.tuiasi.ro (S.D.I.)

Abstract

Adhesion between fused deposition modelling (FDM) printed polymers and textile substrates is critical for durable printed-on-textile hybrids. Since no dedicated test standard exists for additively manufactured textile interfaces, many studies use T-peel methods adapted from adhesive-bond standards. However, printed-on-textile joints are often governed by polymer penetration into the fabric and mechanical interlocking, rather than by a discrete adhesive layer. This work evaluates a fixture-based perpendicular (normal-separation) tensile method, using a circular dolly printed directly onto a cotton plain-weave substrate and a fully 3D-printable, threaded, self-aligning clamping assembly. Three representative filaments, namely polyethylene terephthalate glycol-modified (PETG), polylactic acid (PLA), and thermoplastic polyurethane (TPU), were tested using both the proposed pull-off method and an ISO 11339-type T-peel benchmark, with n = 8 specimens per polymer. The perpendicular method produced complete datasets for all polymers and clearly differentiated adhesion performance (TPU > PLA > PETG). In contrast, for T-peel, the standard evaluation window (25–125 mm) was completed for all PETG specimens but only for a subset of PLA specimens and a single TPU specimen. In the remaining tests, premature substrate failure prevented completion of this window, so the results could not be evaluated. Microscopy confirmed distinct interlocking morphologies across polymers, supporting the observed differences in failure behavior between peel and normal separation. Overall, the results indicate that perpendicular dolly pull-off testing is a practical and reproducible alternative for quantifying adhesion across a wider range of printed-on-textile bonding conditions.

Keywords: fused deposition modelling (FDM); polymer–textile adhesion; printed-on-textile composites; T-peel test; pull-off test; perpendicular tensile testing; mechanical interlocking; textile substrate

Academic Editor: Rajesh Mishra

Received: 5 April 2026
Revised: 23 April 2026
Accepted: 27 April 2026
Published: 1 May 2026

1. Introduction

Fused deposition modelling (FDM) printed directly onto textile substrates enables hybrid structures that combine the comfort and conformability of fabrics with the geometric freedom and functional integration of additive manufacturing (AM). Beyond decorative customization, published studies show that direct FDM printing on textiles can be used to

create polymer–textile composites and that their performance depends strongly on printing parameters, substrate type, and adhesion behavior [1,2]. In protective applications, such structures have been studied for adhesion, quasi-static stab resistance, and air permeability, including stab-proof vest concepts and sandwich structures with textiles placed between FDM-printed layers [3–5]. These studies aimed to balance protection performance with wearer comfort and air permeability. Direct FDM printing on textiles also supports functional applications. Conductive polymers printed on textile substrates have been investigated in terms of adhesion, sensing, and electrical connection [6,7]. More broadly, 3D-printed stretchable smart fibers and textiles have been developed for self-powered e-skin applications [8].

Across these application areas, the integrity of the polymer–textile bond remains a key limitation. If adhesion is too low, the printed elements can detach during bending, abrasion, laundering, or cyclic deformation. If the mechanical interlocking is strong but only local, the textile itself can become the weakest part. For this reason, the quantification of polymer–textile "adhesion" has become a common methodological requirement in FDM-on-textile research. It is important because it supports the comparison of materials, printing parameters, and textile structures [9].

In related upholstery-material testing, mechanical performance is commonly evaluated with established test procedures [10]. This is different from AM polymer–textile adhesion, where standardization is still limited. Because no dedicated standard exists for AM–textile interfaces, most studies focused on adhesion have used peel-based tests, often reported as a "T-peel" approach. In most cases, this was done by adapting two existing standards: DIN 53530 [11], often used as a practical basis for separating a printed strip from a fabric, and ISO 11339 [12], a T-peel standard for bonded flexible adherends, which is the main reference considered in the present study.

This use of the T-peel test in FDM-on-textile testing becomes easier to understand when the original purpose of the standard is stated clearly. As shown in Figure 1a, ISO 11339 defines the T-peel test for determining the peel strength of an adhesive by measuring the peeling force in a bonded assembly made of two flexible adherends. The standard also states that this method was developed to characterize adhesive bonds, not to provide design information [12].

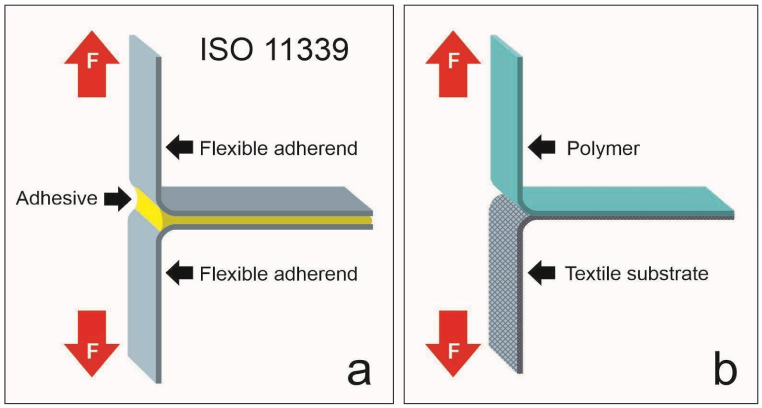

Figure 1. Schematic comparison of the ISO 11339 T-peel concept and its adaptation to 3D printing on textiles: (**a**) flexible adherends bonded by an adhesive layer (ISO 11339 joint); (**b**) printed-on-textile T-peel, where the deposited polymer functions as both the adherend and the bonding medium.

The test is based on the idea that a bond line, meaning an adhesive layer, exists between two adherends and fails before the adherends in a controlled way. In direct FDM printing onto textiles, the situation is different. The joint contains only two components, the polymer and the textile, and the printed polymer acts both as the adherend and as

the bonding medium, as shown in Figure 1b. This difference is important because the measured response does not always represent only interface separation. Depending on the textile construction and the behavior of the polymer, it can also reflect damage to one of the two components.

The limitations become clearer when the failure modes reported in the literature on 3D printing onto textiles are examined in detail. During peel testing, different types of failure can occur. These include failure inside the printed polymer layer (cohesive failure), interfacial delamination, and rupture of the textile substrate itself [9]. There are also clear examples in which the fabric breaks during the adhesion test before the printed element detaches, indicating that the test result is governed by textile failure, not by interface failure [13].

T-peel results can be difficult to compare from one study to another, because these failure modes depend on how the polymer penetrates the textile structure, and on how stresses are redistributed between yarns during peeling. For this reason, the failure mode should be reported and interpreted clearly. In such cases, the result should be understood as a combined measure of interface response and adherend integrity.

The peel geometry itself can also introduce uncertainty. Textiles rarely behave like ideal flexible adherends with a stable peel angle. During testing, deformation of the textile substrate can influence both the measured force and the failure path. This effect has already been reported in earlier studies on textile-based hybrids, where deformation of the textile structure during peeling was shown to affect the peel response [14].

Another practical issue is the way peel data are processed and reported. Many studies based on DIN 53530 show strongly undulating force–displacement curves [11]. These curves are often evaluated with multi-peak methods described in ISO 6133 [15], which is often cited as the "method for more than 20 peaks" [16]. Similar approaches based on peak selection and averaging have also been reported for ISO 11339-type T-peel tests used on AM–textile composites [2]. In practice, this can create a methodological ambiguity. When specimens show early textile damage or polymer fracture, some studies may still report an "average peel force" if enough peaks were recorded before failure. In this way, a complex mixed-mode response is reduced to a single scalar value. This can be useful for comparisons within the same study, but it should be interpreted with caution when the dominant failure mechanism is not interfacial separation.

In response to these limitations, several studies have explored perpendicular (pull-off-type) tensile testing. In this approach, the polymer–textile joint is loaded normal to the fabric surface. This loading direction matches the way the polymer penetrates the textile and forms mechanical interlocks through the thickness. Compared with peel testing, this method reduces the influence of a moving peel front and of large substrate deformations, which can strongly affect the results in compliant textiles. An important contribution was made by Malengier et al., who presented three testing methods for 3D printing on textiles—perpendicular tensile, shear, and peel testing—with the aim of improving the suitability and comparability of adhesion measurements [17].

Although perpendicular or pull-off-type tests are less common than T-peel, they have been used in different studies. Gorlachova and Mahltig used a separation-based method to detach printed features from cotton and to study adhesion trends for different materials and processing conditions [18]. Silvestre et al. proposed a custom tensile adhesion test for polymer-on-textile specimens, showing the need for stable methods when textiles are compliant and failure is mixed [6]. In a broader AM hybridization context, Maier et al. used tensile adhesion testing to evaluate bonding quality in additively manufactured structures on textile-reinforced thermoplastic composites. This showed that perpendicular tests can provide a direct mechanical metric when peel results are difficult to interpret [19].

More recently, Robinson et al. used perpendicular adhesion testing as part of a multi-test evaluation of additive manufacturing on textiles, together with peel and shear tests, again showing that the approach is viable and informative [20].

Perpendicular testing offers clear advantages, but it has not become the main method in AM–textile adhesion research. The reasons seem to be mainly practical rather than theoretical. Earlier versions often used custom fixtures, often with metal parts, together with less accessible specimen geometries and stricter alignment requirements. These conditions can be handled in specialized laboratories, but they can limit wider use in the AM community [9,17].

This work aims to reduce this adoption gap by proposing a fully accessible perpendicular tensile adhesion test. The method is based on an easy-to-make, self-aligning clamping assembly and a circular specimen concept. By design, the method aims to (i) reduce the influence of warp/weft selection as a first-order limitation, (ii) support both rigid and flexible printed polymers, without the instability often seen in peel testing on compliant substrates, and (iii) make perpendicular adhesion testing more practical for typical FDM users and laboratories, enabling more consistent reporting and comparison across future AM–textile studies.

2. Materials and Methods

This study evaluates adhesion between FDM-printed polymers and a woven textile substrate by using two complementary test methods. The first method is a T-peel configuration, used as a benchmark from the literature. The second method is a normal-separation (perpendicular) tensile pull-off test. This test is based on a circular printed dolly and a self-aligning, threaded clamping fixture developed in this work. Three polymer families were selected in order to cover a broad range of interface behavior. These included relatively rigid filaments (PLA and PETG) and one flexible filament (TPU). For each polymer, the specimens were printed on the same textile substrate under controlled and repeatable conditions. Adhesion was then quantified with both test methods, together with systematic documentation of the observed failure mode.

2.1. Materials

Three commercially available FDM filaments (nominal diameter 1.75 mm) were used to cover a practical range of stiffness and interfacial behavior: PLA [M15.1] (eSUN ePLA, Fire Engine Red; Shenzhen Esun Industrial Co., Ltd., Shenzhen, China), PETG (eSUN PETG, Solid White; Shenzhen Esun Industrial Co., Ltd., Shenzhen, China), and TPU (eSUN eTPU-95A, Transparent Red; Shore A 95; Shenzhen Esun Industrial Co., Ltd., Shenzhen, China). All filaments were used as received from the manufacturer.

The textile substrate was a plain-woven cotton fabric. It was selected as a representative apparel-type textile and as a common baseline material in FDM-on-textile adhesion studies [1,17]. Plain weave was also selected because it offers dimensional stability and a more repeatable peel and tensile response than highly extensible textile structures. At the same time, it still provides a porous structure that allows polymer penetration and mechanical interlocking. The fabric had an areal density of about 140 g/m^2 and a thickness of about 0.20 mm, measured according to ISO 5084 [21]. Its thread density was 24 ends/cm in warp and 22 picks/cm in weft. Before printing and testing, the fabric was conditioned for 24 h in the standard atmosphere of 20 $\pm$ 2 °C and 65 $\pm$ 4% relative humidity, in accordance with ISO 139 [22].

2.2. Equipment and Printing Setup

All specimens were manufactured by material extrusion on a Prusa i3 MK2 FDM printer (Prusa Research a.s., Prague, Czech Republic) equipped with a 0.4 mm nozzle. Slicing and toolpath generation were performed in OrcaSlicer, version 2.3.1. Printing was carried out directly on the conditioned textile substrate.

To obtain stable printing of tall features on a compliant textile substrate, the fabric was fixed on the build plate with double-sided adhesive tape. High-tack adhesives were not used because they can make removal of freshly printed specimens more difficult and can damage the textile or cause premature debonding during removal. Instead, a lower-tack fixation arrangement was applied. The specimens were removed only after cooling in order to reduce unintended interfacial damage before testing.

Printing parameters were selected to control the polymer–textile interface and were kept consistent across all specimens. For each filament, the main process settings were fixed within the ranges commonly reported for FDM printing onto textiles. The nozzle/bed temperatures were 215/60 °C for PLA, 225/70 °C for PETG, and 230/30 °C for TPU. The first-layer speed was set to 15 mm/s for PLA and PETG, and to 10 mm/s for TPU. The first-layer parameters governing polymer interpenetration were kept constant for all materials and specimen types: 0.20 mm layer height, 100% infill, and a fixed raster orientation for solid regions. The nozzle-to-plate distance was set to 0.30 mm, measured relative to the bare metallic build plate. This value corresponded to the combined thickness of the double-sided adhesive fixation layer (~0.10 mm) and the cotton fabric (~0.20 mm). Therefore, during first-layer deposition, the nominal nozzle-to-textile clearance was approximately 0 mm. The 0.20 mm first layer was consequently deposited under slight compression into the textile surface rather than as a free-standing layer above it. This setting was selected to promote polymer squeeze-in and penetration into the fabric porosity, while avoiding excessive nozzle drag, textile displacement, or first-layer clogging during the longer T-peel prints. Parameters above the first layer were allowed to follow the standard settings of each specimen type (e.g., to reduce printing time), but they remained consistent within each specimen geometry.

Testing was performed using a SATRA STM 466 universal testing machine (SATRA Technology Centre, Kettering, United Kingdom) equipped with a 2 kN load cell. Data acquisition and test control were conducted using SATRA Material Testing Centre software, version 3.4b (SATRA Technology Centre, Kettering, United Kingdom).

Microscopy imaging was performed using an Optech microscope (Optech Optical Technology, Munich, Germany). Images were acquired and processed using Vision Image Analysis software, version 1.0 (Optech Optical Technology, Munich, Germany).

2.3. Geometry and Method Development for Perpendicular Tensile Testing

2.3.1. Reference Dolly Geometry from Prior Work

The initial pull-off specimen geometry was based on the dolly concept reported in prior adhesion-testing work for 3D printing on textiles, using a circular contact area with the diameter D = 24 mm. This starting geometry was selected to maintain comparability with the literature and to follow an established precedent for perpendicular tensile adhesion measurements in printed-on-textile systems [17].

2.3.2. Dolly Geometry Scaling and Final Selection

Preliminary trials confirmed that the D = 24 mm dolly enabled stable testing for PLA and PETG on the selected woven substrate. For TPU, however, the same geometry frequently produced substrate-limited behavior, i.e., failure by fabric rupture rather than interfacial separation, which reduces the ability of the test to distinguish adhesion differences

at the polymer–textile interface. To keep the method informative across a wide adhesion range—spanning weak to very strong bonding—and to avoid systematic textile failure for high-adhesion polymers, the bonded contact area was reduced by scaling the dolly diameter to D = 15 mm as shown in Figure 2.

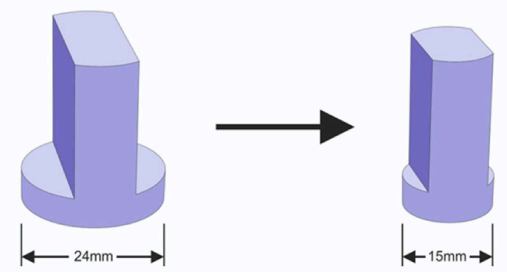

Figure 2. Pull-off dollies: literature-based geometry (D = 24 mm, after Malengier et al.) and the scaled geometry used in this study (D = 15 mm) following preliminary trials.

The final diameter was selected to provide reliable fabrication of a tall dolly on a compliant textile substrate, while maintaining sufficient base stability to avoid print instability or build failure. A detailed description of the final specimen geometry and the corresponding self-aligning fixture is provided in Section 2.3.3.

2.3.3. Dolly and Fixture Design

A normal-separation (pull-off) adhesion test was performed using a circular dolly printed directly onto the textile and a 3D-printable, threaded, self-aligning clamping fixture designed to immobilize the fabric and enforce repeatable alignment during testing. The fixture shown in Figure 3 consists of three parts: (i) a threaded support body (Part e), (ii) a fixing/indexing plate (Part c), and (iii) a threaded cap (Part b).

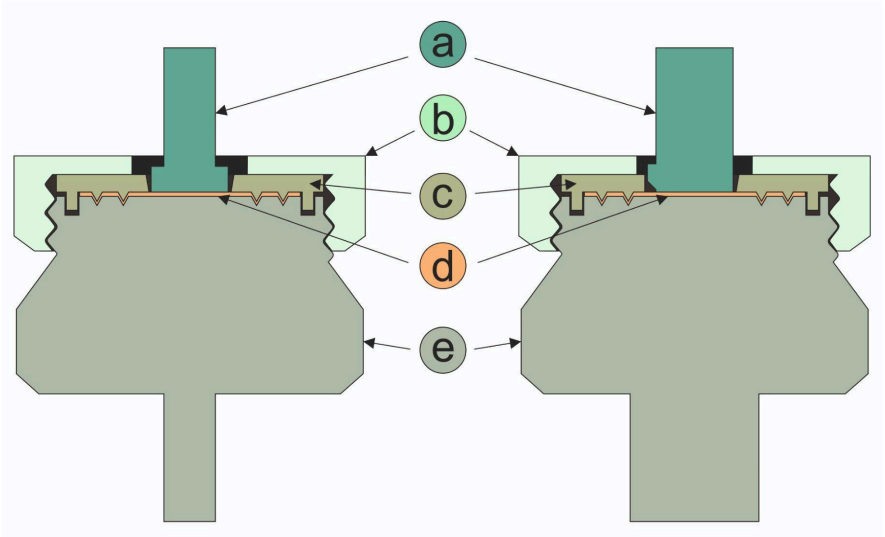

Figure 3. Front and side section of the perpendicular tensile testing fixture. Labelled components: (a) printed dolly; (b) threaded cap; (c) fixing/indexing plate; (d) textile substrate; (e) threaded support body.

The support body presented in Figure 3e acts as the main structural element of the fixture, providing both a lower gripping region for the universal testing machine (UTM) jaws and a geometric reference for axial alignment. It includes an external grip region for manual handling and an internal thread to accept the cap. The upper surface includes a clean, planar seating area around the dolly region to promote predominantly axial loading.

Two guidance/anti-slip systems are integrated on the upper face: (i) two radial rows of recesses that mate with pyramid-like protrusions on the fixing plate, creating mechanical interlocking that stabilizes the plate under compressive clamping, and (ii) two large radial keyways that mate with corresponding protrusions on the fixing plate to prevent rotation of both the plate and the textile during tightening.

The fixing plate presented in Figure 3c maintains the textile in a fixed and repeatable position and defines the clearance geometry around the dolly. It incorporates (i) two radial protrusions that engage the support-body keyways to prevent rotation during tightening and loading, and (ii) a set of radially distributed pyramid-like protrusions that engage the two rows of recesses in the support body, increasing friction and resisting slip under clamp pressure. The central opening for the dolly was designed with a radial clearance of ~0.5 mm relative to the dolly diameter to avoid contact during the test. To minimize parasitic contact and to enable complete vertical separation, this opening is slightly conical (a truncated cone with the smaller diameter oriented downward), rather than a straight cylindrical hole.

To ensure repeatable angular positioning and collinearity between the upper and lower grips, the printed dolly includes a small orientation key/feature, and the fixing plate includes a complementary indexing recess. This indexing prevents rotation of the dolly–textile assembly and ensures that the dolly is consistently presented to the upper jaws in the same orientation.

The cap shown in Figure 3b closes the assembly and applies clamping pressure through the internal thread of the support body. It includes an external grip region for repeatable manual tightening and a central clearance opening around the dolly to avoid contact and eliminate frictional or lateral constraint during pull-off.

The three-part threaded fixture was fabricated by FDM with a 0.20 mm layer height, 4 perimeters (walls), and 98% gyroid infill to ensure sufficient stiffness and dimensional stability during clamping and loading. The geometry was designed to be self-supporting, requiring no support structures, which simplifies fabrication and improves repeatability across printers. The system can be produced in PLA for routine use and method validation; however, for repeated tightening, higher clamp loads, or long-term durability, fabrication in a tougher polymer such as PETG or ABS is recommended. The printable files for the dolly and fixture device can be downloaded at: https://www.mdpi.com/article/10.3390/textiles6020054/s1.

2.3.4. Perpendicular Tensile Testing Using Proposed Method

For each polymer (PLA, PETG, and TPU), n = 8 pull-off specimens were manufactured and tested using the final dolly geometry (D = 15 mm) and the fixture and test protocol. Key procedural steps are documented in Figure 4 (specimen fabrication workflow: dolly printing on textile, specimen cutting, and the full specimen set).

The textile specimen with the printed dolly was placed onto the support body. The fixing/indexing plate was positioned such that the anti-rotation protrusions engaged the support-body keyways and the interlocking features mated. The cap was then tightened until the textile was firmly clamped. The assembled fixture was mounted in the lower jaws of a universal testing machine, while the dolly was gripped in the upper jaws. Figure 5 presents the fixture assembly and mounting in the UTM.

A displacement-controlled tensile test was run at a crosshead speed of 50 mm/min (constant for all specimens), and the force–displacement curve was recorded continuously until complete separation. The primary response was the maximum force, F_{max} (N), for each specimen. Figure 6 shows the specimens after testing, illustrating typical post-test appearance.

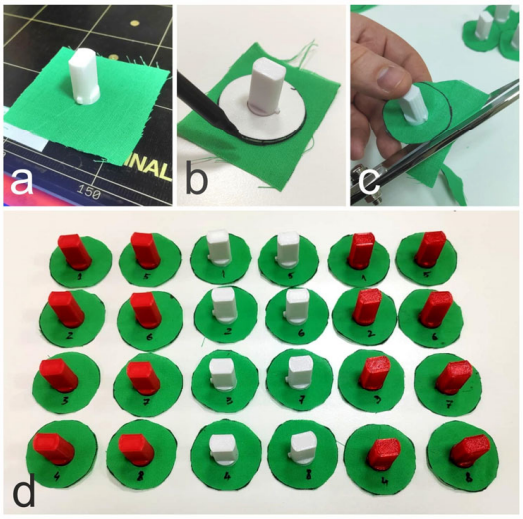

Figure 4. Perpendicular-dolly specimen fabrication workflow: (**a**) dolly printed directly onto the textile substrate; (**b**) marking the cutting outline using a template; (**c**) cutting the circular specimen; (**d**) complete specimen set (n = 8 per polymer).

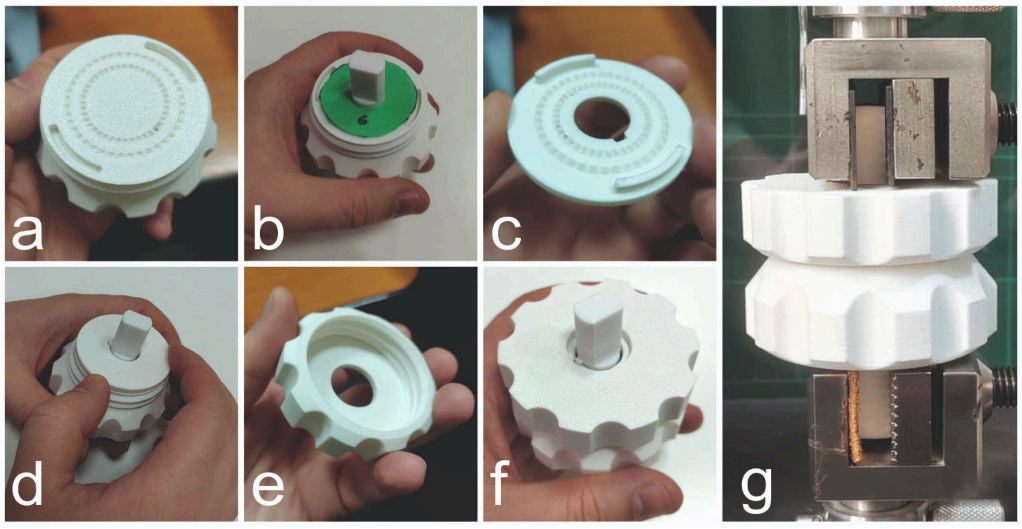

Figure 5. Assembly of the perpendicular-dolly fixture and mounting in the testing machine: (**a**) threaded support body; (**b**) dolly with textile placed on the support; (**c**) fixing/indexing plate; (**d**) plate positioned to clamp the textile; (**e**) threaded cap; (**f**) cap tightened to complete the assembly; (**g**) assembled fixture mounted in the universal testing machine.

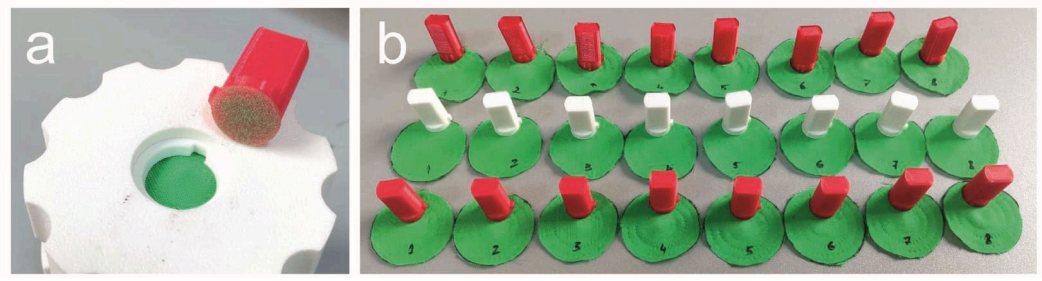

Figure 6. Post-test appearance of perpendicular-dolly specimens: (**a**) PLA specimen immediately after testing; (**b**) complete set of tested specimens, with each dolly placed on its corresponding textile substrate.

2.4. T-Peel Test (Benchmark)

A T-peel adhesion test was used as a benchmark method and performed in accordance with ISO 11339 [12], adapted to FDM-printed polymer strips on a woven textile substrate. For each polymer, n = 8 T-peel specimens were manufactured and tested under identical conditions.

Each T-peel specimen had an overall length of 200 mm, a constant width of 25 mm, and a printed-strip thickness of 0.6 mm (3 layers at 0.20 mm). A 30 mm section at one end of the intended bonded region was covered with masking tape during printing to intentionally prevent bonding between the polymer and the textile, thereby creating a reproducible free "arm" for gripping in the test machine. The fabric was oriented with the warp direction along the specimen length, and the print direction was aligned with the warp to keep textile anisotropy controlled across specimens. As shown in Figure 7, masking-tape was used for polymer–substrate separation during printing. Figure 8 illustrates the complete T-peel specimen set.

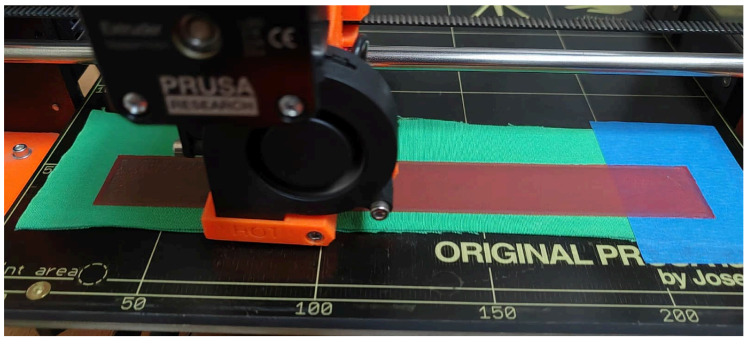

Figure 7. T-peel specimen during printing (PLA).

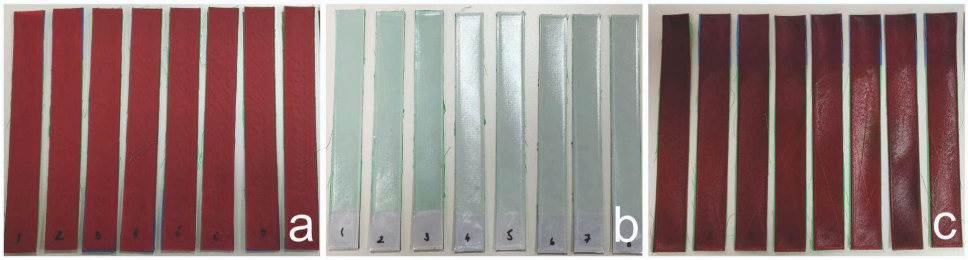

Figure 8. Complete T-peel specimen sets (n = 8 per polymer): (**a**) PLA, (**b**) PETG, (**c**) TPU.

The two free arms (polymer and textile) were clamped in opposing grips of the universal testing machine to form an approximately 180° T-peel configuration. Alignment of the peel arms with the loading axis (collinearity) was ensured manually during clamping, as is typical for this setup when a dedicated self-aligning peel fixture is not used. A displacement-controlled test was run at a constant crosshead speed of 100 mm/min, while force–displacement data were recorded continuously until separation or premature failure. A representative specimen mounted in the grips is shown in Figure 9.

Peel resistance was calculated as the mean peeling force divided by the specimen width, and is therefore reported in N/mm, over the standard evaluation window (25–125 mm) according to ISO 11339, excluding the initial transient region [12]. The failure mode was documented for each specimen (interfacial separation, polymer fracture, or textile damage). Examples of non-interfacial failure cases are illustrated in Figure 10.

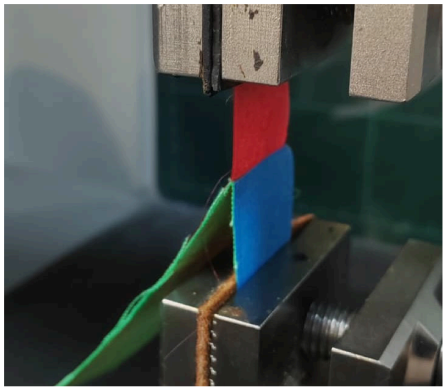

Figure 9. T-peel specimen mounted in the universal testing machine.

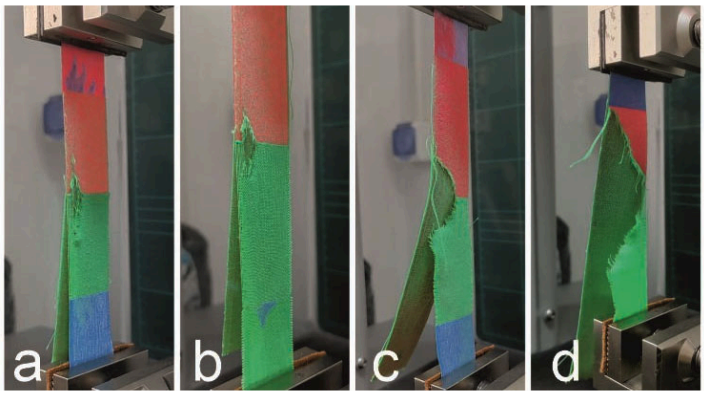

Figure 10. Examples of premature T-peel failures during testing: (**a**,**b**) PLA specimens; (**c**,**d**) TPU specimens.

2.5. Microscopy

Microscopy was used to document interface morphology and post-test surface features relevant to adhesion and failure mode interpretation. Representative specimens were prepared and examined in three complementary views: (i) cross-sections through the polymer–textile interface, obtained by sectioning through the bonded region to expose the through-thickness penetration and yarn encapsulation; (ii) cross-sections through the polymer after textile removal, examined after both T-peel and perpendicular (dolly) tests to visualize the remaining interlocking protrusions/features formed within the fabric structure; and (iii) the fabric surface opposite the printed side (backside) after testing, examined after both test methods to document polymer residue trapped in weave openings and any deformation of the textile structure.

The microscopy observations focused on qualitative comparison of polymer penetration depth/extent, geometry and apparent density of interlocking features, and the presence/distribution of polymer remnants on the textile backside, enabling correlation between interface morphology and the observed test outcomes under peel versus normal separation loading.

3. Results and Discussion

3.1. Dataset and Reported Outputs

A total of 48 specimens were produced and tested (3 polymers × 2 test methods × 8 replicates). Results are reported separately for the T-peel benchmark and the proposed perpendicular tensile (dolly) method, using a clear distinction between valid tests (suitable for quantitative comparison) and premature failures (reported as failure rate and illustrated qualitatively).

For the T-peel benchmark, peel performance is reported as peel resistance in N/mm, calculated by dividing the mean peeling force recorded over the defined evaluation window (25–125 mm) by the specimen width, consistent with ISO 11339 practice [12]. Because multiple specimens—especially for TPU—failed prematurely (e.g., textile rupture or specimen damage before a stable peeling segment could be obtained), the dataset is split into valid tests used for peel-resistance statistics and premature failures excluded from peel-resistance statistics but retained for failure-rate reporting and qualitative interpretation. In the final dataset, the number of tests meeting the analysis criteria was n = 8 for PETG, n = 5 for PLA, and n = 1 for TPU; all remaining T-peel runs are reported as premature failures.

For the perpendicular tensile (dolly) method, all specimens produced a complete normal-to-surface separation without test failures; therefore, all replicates were treated as valid (n = 8 per polymer). The primary reported outcome is the maximum load, F_{max} (N). In addition, an area-normalized metric is reported as a nominal normal tensile strength, calculated as:

$$\sigma_{max} = \frac{F_{max}}{A_0}, A_0 = \pi\left(\frac{D}{2}\right)^2$$

where A_0 is the bonded circular area and D is the dolly diameter used in the final geometry. This normalization supports comparison across geometries and across studies that report strengths as stress rather than force. Summary statistics are reported as mean ± SD, alongside min–max for each polymer.

To document both repeatability and failure behavior, representative mechanical response curves are presented as follows. For T-peel, two representative valid curves and two representative failed curves are shown for PLA; two representative valid curves are shown for PETG; for TPU, a compact panel is used that groups four failed curves together and contrasts them with the single valid curve. For the perpendicular tensile method, two representative curves per polymer are shown to illustrate the typical response and scatter, since no failures occurred in this configuration. Interface morphology is examined using close-up/microscopy images to support failure-mode interpretation; these observations are discussed in Section 3.4 and are used to link the measured responses to polymer penetration and mechanical interlocking at the textile interface.

3.2. Perpendicular Tensile Test (Proposed Method): Quantitative Outcomes and Repeatability

The proposed perpendicular tensile method generated a complete, valid dataset for all three polymers (n = 8 per polymer), with no test interruptions due to specimen slippage, grip-related damage, or fixture-related instability. The primary reported outcome was the maximum load at separation (F_{max}), extracted from each load–displacement curve. In addition, a nominal normal separation stress (σ_{max}) was calculated by dividing F_{max} by the bonded circular area ($A = \pi(D/2)^2 = 176.7$ mm^2 for D = 15 mm). This stress should be interpreted as an apparent (nominal) metric intended for within-study comparison, since non-uniform load transfer and stress concentrations are expected at a rigid–flexible interface.

As summarized in Table 1, the method clearly discriminated the three polymer systems under normal-to-surface loading. σ_{max} was calculated as F_{max}/A, where $A = 176.7$ mm^2 (circular bonded area for D = 15 mm) and N/mm^2 is equivalent to MPa.

PETG exhibited the lowest separation loads ($F_{max} = 291.9 \pm 15.2$ N; $\sigma_{max} = 1.652 \pm 0.086$ MPa), PLA showed intermediate values ($F_{max} = 606.5 \pm 44.4$ N; $\sigma_{max} = 3.432 \pm 0.251$ MPa), and TPU presented the highest resistance to separation ($F_{max} = 830.8 \pm 46.9$ N; $\sigma_{max} = 4.701 \pm 0.265$ MPa). Relative variability was moderate and acceptable for this type of textile–polymer interface test, with coefficients of variation (based on F_{max}) of 5.21% for PETG, 7.32% for PLA, and 5.64% for TPU.

Table 1. Summary statistics for the perpendicular tensile (dolly) test (D = 15 mm).

Polymer	n	F_{max} (N) Mean ± SD	F_{max} (N) Min–Max	σ_{max} (MPa) Mean ± SD	σ_{max} (MPa) Min–Max	CV (%) (F_{max})
PETG	8	291.9 ± 15.2	279–317.9	1.652 ± 0.086	1.579–1.799	5.21
PLA	8	606.5 ± 44.4	536–652.9	3.432 ± 0.251	3.033–3.695	7.32
TPU	8	830.8 ± 46.9	726–886.8	4.701 ± 0.265	4.108–5.018	5.64

CV = coefficient of variation.

Representative nominal stress–displacement curves (two per polymer) are shown in Figure 11a–f. All curves exhibit a short initial seating region followed by a monotonic load increase toward a clearly defined maximum and a rapid drop associated with separation. Unlike peel testing, this method does not depend on identifying a long constant-force evaluation window, because the reported outcome is anchored to a robust peak event. A further practical advantage is geometric: because the bonded region is circular, the response is not inherently direction-sensitive with respect to warp/weft orientation, reducing a common source of variability when testing woven substrates.

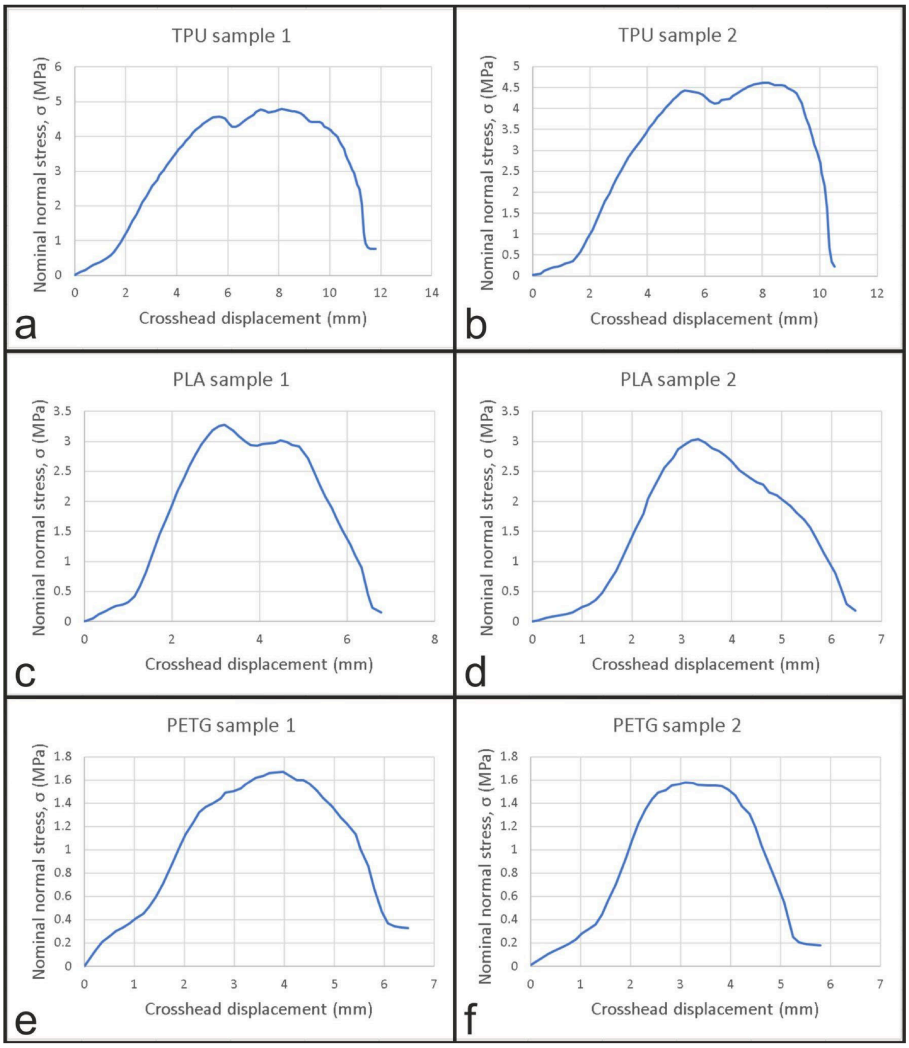

Figure 11. Representative nominal stress–displacement curves from the perpendicular-dolly tensile test: (**a**,**b**) TPU specimens; (**c**,**d**) PLA specimens; (**e**,**f**) PETG specimens. Nominal stress was calculated by dividing the recorded load by the circular dolly area, A = 176.7 mm^2.

3.3. Benchmark T-Peel Results and Failure Modes (ISO 11339)

T-peel testing was used as a benchmark method because it is the most frequently reported approach for assessing polymer–textile bonding in FDM-on-textile studies. Peel resistance was calculated in N/mm by dividing the mean peeling force recorded over the fixed 100 mm evaluation window (25–125 mm) by the specimen width, excluding the initial transient, following ISO 11339 practice [12]. In practice, many specimens—especially at higher adhesion—did not yield usable data across the full evaluation window. The textile often failed before the window was completed, or the T-peel curve showed strong monotonic drift instead of a near-stationary response.

Across the three materials, the ability to obtain "standard-compliant" curves differed markedly. PLA showed partial validity (5/8): several specimens provided a measurable evaluation segment, while others failed early through fabric rupture or mixed failure, preventing extraction of a compliant 100 mm window. Valid sample graphs for PLA are presented in Figure 12, and failed examples in Figure 13.

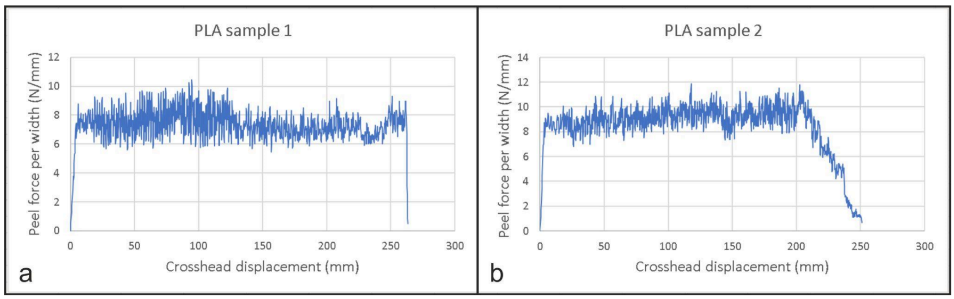

Figure 12. Representative T-peel curves for two valid PLA tests: (**a**) sample 1; (**b**) sample 2.

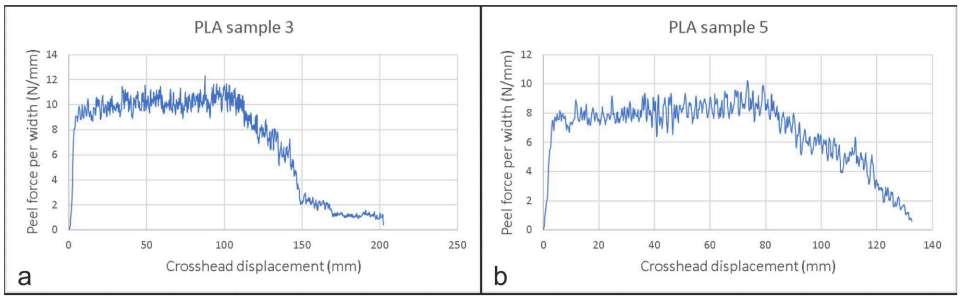

Figure 13. Representative T-peel curves for two failed PLA tests: (**a**) sample 3; (**b**) sample 5.

PETG produced valid curves for all specimens (8/8), typically characterized by an early higher-force phase followed by a gradual decrease toward a lower level, but the same fixed evaluation window (25–125 mm) was applied to ensure consistent processing across materials. Valid sample graphs for PETG are presented in Figure 14.

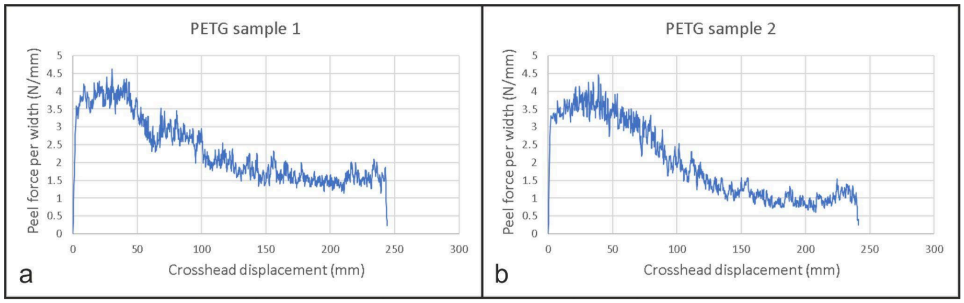

Figure 14. Representative T-peel curves for two valid PETG tests: (**a**) sample 1; (**b**) sample 2.

TPU exhibited the strongest substrate-limited behavior: most TPU specimens could not complete the required 25–125 mm evaluation window (7/8). Only one specimen met the minimum data-length requirement. The valid test graph is shown in Figure 15. Failed sample graphs are presented in Figure 16.

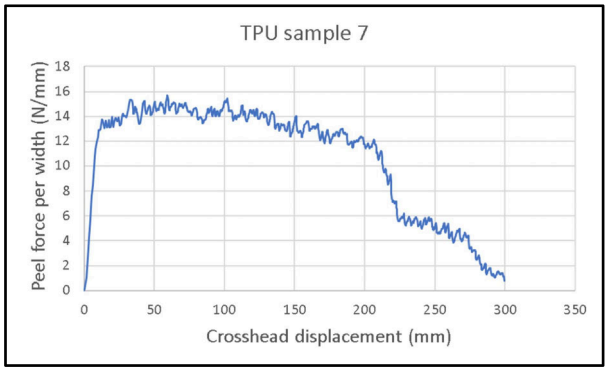

Figure 15. T-peel curve for the single valid TPU test: sample 7.

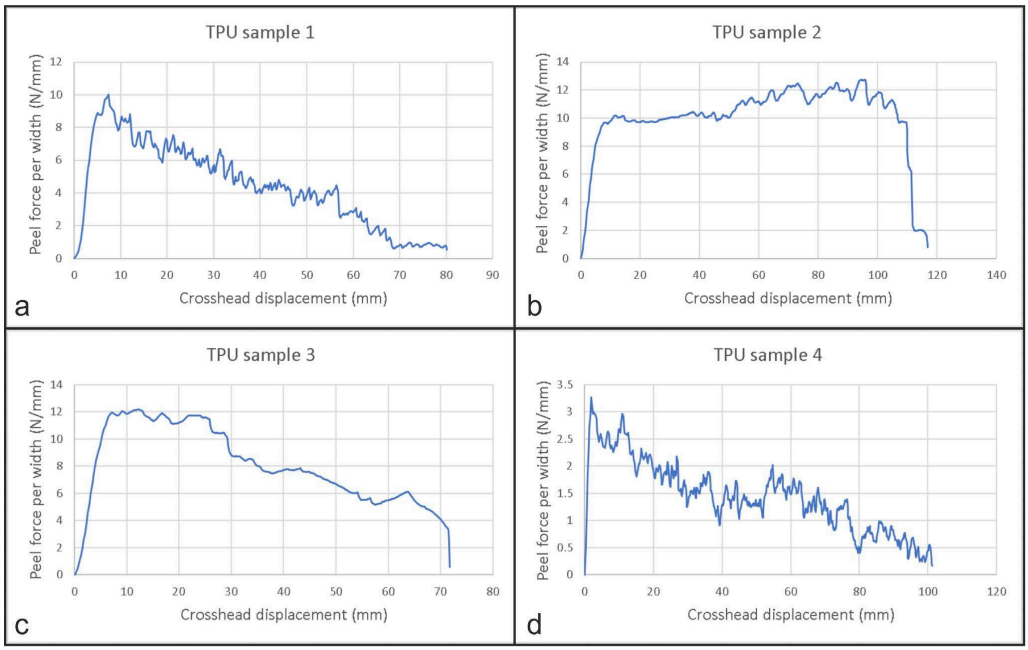

Figure 16. Representative failed TPU T-peel curves: (**a**) sample 1; (**b**) sample 2; (**c**) sample 3; (**d**) sample 4.

Table 2 reports T-peel resistance normalized by the 25 mm specimen width, calculated as the mean peeling force over the ISO 11339 evaluation window (25–125 mm) for specimens that provided the required window [12]. Specimens that ruptured or otherwise did not complete the evaluation segment were excluded from peel-resistance statistics and are reported as invalid counts rather than being averaged. To retain information from all tests, peak-force (F_{max}) statistics include all specimens within each polymer group.

For TPU, only one specimen completed the required ISO 11339 evaluation window. Therefore, the TPU T-peel resistance value is reported only as a single valid observation and should not be interpreted as a statistically representative mean or as a population estimate. No standard deviation or confidence interval can be associated with this value.

Table 2. Summary of T-peel test results (ISO 11339).

Polymer	n (Tested)	n (Valid)	Peel Resistance (N/mm) Mean ± SD	CV (%)	Peak Force, F_{max} (N) Mean ± SD	CV (%)
TPU	8	1	14.43 *	-	277.3 ± 95.9	34.58
PLA	8	5	8.42 ± 0.64	7.66	279.1 ± 20.6	7.37
PETG	8	8	2.92 ± 0.12	4.17	101.7 ± 11.4	11.24

* Single valid observation, not a statistically representative population estimate.

Overall, the T-peel benchmark clearly differentiated PETG (lower, stable peel) from PLA (higher peel with mixed validity), while TPU could not be robustly quantified by T-peel on this woven fabric because the test became dominated by substrate failure rather than interfacial separation—exactly the regime where an alternative normal-to-surface method is needed.

3.4. Interface Morphology and Interlocking Features (Microscopy)

Direct FDM deposition onto textiles rarely creates a simple, planar bond line. Instead, the interface develops as a three-dimensional engagement zone in which molten polymer penetrates the fabric porosity and partially surrounds yarns before solidifying. This penetration generates mechanical interlocking features for the more pronounced cases, which can strongly influence both the measured response and the dominant failure mode, particularly under peel loading where bending and off-axis extraction are inherent to the test. The microscopy sets presented below are therefore used to connect the observed macroscopic behavior (valid tests versus premature failures) to the underlying interface morphology for each polymer. Accordingly, these images are used for qualitative morphological interpretation of polymer penetration, yarn wrapping and interfacial failure features.

Figure 17 illustrates a cross-section through the polymer–textile interface and shows clear differences in penetration and encapsulation. For TPU (a), the polymer visibly envelops the textile structure, forming a continuous film that extends through the fabric thickness and can be observed even on the opposite side, indicating extensive impregnation and strong mechanical interlocking. For PLA (b), a similar—but less pronounced—behavior is observed: the polymer infiltrates the inter-yarn gaps and forms distinct protruding interlock features within the weave openings. For PETG (c), penetration appears more limited; the polymer does not immerse the textile to the same extent, and the resulting interlock features are smaller and less pronounced. Collectively, these sections support a simple morphological ranking that mirrors the adhesion trends: extensive encapsulation/interlocking for TPU, intermediate interlocking for PLA, and more limited interlocking for PETG.

These microscopy observations help explain why TPU produced the highest resistance, despite being a soft elastomer. The stronger TPU response should be interpreted as a process-interface effect rather than as a consequence of higher intrinsic stiffness or strength. Previous FDM-on-textile studies have shown that adhesion is strongly influenced by printing parameters, especially the nozzle-to-textile or nozzle-to-bed distance, because reduced distance can press molten polymer between yarns and fibers and promote mechanical interlocking [1,16]. In the present study, TPU was more compliant than PLA and PETG and could conform more effectively to the yarn architecture during first-layer deposition. Combined with the near-zero effective nozzle-to-textile clearance, this likely promoted deeper squeeze-in, yarn wrapping and stronger mechanical anchoring. Therefore, the higher TPU response under normal separation is consistent with an interface governed by polymer penetration and mechanical interlocking, rather than by polymer stiffness alone.

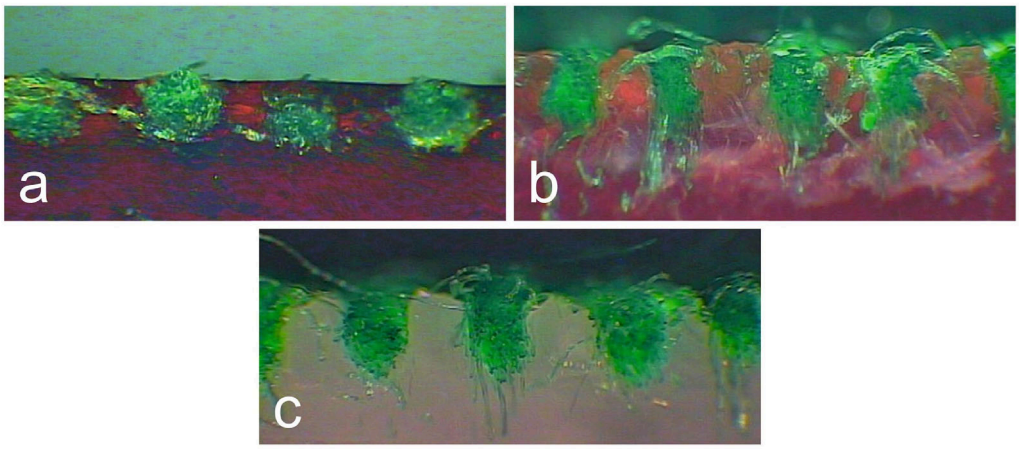

Figure 17. Cross-sectional microscopy images of the printed polymer–textile interface: (**a**) TPU, (**b**) PLA, (**c**) PETG.

Figure 18 compares the polymer surface after textile removal for both loading paths, highlighting how the same interfacial morphology can respond differently under peel versus normal separation. After T-peel, TPU shows evidence of partial damage to the polymer-side interlocking features in some regions, consistent with a mixed response in which the measured force may include not only interface separation but also local rupture of polymer structures formed within the fabric porosity. In contrast, after the perpendicular (pull-off) test, the TPU polymer surface retains a dense population of interlocking features with a more uniformly preserved appearance, suggesting that these features were primarily pulled out from the textile rather than torn within the polymer. For PLA and PETG, the polymer-side surfaces appear broadly similar between the two tests, with interlocking features largely preserved; however, the peel geometry can still promote yarn pull-out and textile damage when the features are more pronounced and rigid, which provides a plausible morphological explanation for the substrate-limited outcomes observed in a subset of PLA T-peel specimens. For PETG, the interlocking features are smaller and smoother, resembling rounded protrusions, which likely reduces snagging of yarns under peel loading and is consistent with the absence of textile rupture during PETG T-peel testing in this study.

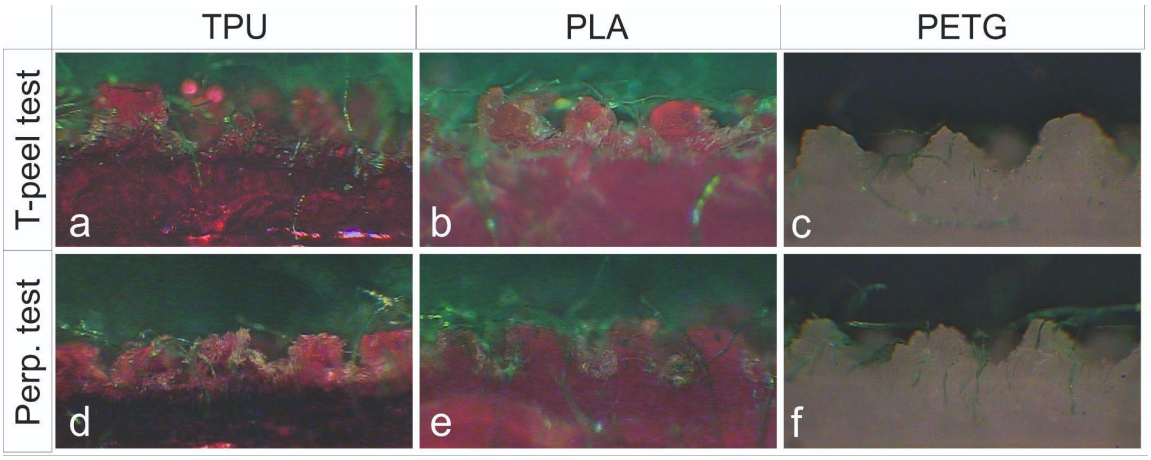

Figure 18. Comparative cross-sectional microscopy of the polymer after textile removal: (**a**–**c**) after T-peel—(**a**) TPU, (**b**) PLA, and (**c**) PETG; (**d**–**f**) after perpendicular-dolly testing—(**d**) TPU, (**e**) PLA, and (**f**) PETG.

Figure 19 compares the fabric surface opposite the printed side after testing for both T-peel and perpendicular pull-off. For TPU under T-peel, polymer residue is distributed across a large area of the back surface, with interlock remnants visibly occupying weave openings—direct evidence that torn interlock material remained embedded in the textile during peeling. In contrast, TPU under perpendicular testing shows only sparse, localized polymer traces, supporting the interpretation that axial extraction favored a cleaner separation without widespread tearing of polymer features. For PLA under T-peel, sporadic polymer remnants are visible together with noticeable deformation of the weave openings, consistent with localized yarn displacement/pull-out during off-axis peel extraction. Under PLA perpendicular testing, polymer traces are again limited and more sporadic, indicating that normal-to-surface extraction reduces lateral yarn displacement and promotes a cleaner detachment pathway. Finally, for PETG, where adhesion was the lowest in both methods, the textile back surfaces show minimal differences between T-peel and perpendicular tests; neither prominent polymer residues nor notable deformation of the weave openings are observed, consistent with a weaker mechanical interlocking contribution overall.

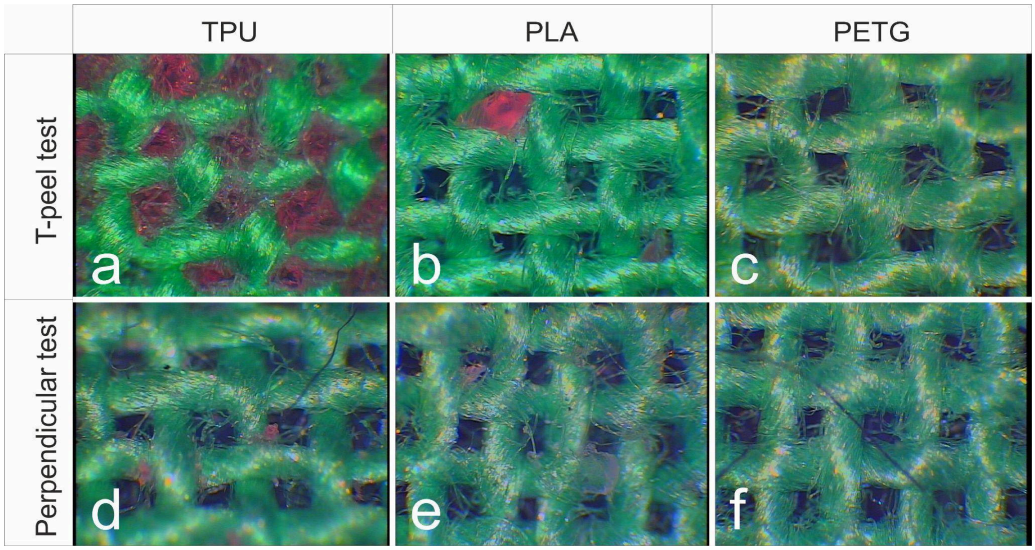

Figure 19. Comparative microscopy of fabric surface opposite the printed side after testing. Woven fabric (**a**–**c**) after T-peel test—(**a**) TPU, (**b**) PLA, and (**c**) PETG; (**d**–**f**) after perpendicular-dolly testing—(**d**) TPU, (**e**) PLA, and (**f**) PETG.

Taken together, these microscopy observations support two conclusions: (i) stronger apparent adhesion in printed-on-textile systems is closely linked to the extent and geometry of polymer penetration/interlocking, and (ii) the same interlocking morphology can lead to fundamentally different measured behavior depending on the loading path—mixed or substrate-limited response under peel versus a cleaner, more interpretable response under normal (perpendicular) extraction.

4. Discussion

Beyond interpretability, the two methods also differ in practical implementation and experimental throughput. T-peel can be perceived as a straightforward "print-and-test" benchmark because it relies on familiar strip specimens and a widely used peel configuration. However, when the full workflow is considered—including specimen fabrication footprint, first-layer reliability over extended toolpaths, test duration, and the proportion of tests that reach a standard-compliant evaluation window—its practical advantage becomes less clear relative to a compact pull-off (dolly) approach.

In this study, the printed polymer mass was similar for both specimen types (≈3.5 g), so the main fabrication penalty of T-peel was not polymer usage but print footprint and exposure time. T-peel specimens require longer, wider first-layer toolpaths over a larger textile area. The most critical process issues were observed at the first layer, where extended continuous deposition increases the likelihood of filament agglomeration and partial nozzle obstruction. This effect is amplified when stronger adhesion strategies are used (e.g., lower stand-off/higher flow), because those settings must be maintained across a large first-layer area. By contrast, the perpendicular-dolly specimen concentrates the interface into a compact circular zone. The first layer is short and localized, which reduces exposure to time-dependent first-layer instabilities and makes it practical to use more assertive first-layer settings to promote penetration without paying the same reliability penalty encountered in long T-peel prints.

Print times were similar for dolly specimens across materials (≈24–26 min per specimen for PLA/PETG/TPU). For T-peel specimens, printing time was comparable for PLA and PETG (≈24 min per specimen) but increased for TPU (≈35 min per specimen), further extending first-layer exposure in the material that also exhibited the highest failure rate in peel. On the testing machine, a typical T-peel run with ~150 mm effective peel length corresponds to ~300 mm total arm travel, which at 100 mm/min requires ~3 min of crosshead travel per specimen, not including mounting and manual alignment. In contrast, the perpendicular pull-off event is completed within seconds once the fixture is mounted and aligned; the full set of eight specimens can therefore be tested in minutes rather than tens of minutes, with lower operator dependence.

T-peel also places more demand on mounting consistency. Gripping, collinearity and the evolving peel angle can influence the effective loading condition, and long peel distances increase the chance that the test transitions into mixed or substrate-limited behavior. This is reflected in the present dataset by the large fraction of non-compliant T-peel outcomes for high-adhesion cases, where premature textile damage prevents steady-state evaluation. The perpendicular-dolly method avoids the need for a long evaluation window and standardizes mounting through a self-aligning fixture, which reduces sensitivity to grip setup and helps ensure that the test reaches a clear separation event.

Finally, the perpendicular approach supports more direct comparison across setups when geometry and bonded area are reported, because results can be expressed as both peak force and nominal pull-off stress based on a defined contact area. Previous work using related perpendicular-separation approaches provides a useful load-range reference for the proposed fixture. For example, Malengier et al. [17] reported a perpendicular tensile test in which directly printed PLA dollies were detached from cotton textile substrates. From their published graph, the maximum forces can be estimated at approximately 80–170 N, depending on textile construction. In the present study, the fully 3D-printable fixture sustained substantially higher pull-off loads, with PLA reaching 606.5 ± 44.4 N and TPU reaching 830.8 ± 46.9 N, with a maximum recorded TPU value of 886.8 N, without fixture failure or loss of alignment. This comparison is not intended to establish direct adhesion equivalence across different polymers, textile systems or printing conditions. Rather, it shows that the proposed fixture is mechanically robust enough to evaluate strong FDM-on-textile interfaces.

T-peel remains useful as a benchmark where steady-state peeling can be achieved, but its practical throughput and completion rate become limiting in strong-bonding regimes—precisely the regimes where routine screening and parameter studies require a robust, repeatable test.

To summarize within-method ranking without implying direct equivalence between peel and pull-off magnitudes, Figure 20 presents normalized trends referenced to each

method's mean. The graph summarizes the available within-method ranking, while highlighting the reduced completeness of the T-peel dataset for TPU, where many specimens could not be evaluated under the ISO window and were therefore excluded from the trend.

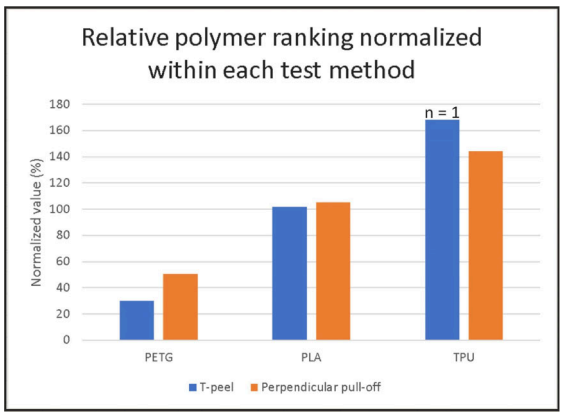

Figure 20. Relative polymer ranking normalized within each test method. T-peel values were normalized from peel resistance (N/mm), while perpendicular pull-off values were normalized from maximum nominal stress (MPa). The TPU T-peel value is labelled as n = 1 because it represents a single valid observation and is shown for indicative comparison rather than as a statistically representative mean.

5. Conclusions

This study evaluated adhesion testing for FDM-printed polymers on a woven cotton substrate using (i) an ISO 11339-type T-peel benchmark and (ii) a fixture-based perpendicular (pull-off) method built around a printed circular dolly and a fully 3D-printable, self-aligning clamping assembly. Across three representative filaments (PETG, PLA, and TPU; n = 8 per polymer), the perpendicular method consistently produced complete datasets and clearly discriminated the normal-separation response of the three polymer–textile systems (TPU > PLA > PETG).

In contrast, T-peel quantification over the ISO evaluation window (25–125 mm) was strongly material-dependent: PETG yielded valid curves for all specimens, PLA produced a mixed dataset, and TPU was largely substrate-limited, with most runs failing before the evaluation window could be completed. These outcomes highlight a practical limitation of peel-based benchmarks for high-interlocking FDM-on-textile systems, where the test can become dominated by textile damage rather than interface separation.

Microscopy supported the mechanical results by revealing distinct penetration and interlocking morphologies across polymers and by showing that the same interfacial architecture can respond differently under peel versus normal separation. From a practical point of view, concentrating the interface into a small, standardized circular area and enforcing alignment through a self-aligning fixture improves robustness and throughput, enabling routine adhesion screening across a wider bonding range than T-peel.

Future work should validate the proposed perpendicular method across a broader range of textile substrates and structures, including fabrics with different weave architectures, knitted constructions (with higher compliance and loop mobility), and nonwoven fabrics (with stochastic porosity and fiber entanglement).

A second direction is further scaling of the dolly contact area to extend the quantifiable range in very-high-adhesion regimes where substrate-limited behavior becomes likely. Reducing dolly diameter below the current geometry could shift failure away from textile rupture and toward measurable separation events, improving discrimination among strong-bonding conditions while preserving the method's key advantage: a compact, repeatable, area-defined normal-separation test.

Supplementary Materials: The following supporting information can be downloaded at: https://www.mdpi.com/article/10.3390/textiles6020054/s1, The printable files for the dolly and fixture device.

Author Contributions: Conceptualization, R.F., M.C.L., C.E.A. and A.T.; methodology, R.F., C.E.A., S.D.I. and E.C.L.; software, E.C.L., A.T. and R.F.; validation, M.C.L., S.D.I. and E.C.L.; formal analysis, M.C.L., S.D.I. and C.E.A.; investigation, R.F., C.E.A. and A.T.; resources, R.F. and E.C.L.; data curation, C.E.A. and S.D.I.; writing—original draft preparation, R.F., C.E.A. and A.T.; writing—review and editing, S.D.I. and E.C.L.; supervision, M.C.L.; project administration, S.D.I. All authors have read and agreed to the published version of the manuscript.

Funding: This research was funded by the European Union's Horizon Europe programme, grant number 101132596. The APC was funded by the same grant.

Data Availability Statement: The original contributions presented in this study are included in the article/Supplementary Material. Further inquiries can be directed to the corresponding authors.

Acknowledgments: The authors acknowledge the information and knowledge support offered by the "Craft Revitalization Action for Future-proofing the Transition to Innovative Technologies for Sustainable Development—CRAFT-IT4SD" project.

Conflicts of Interest: The authors declare no conflicts of interest.

Abbreviations

The following abbreviations are used in this manuscript:

FDM	Fused deposition modelling
PETG	Polyethylene terephthalate glycol
PLA	Polylactic acid
TPU	Thermoplastic polyurethane
ISO	International Organization for Standardization
AM	Additive manufacturing
DIN	Deutsches Institut für Normung
RH	Relative humidity
UTM	Universal testing machine
ABS	Acrylonitrile butadiene styrene

References

1. Spahiu, T.; Al-Arabiyat, M.; Martens, Y.; Ehrmann, A.; Piperi, E.; Shehi, E. Adhesion of 3D printing polymers on textile fabrics for garment production. *IOP Conf. Ser. Mater. Sci. Eng.* **2018**, *459*, 012065. [CrossRef]
2. Loh, G.H.; Sotayo, A.; Pei, E. Development and testing of material extrusion additive manufactured polymer-textile composites. *Fash. Text.* **2021**, *8*, 2. [CrossRef]
3. Cakar, S.; Ehrmann, A. Adhesion and stab-resistant properties of FDM-printed polymer/textile composites. *Tekstilec* **2023**, *66*, 211–217. [CrossRef]
4. Sitotaw, D.B.; Muenks, D.; Kebash, A.K. 3D printing applications on textiles: Measurement of air permeability for potential use in stab-proof vests. *J. Eng. Fibers Fabr.* **2024**, *19*, 15589250241232152. [CrossRef]
5. Özev, M.S.; Ehrmann, A. Sandwiching textiles with FDM printing. *Commun. Dev. Assem. Text. Prod.* **2023**, *4*, 88–94. [CrossRef]
6. Silvestre, R.; Garcia-Breijo, E.; Ferri, J.; Montava, I.; Bou-Belda, E. The influence of the structure of cotton fabrics on the adhesion of conductive polymer printed with 3D printing technology. *Polymers* **2023**, *15*, 668. [CrossRef] [PubMed]
7. Monteiro, E.; Carvalho, H.; Rocha, A.M.; Tama Bırkocak, D.; Puga, H. 3D printing of flexible conductive polymers on textiles for sensing and electrical connection. *Tekst. Muhendis* **2022**, *29*, 315–321. [CrossRef]
8. Chen, Y.; Deng, Z.; Ouyang, R.; Zheng, R.; Jiang, Z.; Bai, H.; Xue, H. 3D printed stretchable smart fibers and textiles for self-powered e-skin. *Nano Energy* **2021**, *84*, 105866. [CrossRef]
9. Popescu, D.; Amza, C.G. 3D printing onto textiles: A systematic analysis of the adhesion studies. *3D Print. Addit. Manuf.* **2024**, *11*, e586–e606. [CrossRef] [PubMed]
10. Costea, M.; Seul, A.; Mihai, A. Slit tear resistance of leather used in upholstery manufacturing. *Ind. Text.* **2023**, *74*, 296–302. [CrossRef]

11. *DIN 53530:1981-02*; Testing of Organic Materials; Separation Test on Fabric Plies Bonded Together. Deutsches Institut für Normung: Berlin, Germany, 1981.
12. *ISO 11339:2010*; Adhesives-T-Peel Test for Flexible-to-Flexible Bonded Assemblies. International Organization for Standardization: Geneva, Switzerland, 2010.
13. Čuk, M.; Bizjak, M.; Muck, D.; Kočevar, T.N. 3D printing and functionalization of textiles. In Proceedings of the 10th International Symposium on Graphic Engineering and Design (GRID 2020), Novi Sad, Serbia, 12–14 November 2020. [CrossRef]
14. Narula, A.; Pastore, C.M.; Schmelzeisen, D.; El Basri, S.; Schenk, J.; Shajoo, S. Effect of knit and print parameters on peel strength of hybrid 3-D printed textiles. *J. Text. Fibrous Mater.* **2018**, *1*, 2515221117749251. [CrossRef]
15. *ISO 6133:2015*; Rubber and Plastics-Analysis of Multi-Peak Traces Obtained in Determinations of Tear Strength and Adhesion Strength. International Organization for Standardization: Geneva, Switzerland, 2015.
16. Meyer, P.; Döpke, C.; Ehrmann, A. Improving adhesion of three-dimensional printed objects on textile fabrics by polymer coating. *J. Eng. Fibers Fabr.* **2019**, *14*, 1558925019895257. [CrossRef]
17. Malengier, B.; Hertleer, C.; Cardon, L.; Van Langenhove, L. 3D printing on textiles: Testing of adhesion. *J. Fash. Technol. Text. Eng.* **2018**, *S4*, 013. [CrossRef]
18. Gorlachova, M.; Mahltig, B. 3D-printing on textiles—An investigation on adhesion properties of the produced composite materials. *J. Polym. Res.* **2021**, *28*, 207. [CrossRef]
19. Maier, J.; Vogel, C.; Lebelt, T.; Geske, V.; Behnisch, T.; Modler, N.; Gude, M. Adhesion studies during generative hybridization of textile-reinforced thermoplastic composites via additive manufacturing. *Materials* **2021**, *14*, 3888. [CrossRef] [PubMed]
20. Robinson, B.; Imam, A.; Sabir, T.; Ahmed, A. Application of additive manufacturing on textiles. In Proceedings of the 93rd Textile Institute World Conference (TIWC 2025), Porto, Portugal, 7–10 October 2025.
21. *ISO 5084:1996*; Textiles-Determination of Thickness of Textiles and Textile Products. International Organization for Standardization: Geneva, Switzerland, 1996.
22. *ISO 139:2005*; Textiles-Standard Atmospheres for Conditioning and Testing. International Organization for Standardization: Geneva, Switzerland, 2005.

Assessing the quality level of the technical fabrics intended for protective equipment for firefighters by determining synthetic indicators

DOI: 10.35530/IT.075.06.202465

EMIL CONSTANTIN LOGHIN
IONUȚ DULGHERIU
LILIANA HRISTIAN

LILIANA BUHU
MANUELA AVĂDANEI
SAVIN DORIN IONESI

ABSTRACT – REZUMAT

Assessing the quality level of the technical fabrics intended for protective equipment for firefighters by determining synthetic indicators

The paper aims to highlight the quality level of technical fabrics by determining synthetic indicators based on durability and comfort functions, which can subsequently be used for modelling the physico-mechanical properties and selecting the most suitable fabrics to meet the requirements of a specific field of use. The study was conducted on two groups of technical fabrics with different compositions (Kevlar and Nomex), intended to manufacture firefighter protective equipment (jackets). Quality indicators represent numerical expressions of the quality level of a product or the relative expression of a certain characteristic, obtained by comparing it to a reference value (norm, standard, model). Quality indicators are converted into grades $I \in [0,1]$, where conventionally, a grade of 0 represents an inadequate product/non-quality, and a grade of 1 represents a superior quality level. The synthetic indicators determined in this study express the quality level of a product through the prism of categories/subcategories of quality characteristics representative of evaluating the comfort and durability functions specific to the groups of fabrics intended for the manufacture of protective equipment. Based on the values obtained for the synthetic indicators, a ranking of fabric variants is made according to the importance of durability and comfort characteristics. Thus, optimal fabric variants from each group can be highlighted, and solutions for improving the quality level for other variants can be proposed.

Keywords: *synthetic indicators, durability characteristics, comfort characteristics, Nomex fabrics, Kevlar fabrics*

Aprecierea nivelului calitativ al țesăturilor tehnice destinate echipamentelor de protecție pentru pompieri prin determinarea indicatorilor sintetici

Lucrarea și-a propus să evidențieze nivelul calitativ al țesăturilor tehnice, prin determinarea indicatorilor sintetici, pe baza funcțiilor de durabilitate și confort, care pot fi folosiți ulterior pentru modelarea proprietăților fizico-mecanice și pentru selectarea celor mai adecvate țesături privind satisfacerea cerințelor unui anumit domeniu de întrebuințare. Studiul a fost efectuat pe două grupe de țesături tehnice din compoziții diferite (Kevlar și Nomex), destinate confecționării echipamentelor de protecție pentru pompieri (jachete). Indicatorii calității reprezintă expresiile numerice ale nivelului calității unui produs sau expresia relativă a unei anumite caracteristici, obținută prin raportarea la valoarea de referință (normă, standard, model). Indicatorii calității sunt convertiți în calificative, $I \in [0,1]$, unde convențional, prin calificativul 0 se reprezintă un produs necorespunzător/noncalitate, iar prin calificativul 1 se reprezintă nivelul calitativ superior. Indicatorii sintetici determinați în cadrul acestui studiu exprimă nivelul calității unui produs prin prisma unor categorii/subcategorii de caracteristici de calitate reprezentative pentru evaluarea funcțiilor de confort și durabilitate specifice grupelor de țesături destinate confecționării echipamentelor de protecție. Pe baza valorilor obținute pentru indicatorii sintetici se realizează o ierarhizare a variantelor de țesături în funcție de gradul de importanță al caracteristicilor de durabilitate și confort. Astfel, pot fi evidențiate variantele optime de țesături din fiecare grupă și pot fi propuse soluții de îmbunătățire a nivelului calității pentru celelalte variante.

Cuvinte-cheie: *indicatori sintetici, caracteristici de durabilitate și confort, Nomex, Kevlar*

INTRODUCTION

In general, when creating firefighter protective equipment (jackets), fabrics that meet the highest levels of protection and comfort are sought, despite their high costs. Most companies use fabrics made from aramid fibres, which dominate the sector, as they offer high levels of mechanical tensile strength and durability while being completely flame-resistant. For these reasons, a range of technical fabrics necessary for the manufacture of firefighter protective equipment has been developed using blends of the latest meta-aramids and para-aramids with comparable effectiveness and protection at reasonable prices [1–3]. Depending on the application, the choice between Kevlar and Nomex is one of the requirements for comfort and protection, which can be used in the seven layers that make up firefighter protective equipment. Kevlar is much more resistant to abrasion than Nomex and is therefore used in a higher concentration percentage in firefighter protective equipment [4–6]. Nomex is a softer-feeling fibre and is

used to a greater extent in everyday clothing articles due to the greater comfort it offers the wearer [7–9]. Simple weave structures such as plain or twill, as well as some of their derivatives like rip-stop and twill, are most commonly used for the outer fabric of firefighter protective equipment due to their exceptional tear resistance and increased tensile strength [10–12]. Nomex provides heat and flame resistance to the protective equipment, while Kevlar offers flexibility, comfort, and breathability [13–15]. Kevlar has been extensively utilized in the production of advanced composites in aerospace, military, marine, and sports sectors due to its mechanical properties, thermal stability, and high energy absorption properties [16–18]. Nomex®, manufactured by DuPont, is made of aramid fibres and is lightweight with high tensile strength and heat resistance (degrading at 480°C) [19–20]. Its high breathability and low water vapour resistance make it suitable for use as an outer layer. Fabrics face complex demands in fire situations [21–26]. The fabric's performance in these situations is related to comfort, time, warmth, durability, and other specific appearance features [27–30]. The performance of firefighter protective clothing is primarily based on the thermophysical properties of the materials used in their construction [31–36].

EXPERIMENTAL PART

Materials and methods

The experimental matrix included twelve samples from two groups of technical fabrics with different compositions, intended for the manufacture of firefighter protective equipment, whose characteristics are presented in table 1.

Group A of fabrics contains six articles, coded K1, K2, K3, K4, K5, and K6, made from yarns composed of Kevlar fibres, balanced in fineness with $Nm_{warp} = Nm_{weft}$ and density $P_{warp} = P_{weft}$, with plain and twill weave structures.

Group B of fabrics contains six articles, coded N1, N2, N3, N4, N5, and N6, made from yarns composed of Nomex fibres, balanced in fineness with $Nm_{warp} = Nm_{weft}$ and density $P_{warp} = P_{weft}$, with plain and twill weave structures.

The fibrous composition, properties of the component fibres, structural parameters of the fabrics, mechanical and physical properties of the yarns, as well as finishing treatments, influence the quality characteristics regarding the durability and physiological comfort of firefighter protective equipment. To highlight the influence of the weave structure on certain surface characteristics of the fabrics in the studies conducted within this work, the weave structure was expressed by the warp floating for the warp yarns F_{warp} and the weft floating for the weft yarns F_{weft}. The intersection between a warp yarn and a weft yarn is called a binding point, so the weave structure contains the set of all binding points with a warp or weft effect in the longitudinal or transverse direction. The floating size, like the binding segment, has a minimum value of $F = 1$, which is specific to the plain weave structure.

Due to its unique properties such as high strength-to-weight ratio and greater modulus, Kevlar fibre has become very popular as reinforcement in composite materials, and its application has increased considerably. Kevlar® is an example of a para-aramid fibre, while Nomex® is considered a meta-aramid. The key difference between meta and para-aramid is that

Table 1

CHARACTERISTICS OF TWELVE SAMPLES OF TECHNICAL FABRICS WITH DIFFERENT COMPOSITIONS

Group/ Composition	Article code	Yarn count $Nm_{warp} = Nm_{weft}$	Technological density, (yarns/10 cm) $P_{warp} = P_{weft}$	Mean flotation F	Type of bonding
Group A/Kevlar	K1	68/2	265	2	Twill $D\frac{2}{2}/$
	K2	54/2	260	2	Twill $D\frac{2}{2}/$
	K3	48/2	290	1.5	Twill $D\frac{2}{1}/$
	K4	60/2	280	1.5	Twill $D\frac{2}{1}/$
	K5	68/2	285	1	Plain
	K6	60/2	275	1	Plain
Group B/Nomex	N1	64/2	270	2	Twill $D\frac{2}{2}/$
	N2	60/2	260	2	Twill $D\frac{2}{2}/$
	N3	48/2	370	1.5	Twill $D\frac{2}{1}/$
	N4	56/2	360	1.5	Twill $D\frac{2}{1}/$
	N5	56/2	355	1	Plain
	N6	68/2	350	1	Plain

meta-aramid has a semi-crystalline molecular structure, while para-aramid is crystalline. Fabrics woven from Nomex® fibres are used in applications requiring good textile properties, good dimensional stability, and excellent heat resistance. Fabrics woven of Nomex® fibre have good resistance to many chemicals and are highly resistant to most hydrocarbons and many other organic solvents.

The database used in this study was obtained by quantifying the physical-mechanical properties of the two groups of fabrics using standardized methods and evaluated through a series of indices determined directly on the measuring apparatus or by calculation.

In determining the synthetic indicators of the two groups of technical fabrics intended for the manufacture of firefighter protective equipment, a series of representative characteristics reflecting durability were selected: tensile strength, *Pr* (daN); fabric tenacity, τ (cN/tex); puncture resistance, *T* (N); work of mechanical deformation at rupture, W_s (N·m); and flexural stiffness, *R* (mg·cm). In determining the synthetic indicators reflecting physiological comfort, the following representative characteristics were selected: air permeability index, *I* (kg/m^2·h); relative elongation at break, ε (%); thermal conductivity coefficient, λ (kcal/m·h·°C); vapour permeability coefficient, μ (g/m^2·h) and fabric mass, *M* (g/m^2).

The representative characteristics used in calculating the synthetic indicators of durability and comfort were selected using the correlation method. Tensile properties tests of the fabrics were conducted on the Honsfield electronic dynamometer, according to SR EN ISO 2062. Analysis of fabric behaviour during wearing indicates that they are subjected to simple or repeated uniaxial or biaxial stretching stresses. The level of these stresses can be close to the breaking limit or may have low, insignificant values, so the designer must anticipate the behaviour under such stresses. This can be appreciated by determining indices derived from the stress-strain diagram. The behaviour under the bending stress of fabrics is structurally determined by the transfer of fibre-yarn-fabric properties, influenced by mechanical and chemical processing processes, and is expressed by the bending length and flexural stiffness. In this study, we used the values obtained for the flexural stiffness of the two groups of fabrics, determined according to the ASTM D1388-18 standard.

Protective equipment for firefighters must be designed to ensure conditions of comfort (being permeable to air and vapours, impermeable to water and toxic substances), of operation (comfortable, resistant, easy to wear), but also to contribute to the prevention of accidents and occupational illnesses.

The mass of the fabrics was determined according to the SR EN 12127:2013 standard, which allows for comparative evaluation, essential for the intended use of the fabric.

Air permeability was determined in accordance with the EN ISO 9237:1995 standard, which for fabrics intended for clothing must ensure comfort conditions during wearer activity.

Experimental values for determining the thermal conductivity coefficient, vapour permeability coefficient, and air permeability index for the two groups of fabrics were obtained through standardized methods, depending on treatment parameters (temperature, pressure, and speed) and material characteristics.

The quality level of the two groups of technical fabrics intended for the manufacture of protective equipment is assessed by determining synthetic quality indicators based on comfort and durability functions.

Quality indicators are numerical expressions of the quality level of a product. A quality indicator must meet a series of conditions:

- it should be simple, so that the calculation method, expression, and meaning are easy to understand;
- it should be relevant to ensure the most accurate description of the actual quality level;
- it should be verifiable so that it can be recalculated anytime based on the method used.

The quality index is a relative expression of a specific characteristic, obtained by comparing it to a reference value (norm, standard, model).

The index can be converted into a rating $I \in [0,1]$, where conventionally, a rating of 0 represents an inadequate product/non-quality, and a rating of 1 represents a superior quality level.

To determine the indices, it is necessary to apply methods for evaluating quality characteristics. Specific methods for the textile industry include:

- measurement with known precision using standardized means;
- expertise conducted through sensory analysis by specialists in the field;
- sociological evaluation based on survey questionnaires addressed to potential users.

In the study, quality characteristics representative of evaluating the comfort and durability functions specific to the groups of fabrics intended for the manufacture of protective equipment were measured. The expertise method was applied to assess the importance of the characteristics expressing the functions of the analysed products. Quality indicators can be simple, synthetic, or global based on the level of complexity. The emphasis of the study was on evaluating the quality level of the analyzed textile surfaces through synthetic and global indicators. The synthetic indicator expresses the quality level of a product through the prism of categories/subcategories of quality characteristics.

The algorithm for calculating the synthetic indicator is as follows:

1. Select representative characteristics.
2. Obtain the sample consisting of representative samples (n).
3. Measure the characteristics using standardized methods.
4. Determine the preferred direction of increase/decrease for each characteristic, depending on the product's purpose.

5. Report the obtained values for each characteristic on a unique scale within the interval [0;1].
6. By reporting, the degree of utility U_i is obtained depending on the preferred direction of increase/decrease of the quality characteristic values, as follows:
   - for the preferred direction of increase in characteristic values (positive characteristic), U_i is calculated using the following relationship:

$$U_i = \frac{x_i - x_{min}}{x_{max} - x_{min}} \quad (1)$$

   - for the preferred direction of decrease in characteristic values (negative characteristic), U_i is calculated using the following relationship:

$$U_i = \frac{x_{max} - x_i}{x_{max} - x_{min}} \quad (2)$$

   - the hierarchy of quality characteristics based on the coefficient of significance (degree of importance) is calculated using the following relationship:

$$\gamma_i = \left(100 / \sum_{j=1}^{m} R_{ij}\right) / \left(\sum_{i=1}^{n}\left(100 / \sum_{j=1}^{m} R_{ij}\right)\right) \quad (3)$$

where R_{ij} = 1 represents the rank assigned to the characteristic considered the most important (with maximum score); R_{ij} = n represents the rank assigned to the characteristic considered the least important (with minimum score); n is the number of characteristics i = 1, ..., n; m is the number of experts j = 1, ..., m.

To establish the significance coefficient, the expertise method was applied. The ranks corresponding to the quality characteristics were evaluated by a team of six specialists in the textile field. Based on the evaluations, the experts fill out survey sheets assigning different ranks to the quality characteristics. The consistency of opinions among experts is verified using the following relationship:

$$W = \sum_{i=1}^{n}\left(\sum_{j=1}^{m} R_{ij} - R_{ij}\right)^2 / \left[m^2 \cdot (n^3 - n)/6\right] \quad (4)$$

where:

$$R_{ij} = \left(\sum_{i=1}^{n}\sum_{j=1}^{m} R_{ij}\right) / 6 \quad (5)$$

The verification of agreement among experts is conducted based on the χ^2 test, where the test statistic is calculated using the following relationship:

$$\chi^2 = W \cdot m(n - 1) \quad (6)$$

If $\chi^2_{calc} > \chi^2_{\nu-1,\alpha=0.05}$, it follows that the opinions of the experts are in agreement (W is significant).

For $W \geq 0.8$, the significance coefficient γ_i is determined using the following relationship:

$$\gamma_i = \left(100 / \sum_{j=1}^{m} R_{ij}\right) / \left(\sum_{i=1}^{n} 100 / \sum_{j=1}^{m} R_{ij}\right) \quad (7)$$

The hierarchy of characteristics is determined based on the criterion of decreasing values of γ_i.The representative values must satisfy the condition $\gamma_i > 1/n$ [37–40]. Calculation of the synthetic indicator using the relationship:

$$Is = \sum_{i=1}^{n} U_i \cdot \gamma_i \quad (8)$$

Synthetic indicators express the quality level of a product through the prism of categories/subcategories of quality characteristics considered to be representative of a product.

RESULTS AND DISCUSSIONS

According to the steps in the workflow algorithm, the following are calculated:

- Synthetic durability indicators $Is_{1-gr.A}$ and $Is_{1-gr.B}$ for Group A and Group B of fabrics, respectively.
- Comfort indicators $Is_{2-gr.A}$ and $Is_{2-gr.B}$ for Group A and Group B of fabrics intended for the manufacture of firefighter protective equipment.

The calculation of the synthetic durability indicator for the fabrics in Group A (Kevlar)

Selection of representative characteristics:

- tensile strength, Pr (daN);
- fabric tenacity, τ (cN/tex);
- puncture resistance, T (N);
- work of deformation at rupture, W_s (N·m);
- flexural rigidity, R (mg·cm).

The average values of durability characteristics for the fabrics in Group A (Kevlar) are presented in table 2.

Table 2

AVERAGE VALUES OF DURABILITY CHARACTERISTICS FOR THE FABRICS IN GROUP A (KEVLAR)

Group/ Composition	Article code	Tensile strength Pr (daN)	Fabric tenacity τ (cN/tex)	Puncture resistance T (N)	Mechanical work W_s (N·m)	Flexural rigidity R (mg·cm)
Group A/ Kevlar	K1	79.03	16.70	1539.72	6.247	52.92
	K2	77.76	16.15	1487.52	6.065	50.86
	K3	72.47	12.00	1224.64	3.287	58.85
	K4	71.59	15.34	1342.78	3.849	54.66
	K5	87.05	20.77	1380.58	6.393	62.44
	K6	85.24	18.60	1420.51	5.919	58.85
Min		**71.59**	**12.00**	**1224.64**	**3.287**	**50.86**
Max		**87.05**	**20.77**	**1539.72**	**6.393**	**62.44**

The preferred direction of variation for durability characteristics has been adopted as follows:

- positive characteristics: *Pr* (daN), τ (cN/tex), *T* (N) and W_s (N·m);
- negative characteristics: *R* (mg·cm).

The values obtained for each characteristic are reported on a single scale in the interval [0;1] as shown in table 3; the degree of utility U_i based on the preferred direction of increase/decrease of the quality characteristic values was determined as follows:

- For the preferred direction of increasing the values of the characteristic (positive characteristic), U_i is calculated using the relationship:

$$U_i = \frac{x_i - x_{min}}{x_{max} - x_{min}} \quad (9)$$

- For the preferred direction of decreasing the values of the characteristic (negative characteristic), U_i is calculated using the relationship:

$$U_i = \frac{x_{max} - x_i}{x_{max} - x_{min}} \quad (10)$$

The values of the synthetic durability indicator for the fabrics in Group A (Kevlar) are presented in table 3. To calculate the indicator $Is_{1-gr.A}$, the values of the importance degree of durability characteristics presented in table 4 were required. The importance degree of durability characteristics was evaluated using the expert method (table 5).

The consistency of expert opinions was checked using the relationship:

$$W = \sum_{i=1}^{n}\left(\sum_{j=1}^{m} R_{ij} - R_{ij}\right)^2 / \left[m^2 \cdot (n^3 - n)/6\right] = \quad (11)$$

$$= \frac{25960}{36 \cdot \frac{(125-5)}{6}} = 36$$

From a statistical point of view, the agreement of expert opinions is verified using the test, where the χ^2 test statistic is calculated using the relationship:

$$\chi^2 = W \cdot m(n-1) \quad (12)$$

If $\chi^2_{calc} > \chi^2_{\nu-1,\alpha=0.05}$, it follows that the expert opinions are in agreement (*W* is significant). So, from a statistical perspective, $\chi^2_{calc} = 720 > \chi^2_{tab}$, the expert opinions are in agreement (*W* is significant). The ranking of characteristics is based on the criterion of decreasing values of γ_{ij}, as presented in table 5.

The calculation of the synthetic durability indicator for the fabrics in Group B (Nomex)

The average values of durability characteristics for fabrics in Group B (Nomex) are presented in table 6. To calculate the indicator $Is_{1-gr.B}$, the values of the importance degree of durability characteristics presented in table 7 were required. The importance degree of durability characteristics was evaluated using the expert method (table 5).

The ranking of durability characteristics for fabrics in Group B was conducted similarly to fabrics in Group A, according to table 5. This method of calculation allows for drawing direct conclusions based on the quality indicators: the closer the indicator value is to 1, the higher the quality it represents. The synthetic indicator $Is_{1-gr.A}$ includes all the characteristics that are reflected in the durability of the analysed fabrics, as observed from the experimental data for fabrics in Group A (Kevlar). Article K5, characterized by $Nm_{warp} = Nm_{weft} = 68/2$, $P_{warp} = P_{weft} = 285$ yarns/10 cm plain weave, with floating $F = 1$, has the highest value of the synthetic indicator $Is_{1-gr.A} = 0.889$. This is justified by the fact that the utility of positive characteristics for tensile strength, fabric tenacity, and mechanical work of rupture deformation has the maximum value, indicating a higher quality level, except for puncture resistance, which is 0.5. Also, the utility of the negative characteristic for bending stiffness has the maximum value, indicating a higher quality level.

Table 3

VALUES OF THE SYNTHETIC DURABILITY INDICATOR FOR THE FABRICS IN GROUP A (KEVLAR)

Group/ Composition	Article code	Positive	Positive	Positive	Negative	Negative	$Is_{1-gr.A}$
		Pr (daN)	τ (cN/tex)	*T* (N)	W_s (N·m)	*R* (mg·cm)	
Group A/ Kevlar	K1	0.481	0.317	1.000	0.863	0.178	0.553
	K2	0.399	0.357	0.834	0.567	0.000	0.428
	K3	0.057	0.000	0.000	0.106	0.690	0.170
	K4	0.000	0.040	0.375	0.000	0.328	0.160
	K5	1.000	1.000	0.495	1.000	1.000	**0.889**
	K6	0.883	0.994	0.622	0.992	0.690	**0.828**

Table 4

VALUES OF THE IMPORTANCE DEGREE OF DURABILITY CHARACTERISTICS OF GROUP A (KEVLAR)

Degree of importance	*Pr* (daN)	τ (cN/tex)	*T* (N)	W_s (N·m)	*R* (mg·cm)
γ_i	0.19	0.23	0.22	0.15	0.21

Table 5

RANKING OF CHARACTERISTICS OF GROUP A (KEVLAR)						
Characteristics / Experts	*Pr* (daN)	τ (cN/tex)	*T* (N)	W_s (N·m)	*R* (mg·cm)	$\sum_{i=1}^{n} R_{ij}$
E1	5	3	4	2	1	15
E2	4	2	1	5	3	15
E3	1	4	2	3	5	15
E4	2	3	4	5	1	15
E5	1	3	2	4	5	15
E6	2	1	4	5	3	15
$\sum_{j=1}^{m} R_{ij}$	19	15	16	23	17	90
$100/\sum_{j=1}^{m} R_{ij}$	5.26	6.67	6.25	4.35	5.88	28
γ_{ij}	0.19	0.23	0.22	0.15	0.21	1.0
Rank	4	1	2	5	3	15.0
$\sum_{j=1}^{m} R_{ij} - R_{ij,n}$	5041	5625	5476	4489	5329	$\sum_{i=1}^{n}\left(\sum_{j=1}^{m} R_{ij} - R_{ij}\right)^2$

Table 6

AVERAGE VALUES OF DURABILITY CHARACTERISTICS FOR FABRICS IN GROUP B (NOMEX)						
Group/ Composition	**Article code**	***Pr* (daN)**	**τ (cN/tex)**	***T* (N)**	**W_s (N·m)**	***R* (mg·cm)**
Group B/ Nomex	N1	35.05	5.13	674.17	4.068	52.92
	N2	34.89	5.18	642.21	4.039	50.86
	N3	33.27	4.38	538.33	4.051	58.85
	N4	32.86	4.32	524.16	4.04	52.66
	N5	37.24	9.01	706.67	3.339	62.75
	N6	36.58	8.83	716.85	3.348	58.64
Min		**32.86**	**4.32**	**524.16**	**3.34**	**50.86**
Max		**37.24**	**9.01**	**716.85**	**4.07**	**62.75**

Table 7

VALUES OF THE IMPORTANCE DEGREE OF DURABILITY CHARACTERISTICS OF GROUP B (NOMEX)							
Group/ Composition	**Article code**	**Positive**	**Positive**	**Positive**	**Positive**	**Negative**	$Is_{1-gr.B}$
		***Pr* (daN)**	**τ (cN/tex)**	***T* (N)**	**W_s (N·m)**	***R* (mg·cm)**	
Group B/ Nomex	N1	0.500	0.173	0.779	0.960	0.827	0.623
	N2	0.463	0.183	0.613	1.000	1.000	0.624
	N3	0.094	0.013	0.074	0.977	0.328	0.254
	N4	0.000	0.000	0.000	0.962	0.849	0.323
	N5	1.000	1.000	0.947	0.000	0.000	0.628
	N6	0.849	0.962	1.000	0.012	0.346	**0.676**

At Article K4 in Group A, characterized by Nm_{warp} = Nm_{weft} = 60/20, P_{warp} = P_{weft} = 280 yarns/10 cm, diagonal $D\frac{2}{1}/$, with floating F = 1.5, the lowest value of the synthetic indicator $Is_{1-gr.A}$ = 0.160 was obtained. This is justified by the fact that the utility of positive characteristics for tensile strength and mechanical work of rupture deformation has the minimum value. Additionally, fabric tenacity and puncture resistance have values lower than 0.4, closer to the lower limit, indicating a lower quality level. Moreover, the utility of the negative characteristic for bending stiffness has a value lower than 0.4, indicating a lower quality level.

At Article N6 in Group B (Nomex), characterized by Nm_{warp} = Nm_{weft} = 68/2, P_{warp} = P_{weft} = 350 yarns/10 cm, plain weave, with floating F = 1, the highest value

of the synthetic indicator $Is_{1-gr.B}$ = 0.676 was obtained. This is justified by the fact that the utility of positive characteristics for tensile strength, fabric tenacity, and puncture resistance, except for the mechanical work of rupture deformation, is close to the maximum value, indicating a higher quality level. However, the utility of the negative characteristic for bending stiffness has a value lower than 0.4, close to the lower limit, indicating a lower quality level.

At Article N3 in Group B, characterized by Nm_{warp} = Nm_{weft} = 48/2, P_{warp} = P_{weft} = 370 yarns/10 cm, diagonal $D\frac{2}{1}/$, with floating F = 1.5, the lowest value of the synthetic indicator $Is_{1-gr.A}$ = 0.254 was obtained. This is justified by the fact that the utility of positive characteristics for tensile strength, fabric tenacity, and puncture resistance is at the minimum value, indicating a lower quality level, except for the mechanical work of rupture deformation. However, the utility of the negative characteristic for bending stiffness is close to the upper limit, indicating a higher quality level.

Among the analysed characteristics, the team of experts considered that fabric tenacity best reflects the durability of the fabrics, assigning it the highest weight for assessing the quality level of fabric assortments needed for the production of firefighting equipment.

Calculating the synthetic physiological comfort indicator for fabrics in Group A (Kevlar)

According to the steps within the algorithm, synthetic comfort indicators $Is_{2-gr.A}$ and $Is_{2-gr.B}$ are calculated for each group of fabrics.

Selection of representative characteristics:

- Air permeability index, I (kg/m^2·h)
- Relative elongation at break, ε (%)
- Thermal conductivity coefficient, λ (kcal/m·h·°C)
- Vapor permeability coefficient, μ (g/m^2·h)
- Fabric mass, M (g/m^2)

The average values of comfort characteristics for fabrics in Group A (Kevlar) are presented in table 8. The preferred direction of variation for physiological comfort characteristics has been adopted as follows:

- positive characteristics: I (kg/m^2·h) and ε (%);
- negative characteristics: λ (kcal/m·h·°C), μ (g/m^2·h) and M (g/m^2).

The values obtained for each characteristic are reported on a single scale in the interval [0;1] in table 9. The degree of utility U_i depending on the preferred direction of increase/decrease of the quality characteristic values was determined as follows:

- for the preferred direction of increasing the values of the characteristic (positive characteristic), U_i is calculated using the relationship:

$$U_i = \frac{x_i - x_{min}}{x_{max} - x_{min}} \quad (13)$$

Table 8

AVERAGE VALUES OF COMFORT CHARACTERISTICS FOR FABRICS IN GROUP A (KEVLAR)

Group/ Composition	Article code	Air permeability index I (kg/m^2·h)	Relative elongation at break ε (%)	Thermal conductivity coefficient λ (kcal/m·h·°C)	Vapour permeability coefficient μ (g/m^2·h)	Fabric mass M (g/m^2)
Group A/ Kevlar	K1	35.4	7.3	0.044	4.28	147
	K2	24.2	6.8	0.047	4.22	160
	K3	34.5	7.6	0.052	4.35	156
	K4	32.8	7.8	0.048	4.42	180
	K5	33.6	5.4	0.053	4.75	162
	K6	34.2	5.6	0.050	4.68	174
Min		**24.2**	**5.4**	**0.044**	**4.22**	**147**
Max		**35.4**	**7.8**	**0.053**	**4.75**	**180**

Table 9

VALUES OF THE SYNTHETIC COMFORT INDICATOR FOR THE FABRICS IN GROUP A (KEVLAR)

Group/ Composition	Article code	Positive I (kg/m^2·h)	Positive ε (%)	Negative λ (kcal/m·h·°C)	Negative μ (g/m^2·h)	Negative M (g/m^2)	$Is_{2-gr.A}$
Group A/ Kevlar	K1	1.000	0.792	1.000	0.887	1.000	**0.939**
	K2	0.000	0.583	0.667	1.000	0.606	0.561
	K3	0.920	0.917	0.111	0.755	0.727	0.694
	K4	0.768	1.000	0.556	0.623	0.000	0.586
	K5	0.839	0.000	0.000	0.000	0.545	**0.296**
	K6	0.893	0.083	0.333	0.132	0.182	0.341

- for the preferred direction of decreasing the values of the characteristic (negative characteristic), U_i is calculated using the relationship:

$$U_i = \frac{x_{max} - x_i}{x_{max} - x_{min}} \quad (14)$$

The values of the synthetic comfort indicator $Is_{2-gr.A}$ for fabrics in Group A (Kevlar) are presented in table 9. For the calculation of the indicator $Is_{2-gr.A}$, the values of the importance degree of comfort characteristics presented in table 10 were required. The importance degree of durability characteristics was evaluated using the expert method (table 11).

The consistency of expert opinions was checked using the relationship:

$$W = \sum_{i=1}^{n}\left(\sum_{j=1}^{m} R_{ij} - R_{ij}\right)^2 / \left[m^2 \cdot (n^3 - n)/6\right] = \quad (15)$$

$$= \frac{25960}{36 \cdot \frac{(125-5)}{6}} = 36$$

From a statistical point of view, the agreement of expert opinions is verified using the test, where the χ^2 test statistic is calculated using the relationship:

$$\chi^2 = W \cdot m(n-1) \quad (16)$$

So, from a statistical perspective, $\chi^2_{calc} > \chi^2_{\nu-1,\alpha=0.05}$, the expert opinions are in agreement (W is significant). The ranking of characteristics is based on the criterion of decreasing values of γ_{ij}, as presented in table 11.

Calculating the synthetic physiological comfort indicator for fabrics in Group B (Nomex)

The average values of physiological comfort characteristics for fabrics in Group B (Nomex) are presented in table 12. The values of the synthetic comfort indicator $Is_{2-gr.B}$ for fabrics in Group B (Nomex) are presented in table 13. For the calculation of the indicator $Is_{2-gr.A}$, the values of the importance degree of comfort characteristics presented in table 10 were required. The importance degree of durability characteristics was evaluated using the expert method (table 11).

The ranking of comfort characteristics for fabrics in Group B was conducted similarly to fabrics in Group A, according to table 4. From the analysis of the values obtained for the synthetic comfort indicators $Is_{2-gr.A}$ and $Is_{2-gr.B}$, the following aspects can be deduced:

- The synthetic indicator $Is_{2-gr.A}$ includes all the characteristics that are reflected in the comfort of the analysed fabrics, as observed from the experimental data for fabrics in Group A (Kevlar). Article K1, characterized by $Nm_{warp} = Nm_{weft} = 56/2$, $P_{warp} = P_{weft} = 365$ yarns/10 cm, diagonal $D\frac{2}{2}/$, with floating $F = 2$, has the highest value of the synthetic indicator $Is_{1-gr.A} = 0.939$. This is justified by the fact that the utility of positive characteristics for the air permeability index has the maximum value, and the relative elongation at break is close to the upper limit, indicating a higher quality level.

Table 10

VALUES OF THE IMPORTANCE DEGREE OF COMFORT CHARACTERISTICS OF GROUP A (KEVLAR)

Degree of importance	l (kg/m^2·h)	ε (%)	λ (kcal/m·h·°C)	μ (g/m^2·h)	M (g/m^2)
γ_i	0.22	0.18	0.19	0.21	0.20

Table 11

RANKING OF CHARACTERISTICS OF GROUP A (KEVLAR)

Characteristics / Experts	l (kg/m^2·h)	ε (%)	λ (kcal/m·h·°C)	μ (g/m^2·h)	M (g/m^2)	$\sum_{j=1}^{m} R_{ij}$
E1	1	2	3	4	5	15
E2	3	4	1	5	2	15
E3	4	5	3	1	2	15
E4	1	4	5	2	3	15
E5	2	3	4	1	5	15
E6	5	2	3	4	1	15
$\sum_{i=1}^{n} R_{ij}$	16	20	19	17	18	90
$100/\sum_{j=1}^{m} R_{ij}$	6.25	5.00	5.26	5.88	5.56	28
γ_{ij}	0.22	0.18	0.19	0.21	0.20	1
Rank	1	5	4	2	3	15
$\sum_{j=1}^{m} R_{ij} - R_{ij,n}$	5476	4900	5041	5329	5184	$\sum_{i=1}^{n}\left(\sum_{j=1}^{m} R_{ij} - R_{ij}\right)^2$

Table 12

AVERAGE VALUES OF PHYSIOLOGICAL COMFORT CHARACTERISTICS FOR FABRICS IN GROUP B (NOMEX)						
Group/ Composition	**Article code**	**Air permeability index I (kg/m^2·h)**	**Relative elongation at break ε (%)**	**Thermal conductivity coefficient λ (kcal/m·h·°C)**	**Vapour permeability coefficient μ (g/m^2·h)**	**Fabric mass M (g/m^2)**
Group B/ Nomex	N1	26.30	21.90	0.056	5.45	217
	N2	30.60	22.70	0.054	5.32	214
	N3	28.80	25.30	0.059	5.73	220
	N4	27.40	26.80	0.057	5.66	230
	N5	29.10	17.60	0.063	6.17	292
	N6	32.20	16.30	0.060	5.81	288
Min		**26.30**	**16.30**	**0.054**	**5.32**	**214**
Max		**32.20**	**26.80**	**0.063**	**6.17**	**292**

Table 13

VALUES OF THE SYNTHETIC COMFORT INDICATOR FOR FABRICS IN GROUP B (NOMEX)							
Group/ Composition	**Article code**	**Positive**	**Positive**	**Negative**	**Negative**	**Negative**	**$Is_{2-gr.B}$**
		I (kg/m^2·h)	**ε (%)**	**λ (kcal/m·h·°C)**	**μ (g/m^2·h)**	**M (g/m^2)**	
Group B/ Nomex	N1	0.000	0.533	0.778	0.847	0.962	0.611
	N2	0.729	0.610	1.000	1.000	1.000	**0.870**
	N3	0.424	0.857	0.444	0.518	0.923	0.624
	N4	0.186	1.000	0.667	0.600	0.795	0.630
	N5	0.475	0.124	0.000	0.000	0.000	**0.128**
	N6	1.000	0.000	0.333	0.424	0.051	0.386

Additionally, the utility of the negative characteristics, such as the thermal conductivity coefficient and fabric mass, has maximum values. Moreover, the vapour permeability coefficient has a value greater than 0.8, close to the upper limit, indicating a higher quality level.

- At Article K5 in Group A, characterized by Nm_{warp} = Nm_{weft} = 68/2 and P_{warp} = P_{weft} = 285 yarns/10 cm, plain weave, with floating F = 1, the lowest value of the synthetic indicator $Is_{2-gr.A}$ = 0.296 was obtained. This is justified by the fact that the utility of positive characteristics for relative elongation at break is at the minimum value, indicating a lower quality level. Additionally, the utility of negative characteristics, such as the thermal conductivity coefficient and vapour permeability coefficient, has minimum values. Moreover, the fabric mass has an average value, indicating a lower quality level.
- At Article N2 in Group B (Nomex), characterized by Nm_{warp} = Nm_{weft} = 60/2, P_{warp} = P_{weft} = 260 yarns/10 cm, diagonal $D\frac{2}{2}/$, with floating F = 2, the highest value of the synthetic indicator $Is_{2-gr.B}$ = 0.870 was obtained. This is justified by the fact that the utility of positive characteristics, such as the air permeability index and relative elongation at break, is close to the upper limit, indicating a higher quality level. Additionally, the utility of negative characteristics, such as the thermal conductivity coefficient, vapour permeability coefficient, and fabric mass, has maximum values, indicating a higher quality level.
- At Article N5 in Group B, characterized by Nm_{warp}= Nm_{weft} = 56/2, P_{warp} = P_{weft} = 355 yarns/10 cm, plain weave, with floating F = 1, the lowest value of the synthetic indicator $Is_{1-gr.A}$ = 0.128 was obtained. This is justified by the fact that the utility of positive characteristics, such as the air permeability index and relative elongation at break, is close to the lower limit, indicating a lower quality level. Additionally, the utility of negative characteristics, such as the thermal conductivity coefficient, vapour permeability coefficient, and fabric mass, has minimum values, indicating a lower quality level.
- Among the analysed characteristics, the team of experts considered that the air permeability index best reflects the comfort of the fabrics, assigning it the highest weight for assessing the quality level of fabric assortments needed for the production of firefighting equipment.

CONCLUSIONS

In conclusion, it is noted that the highest values for the synthetic durability indicators of fabrics, both in Group A (Kevlar) and Group B (Nomex), were obtained for fabrics with a plain weave structure,

$Is_{1-gr.A}$ = 0.889, Art. K5 and $Is_{1-gr.B}$ = 0.676, Art. N6, while the lowest values were obtained for fabrics with a diagonal $D\frac{2}{1}$/ structure, $Is_{1-gr.A}$ = 0.160, Art. K4 and $Is_{1-gr.B}$ = 0.254, Art. N3.

The highest values for the synthetic comfort indicators of fabrics, both in Group A (Kevlar) and Group B (Nomex), were obtained for fabrics with a Diagonal $D\frac{2}{1}$/ structure, $Is_{2-gr.A}$ = 0.939, Art. K1 and $Is_{2-gr.B}$ = 0.870, Art. N2 respectively, while the lowest values were obtained for fabrics with a plain weave structure, $Is_{2-gr.A}$ = 0.296, Art. K5 and $Is_{2-gr.B}$ = 0.128, Art. N5.

Fabrics with a Plain weave structure provide better stability of the yarns in the woven structure, regardless of the fibre composition. However, it should be noted that the raw materials used in the production of firefighting equipment must have special characteristics, which Kevlar and Nomex fibres fulfil, thus ensuring the performance of activities involving risk factors of thermal, chemical, biological, mechanical, physical, or electrical nature and have direct influences on the health and life of the individual performing a certain activity.

The values of the synthetic indicators determined based on durability and comfort functions can be used subsequently for modelling the physical-mechanical properties and for selecting the most suitable fabrics to meet the requirements of a particular field of use.

Articles in each group where the value of both the synthetic durability indicator and the synthetic comfort indicator is close to the maximum, indicating a superior quality level, can be considered reference elements. Therefore, articles, where the value of both the synthetic durability indicator and the synthetic comfort indicator is minimal, can have their quality improved by modifying structural parameters (such as fineness, technological density, and weave type), with the high-quality article from each group serving as a reference. This approach allows for finding optimal operating conditions in a short time and with reduced material costs compared to laboratory research.

The choice of raw material for making firefighter suits is a meticulous and rigorous process, considering that this equipment must provide maximum protection under extreme conditions.

By calculating the synthetic durability indicators for the fabrics from Group A (Kevlar), manufacturers can select plain weave fabrics, such as: Art. K5 ($Is_{1-gr.A}$ = 0.889) and Art. K6 ($Is_{1-gr.A}$ = 0.828), to be used in the outer layer of the protective jacket for firefighters, because through their structural characteristics (fineness, technological density, type of weave) and the values of durability assessment properties, they offer good resistance to cuts and abrasions, as well as thermal protection.

Diagonal $D\frac{2}{2}$/ weave fabrics, namely Art. K1 ($Is_{1-gr.A}$ = 0.553) and Art. K2 ($Is_{1-gr.A}$ = 0.428), can be used for the collar and cuff areas. These areas can be reinforced with Kevlar fabric to prevent fire penetration and provide additional protection against heat.

Additionally, $D\frac{2}{1}$/ weave fabrics, namely Art K3 ($Is_{1-gr.A}$ = 0.170) and Art. K4 ($Is_{1-gr.A}$ = 0.160), can be used for the shoulder and elbow areas as an additional layer of protection to provide better protection against impact and heat.

Based on the obtained values of the synthetic comfort indicators for the fabrics from Group A (Kevlar), manufacturers can select Diagonal $D\frac{2}{1}$/, weave fabrics, such as: Art K1 ($Is_{2-gr.A}$ = 0.939) and Art. K2 ($Is_{2-gr.A}$ = 0.561), to be used in the elbow and knee areas in the case of pants, as an additional layer of protection.

Diagonal $D\frac{2}{1}$/ weave fabrics, namely Art. K3 ($Is_{1-gr.A}$ = 0.694) and Art. K4 ($Is_{1-gr.A}$ = 0.586), can be used for the pocket area. This area can be reinforced with Kevlar fabric to prevent the penetration of fire and water, providing additional protection against heat and for the radio/phone.

Plain weave fabrics, namely Art. K5 ($Is_{1-gr.A}$ = 0.296) and Art. K6 ($Is_{1-gr.A}$ = 0.341), can be used for the shoulder and collar areas as an insulation layer to keep heat away and protect against extreme temperatures.

By calculating the synthetic durability indicators for the fabrics from Group B (Nomex), manufacturers can select plain weave fabrics, such as: Art. N6 ($Is_{1-gr.B}$ = 0.676) and Art. N5 ($Is_{1-gr.B}$ = 0.628), to be used in the outer layer of the jacket, providing a barrier against flames and intense heat.

Diagonal $D\frac{2}{2}$/ wave fabrics, namely Art. N1 ($Is_{1-gr.B}$ = 0.623) and Art. N2 ($Is_{1-gr.B}$ = 0.624), can be used for the protective hood, which covers the head, neck, and sometimes shoulders, often made of Nomex to protect these sensitive areas from exposure to fire and heat.

Diagonal $D\frac{2}{1}$/ wave fabrics, namely Art. N3 ($Is_{1-gr.B}$ = 0.254) and Art. N4 ($Is_{1-gr.B}$ = 0.323), can be used for the collar and cuff areas. These areas can be reinforced with Nomex fabric to prevent fire penetration and provide additional protection against heat.

Based on the obtained values of the synthetic comfort indicators for the fabrics from Group B (Nomex), manufacturers can select Diagonal $D\frac{2}{2}$/ weave fabrics, such as Art. N2 ($Is_{2-gr.B}$ = 0.870) and Art. N1 ($Is_{2-gr.B}$ = 0.611), to be used in the making of base clothing, worn under the main suit, which can be made from Nomex to provide additional protection at the skin level.

Diagonal $D\frac{2}{1}$/ weave fabrics, namely Art. N3 ($Is_{1-gr.B}$ = 0.624) and Art. N4 ($Is_{1-gr.B}$ = 0.630), can be used for making full suits to provide complete protection.

Plain weave fabrics, namely Art. N5 ($Is_{1-gr.B}$ = 0.128) and Art. N6 ($Is_{1-gr.B}$ = 0.386), can be used in the inner layers including lining to ensure additional protection and enhance the comfort of the firefighter.
Based on the obtained values of durability and comfort synthetic indicators, manufacturers ensure that the selected materials used in various areas of firefighter protective equipment meet the highest safety and performance standards, thereby protecting the lives of those on the front lines of firefighting efforts.

ACKNOWLEDGEMENTS

This work was supported by a grant from the Ministry of Research, Innovation and Digitization, UEFISCDI, project number PN-IV-P8-8.1-PRE-HE-ORG-2023-0039, within PNCDI IV.

REFERENCES

[1] Zhang, S.H., He, G.Q., Liang, G.Z., Cui, H., Zhang, W., Wang, B., *Comparison of f-12 aramid fiber with domestic armid fiber iii on surface feature*, In: Applied Surface Science, 2010, 256, 2104–2109

[2] Ertekin, M., Kırtay, E., *Burning behaviour and mechanical properties of fabrics woven with ring spun aramid and flame retardant polyester yarns*, In: Tekstil ve Konfeksiyon, 2014, 24, 3, 286–290

[3] Singh, T.J, Samanta, S., *Characterization of Kevlar Fiber and its Composites: A Review*, In: Mater. Today Process, 2015, 2, 4, 1381–1387

[4] Ozgen, B., *Physical properties of Kevlar and Nomex plied and covered yarns*, In: Textile Research Journal, 2013, 83, 7, 752–760

[5] Hristian, L., Bordeianu, D.L., Iurea, P., Sandu, I., Earar, K., *Study of the Tensile Properties of Materials Destined to Manufacture Protective Clothing for Firemen*, In: Journal of Plastics, 2014, 51, 4, 405–409

[6] Zhu, D., Mobasher, B., Rajan, S.D., *Experimental studyof dynamic behavior of Kevlar 49 single yarn*, In: Mech. Ser., 2011, 1, 147–152

[7] Huang, G., *Research on thermal properties of Nomex Viscose FR fiber blended fabric*, In: Mater Design, 2009, 30, 4324–4327

[8] Dulgheriu, I., Ionesi, S.D., Avadanei, M.L., Hristian, L., Loghin, E.C., Buhu, L., Ionescu, I., *ANCOVA analysis of penetration force on Kevlar fabrics used for ballistic protective equipment*, In: Industria Textila, 2022, 73, 1, 69–76, http://doi.org/10.35530/IT.073.01.202197

[9] Boorady, L.M., Barker, J., Lee, Y.A., Lin, S.H., Cho, E., Ashdon, S.P., *Exploration of firefighter turnout gear; Part 1-identifying male firefighter use needs*, In: J. of Textile and Apparel, Technol. and Management, 2013, 8, 1, 1–13

[10] Dong, Z., Sun, C.T., *Testing and modeling of yarn pull-out in plain woven Kevlar fabrics*, In: Composites Part A, 2009, 40, 1863–1869

[11] Yue, C.Y, Sui, G.X., Looi, H.C., *Effects of heat treatment on the mechanical properties of Kevlar-29 fibre,* In: Composites Science and Technology. 2000, 60, 3, 421–427

[12] Barker, R.L., Guerth-Schacher, C., Grimes, R.V., Hamouda, H., *Effects of moisture on the thermal protective performance of firefighter protective clothing in low-level radiant heat exposures*, In: Textile Research Journal, 2006, 76, 1, 27–31

[13] Lawson, L.K., Crown, E.M., Ackerman, M.Y., Douglas Dale, J., *Moisture effects in heat transfer through clothing systems for wildland firefighters*, In: Inter. J. of Occupational Safety and Ergonomics, 2004, 10, 3, 227–238

[14] DuPont, Nomex® and Kevlar® for Emergency Response, 2024

[15] Devanand, Uttam, R., *Thermophysiological clothing comfort*, In: Journal of Textile Engineering & Fashion Technology, 2021, 7, 3, 98–103

[16] Kirkwood, J.E., Kirkwood, E.M., Lee, Y.S., Egres, R.G., Wagner, N.J., Wetzel, E.D., *Yarn pull-out as a mechanism for dissipating ballistic impact energy in Kevlar KM-2 fabric Part II: Predicting ballistic performance*, In: Text. Res. J., 2004, 74, 11, 939–948

[17] Hristian, L., Ostafe, M.M., Dulgheriu, I., Buhu, L., Buhu, A., Negru, D., *Identification of influence factors on physical-mechanical properties, using the principal component analysis, in selecting the textile fabrics for the clothing products*, In: Industria Textila, 2020, 71, 5, 438–445, http://doi.org/10.35530/IT.071.05.1754

[18] Woo, S.C, Kim, T.W., Rate, H.S., *Impact in Kevlar-Woven Composites and Fracture Analysis Using Acoustic Emission*, In: Compos. Part B Eng., 2014, 60, 125–136

[19] Lee, Y.S., Wetzel, E.D., Wagner, N.J., *The Ballistic Impact Characteristics of Kevlar Woven Fabrics Impregnated with a Colloidal Shear Thickening Fluid*, In: J. Mater. Sci., 2003, 38, 2825–2833

[20] Zhu, D., Mobasher, B., Rajan, S.D., *High Strain Rate Testing of Kevlar 49 Fabric. Society for Experimental Mechanics*, In: 11th International Congress and Exhibition on Experimental and Applied Mechanics, 2008, 1, 34–35

[21] Hristian, L., Sandu, A.V., Manea, L.M., Tulbure, E.A., Earar, K., *Analysis of the Principal Components on the Durability and Comfort Indices of the Fabrics Made of Core-coating Filament Yarns*, In: J. Chem., 2015, 66, 3, 342–347

[22] Coca, A, Williams, W.J., Roberge, R.J., Powell, J.B., *Effects of fire fighter protective ensembles on mobility and performance*, In: Applied ergonomics, 2010, 41, 4, 636–641

[23] Dolez, P.I., Marsha, S., McQueen, R.H., *Fibers and Textiles for Personal Protective Equipment: Review of Recent Progress and Perspectives on Future Developments*, In: Textiles, 2022, 2, 349–381

[24] Arvinte, C., Hristian, L., Burduhos-Nergis, D.P., Bernevig, M.A., Toma, S.L., Sandu, I.G., Bejinariu, C., *Protection against mechanical risks provided by gloves used by firefighters in intervention actions*, In: Journal of Physics: Conference Series, 1960, 2021, 1, 012016

[25] Hristian, L., Ostafe, M.M., Manea, L.R., Apostol, L.L., *Study of Mechanical Properties of Wool Type Fabrics using ANCOVA Regression Model,* In: International Conference on Innovative Research (ICIR Euroinvent), Book Series: IOP Conference Se-ries-Materials Science and Engineering, 2017, 209, 012075

[26] Wang, M., Li, X.H., Li, J., Xu, B., *A new approach to quantify the thermal shrinkage of fire protective clothing after flash fire exposure*, In: Text. Res. J., 2015, 86, 580–592

[27] Houshyar, S., Padhye, R., Troynikov, O., Nayak, R., Ranjanet, S., *Evaluation and improvement of thermophysiological comfort properties of firefighters' protective clothing containing super absorbent materials*, In: Journal of the Textile Institute 2015, 106, 12, 1394–1402

[28] Manea, L.R., Hristian, L., Ene, D., Amariei, N., Popa, A., *Fundamental Aspects on Conductive Textiles Implemented in Intelligent System*, In: IOP Conference Series: Mat. Science and Engineering, 2009, 1, 012062

[29] Surdu, L., Radulescu, I.R., Ghituleasa, C., Subtirica, A., Mihai, C., Cioara, I., Ene, A., *Comfort properties of multilayer textile materials for clothing,* In: Industria Textila, 2013, 64, 2, 75–79

[30] Fu, M., Yuan, M.Q., Weng, WG., *Modeling of heat and moisture transfer within firefighter protective clothing with the moisture absorption of thermal radiation*, In: International Journal of Thermal Sciences, 2015, 96, 201–210

[31] Hristian, L., Dulgheriu, I., Negru, D., *Study of characterization indices of worsted wool fabrics using as a statistical tool correlation method*, In: Proceedings of the 7th International Symposium Technical Textiles-Present and Future, Sciendo, 2021, 37–44

[32] Hirschler, M.M., *Analysis of thermal performance of two fabrics intended for use as protective clothing*, In: Fire & Materials, 2015, 21, 3, 115–121

[33] Hristian, L., Ostafe, M.M., Bordeianu, D.L., Apostol, L.L., *The study of the characterization indices of fabrics by Principal Component Analysis method*, In: Journal Fascicle of Textiles, Leatherwork, 2017, XVIII, 1, 49–54

[34] Houshyar, S., Padhye, R., Nayak, R., *Effect of moisture-wicking materials on the physical and thermo-physiological comfort properties of firefighters' protective clothing,* In: Fibers and Polymers, 2017, 18, 2, 383–389

[35] Toma, D., Popescu, G., Popescu, A., Olaru, S., Salistean, A., Badea, I., *Protective clothing system for interventions in emergency situations*, In: Industria Textila, 2023, 74, 1, 121–129, http://doi.org/10.35530/IT.074.01.1839

[36] Gohar, E.S., Mazari, A.A., *Thermal performance of protective clothing (firefighter) under extreme ambient conditions*, In: Industria Textila, 2023, 74, 5, 542–546, http://doi.org/10.35530/IT.074.05.20237

[37] Weedall, P.J., Harwood, R.J., Shaw, N., *An assesment of the Kawabata Transformation equations for Primary-hand Values*, 1995, 86(3), Journal of Textile Institute

[38] Taloi, D., Bratu C., *Optimizarea proceselor metalurgice*,1983, Ed. Didactica si Pedagogica, Bucuresti

[39] Bona, M., *Statistical Methods for the Textile Industry*, 1993, Eurotex-Textilia

[40] Dulgheriu, I., Avadanei, M., Ionesi, S.-D., Ionescu, I., Loghin, E.-C., *Rationalisation methods for managing the production processes of textile products from the regulated field*, In: Industria Textila, 2022, 73, 6, 645–653, http://doi.org/10.35530/IT.073.06.2021108

Authors:

EMIL CONSTANTIN LOGHIN, IONUȚ DULGHERIU, LILIANA HRISTIAN, LILIANA BUHU, MANUELA AVĂDANEI, SAVIN DORIN IONESI

"Gheorghe Asachi" Technical University of Iasi, Faculty of Industrial Design and Business Management, 29 D. Mangeron, 70050, Iasi, Romania

Corresponding author:

SAVIN DORIN IONESI
e-mail: savin-dorin.ionesi@academic.tuiasi.ro

materials

MDPI

Article

FEM Analysis of Textile Reinforced Composite Materials Impact Behavior

Savin Dorin Ionesi [1,*], Luminita Ciobanu [1,*], Catalin Dumitras [2], Manuela Avadanei [1], Ionut Dulgheriu [1], Irina Ionescu [1] and Maria Carmen Loghin [1,*]

[1] Faculty of Industrial Design and Business Management, "Gheorghe Asachi" Technical University of Iasi, Blvd. Mangeron, No. 29, 700050 Iasi, Romania; mavad@tuiasi.ro (M.A.); idulgheriu@tuiasi.ro (I.D.); iirina@tuiasi.ro (I.I.)

[2] Faculty of Machine Manufacturing and Industrial Management, "Gheorghe Asachi" Technical University of Iasi, Blvd. Mangeron, No. 59, 700050 Iasi, Romania; dumitrascata@yahoo.com

* Correspondence: dionesi@tuiasi.ro (S.D.I.); luminita.ciobanu@tuiasi.ro (L.C.); cloghin@tuiasi.ro (M.C.L.)

Abstract: Composite materials reinforced with textile fabrics represent a complex subject. When explaining these materials, one must consider their mechanical behavior in general, and impact resistance in particular, as many applications are characterized by dynamic strains. Impact characteristics must be considered from the early stages of the design process in order to be controlled through structure, layer deposition and direction. Reinforcement materials are essential for the quality and behavior of composites, and textile reinforcements present a large range of advantages. It takes a good understanding of the requirements specific to an application to accurately design textile reinforcements. Currently, simulations of textile reinforcements and composites are efficient tools to forecast their behavior during both processing and use. The paper presents the steps that must be followed for modelling the impact behavior of composite materials, using finite element analysis (FEM). The FEM model built using Deform 3D software offers information concerning the behavior structure during impact. The behavior can be visualized for the structure as a whole and, for different sections, be considered significant. Furthermore, the structure's strain can be visualized at any moment. In real impact tests, this is not possible due to the very short time interval and the impossibility to record inside the structure, as well as to record all significant stages using conventional means.

Keywords: FEM; impact behavior; composite materials; knitted fabrics

Citation: Ionesi, S.D.; Ciobanu, L.; Dumitras, C.; Avadanei, M.; Dulgheriu, I.; Ionescu, I.; Loghin, M.C. FEM Analysis of Textile Reinforced Composite Materials Impact Behavior. *Materials* **2021**, *14*, 7380. https://doi.org/10.3390/ma14237380

Academic Editor: Abbas S. Milani

Received: 5 November 2021
Accepted: 28 November 2021
Published: 2 December 2021

1. Introduction

Mechanical properties of textile reinforced composites are essential in applications characterized by a high level of strains, and predicting their behavior during use is a determinant for the design stage and ensures its quality. The complexity of textile structures and geometries, their anisotropy and discontinuous nature make the process of modelling mechanical behavior extremely difficult.

In terms of prediction, applied mathematics is used to define boundary conditions in solving continuum mechanics. The scientific literature contains studies of applied physics aimed at solving similar problems, but is directed to obtain continuous functions based on approximated areas. Aerospace engineering researches focus on finding optimal ways of expressing the influence of the rigidity coefficients. All these results can be summed up in three distinct approaches and solutions, each expressing a different view on the same issue, namely modelling the behavior of composite materials.

The term finite element method (FEM) defines a broad range of computing techniques that have certain common characteristics. Currently the main drawbacks related to application difficulties have been removed with the widespread use of computers and the development of a large range of analytic software such as ANSYS, Algor or Deform 3D.

In the textile domain, modelling using the finite element method has experienced an accelerated growth in the last decade, most models predicting the mechanical behavior of composite materials with woven reinforcement [1–5].

Even if they have a lower mechanical resistance, knitted fabrics are widely used for composite reinforcement. The complexity of their specific geometry and the large number of structural possibilities, as well as the direct influence of the mechanical strains introduced during knitting at yarn level, led to the formulation of different geometrical and mechanical models for knitted fabrics, each one based on different assumptions and production conditions, and considered the micro, meso or macro level of the fabrics. Mechanical models of knitted fabrics can be divided into models based on force analysis, models based on energy minimization, and FEM models [6].

The situation is even more complicated in the case of knitted fabrics built along all the three axes, the so-called 3D knitted fabrics, as it is not only the fabric structure that has to be modelled, but also the 3D geometry of that fabric and its particularities in connection between stitches.

This is the case of weft/warp knitted spacer fabrics, materials characterized by the presence of (at least) two independent layers connected by yarns or by knitted layers [7,8]. Connection through yarns limits the spatial geometry of the 3D fabrics but is widely used in technical applications, especially as warp knitted fabrics. A large range of possibilities is offered by the flexibility of weft knitted spacers with connections through knitted layers [9–12]. Such possibilities are beneficial for developing preforms for composite materials with the final shape of the product.

In the literature, there are fewer FEM models for the mechanical behavior of knitted fabrics mainly due to the complexity of the yarn geometry in the stitches and the high number of factors influencing their properties.

All FEM models are based on geometrical models developed for knitted fabrics in general, there is an exhaustive review being carried out in this [13], or for knitted fabrics for composite reinforcement, considering the particularities of high-performance fibers [14–16]. These models concern mainly 2D knitted fabrics. Still, a literature survey shows a limited number of models dealing with the mechanical behavior of warp knitted spacers exemplified by [17–19], as well as weft knitted spacers [20,21]. The model proposed by Hamedi [21], simulates the flexural behavior of weft knitted spacer fabrics with a constant width (connected through knitted layers), considering the geometrical specificities proposed by Vassiliadis [22].

The paper presents a different approach for the modelling of mechanical behavior of composite materials reinforced with weft knitted spacer fabrics, by replacing the composite with an equivalent continuous material, with similar mechanical characteristics. The advantage of such an equivalence is given by the elimination of the numerical models for the knitted structure with all their restrictions and limitations. Furthermore, an equivalent continuous material can be placed easily to form the required specific geometry. This is an innovative approach to modelling composites reinforced with knitted fabrics that simplifies the behavior simulation. The approach requires careful consideration in determining the characteristics of the equivalent continuous material to correspond to the properties of real composite.

The equivalent model proposed in the paper deals with low velocity impact behavior of a composite material reinforced with knitted spacers of predetermined geometry (distance between connecting layers and distance between independent layers). The proposed model is described and used to predict impact behavior. Validation is carried out based on experimental results to see the level of conformity the model presents.

2. Materials and Methods

The knitted reinforcement selected for this study is a sandwich fabric where the independent outer layers (plain jersey) are connected through knitted layers placed perpendicularly to them. The distance between the connecting layers is 10 mm. The samples were

designed without or with inlay yarns in the exterior layers (yarns placed horizontally in the fabric, without looping it into stitches). Inlay yarns are an efficient way to enhance fabric strength. Figure 1 presents the production of the textile reinforced composite, starting with the knitting of the reinforcement.

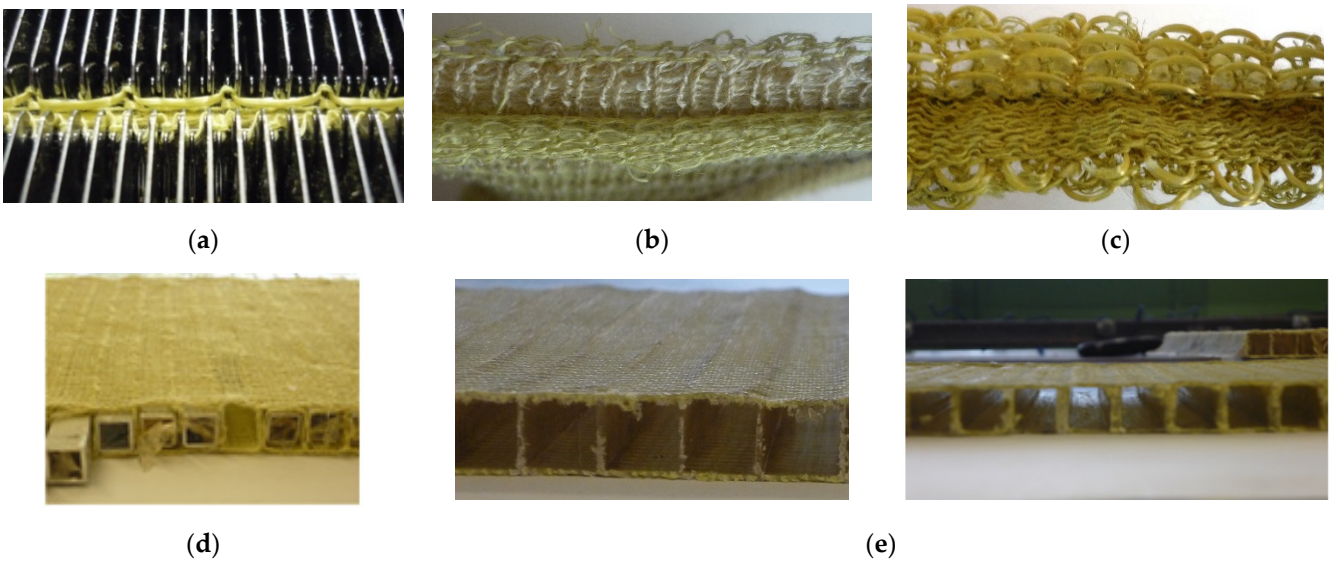

(**a**) (**b**) (**c**)

(**d**) (**e**)

Figure 1. Composite reinforced with sandwich knitted fabrics—machine view (**a**), aspect of the outer layers with (**b**) and without in-lay yarns (**c**), preparation of the knitted reinforcement–insertion of moulds (**d**) and final aspect of the knitted spacer reinforced composite (**e**).

The 3D knitted fabric variants were produced on a STOLL CMS 320 TC flat knitting machine, Reutlingen, Germany, gauge 10E. The fabrics were made of para-aramid (Steel Kevlar and Twaron, DuPont, Wilmington, DE, USA) and technical natural yarns (Linen). The use of natural fibers was designed so as not to affect the performance of the spacer fabrics, and target an increase in sustainability. Different raw materials were used to produce the outer and connecting layers, as presented in Table 1. The volume fraction of the composite samples required to increase fabric compactness was obtained by introducing transversal Twaron yarns.

Table 1. Characterisation of the experimental variants (weft knitted spacer fabrics).

Fabric	Outer Layers			Connecting Layer		
	Yarn Type	Layer Structure	Yarn Linear Density (Tex)	Yarn Type	Layer Structure	Yarn Linear Density (Tex)
1	Kevlar 49®	Plain jersey	28	Kevlar 49®	Plain jersey	28
2	Kevlar 49®	Plain jersey	28	Linen	Plain jersey	20
3	Kevlar 49®	Plain jersey	28	Kevlar 49®	Plain jersey	28
	Twaron®	Plain jersey with inlay	6			
4	Kevlar 49®	Plain jersey	2	Linen®	Plain jersey	20
	Twaron®	Plain jersey with inlay	6			

The 3D composite materials studied in this paper were produced using the 4 variants of the spacer fabrics presented in Table 1 as performs, and epoxy EPICURE 04908, Hexion, Columbus, OH, USA, and polyester DISTITRON 3501S, Polynt, Bergamo, Italy, as matrices,

resulting in two sets of composites. The epoxy matrix had a mixing ratio of 30% EPIKURE Curing Agent 04908 and 5% Dearing agent BYK A535, while for the polyester resin the mixing contained 1.5% of initiator for unsaturated polyester resin NOROX MCP 75 and 0.08% polyester inhibitor NLC 10. The composite materials were processed using the Vacuum Assisted Resin Transfer Molding (VARTM) technology. All experimental samples were cured at room temperature (23 °C), the ones with epoxy matrix for 46 h and the ones with polyester for 23 h.

The modelling of the behavior to low intensity impact of the composite materials has to be based on the physical-mechanical properties of the reinforcement and matrix used for composite materials. The experimental values obtained for these properties are shown in Table 2.

Table 2. Physical mechanical characteristics of composite materials.

	Structure Variant				**Polymeric Matrix**	
	Kevlar–Twaron		**Kevlar–Linen**		**Epoxy Resin**	**Polyester Resin**
	Row	**Wale**	**Row**	**Wale**		
Young module [N/mm^2]	6376	30,411	6161	5513	2900	4000
Force [N]	2430.59		745.18		-	-
Thread weight [g]	6.4		3.7		-	-
Composite sample weight [g]	19.3		14		-	-
Dimension of the impactor head [mm]	20					

3. Definition of the Model

The general geometry of the composite material to be analyzed using FEM is defined in Figure 2a, where the exterior walls and connecting layers form the repetitive element, the partition.

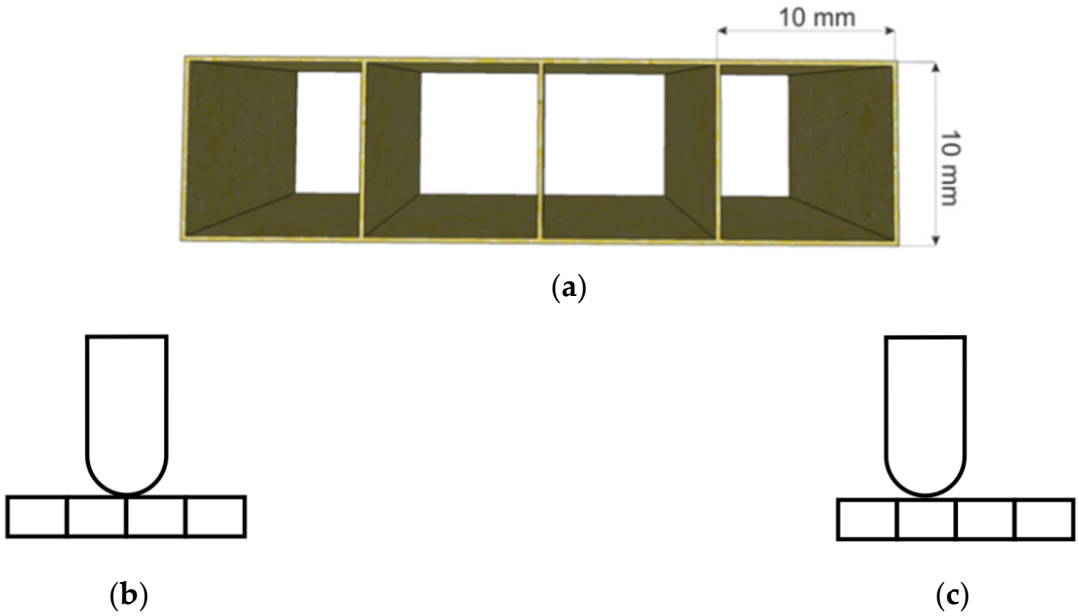

Figure 2. *Cont.*

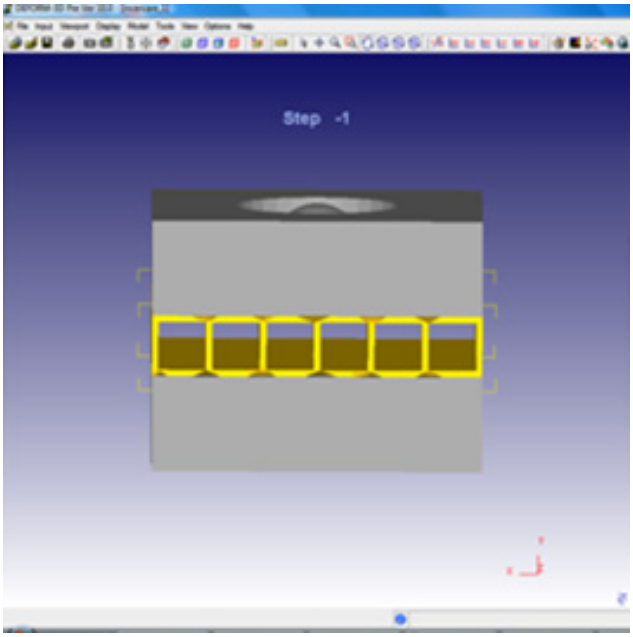

(**d**)

Figure 2. Model design. (**a**) Geometrical model for the equivalent continuous material. (**b**) Impactor position on connection layer. (**c**) Impactor position between connection layers. (**d**) Aspect of processed model.

Taking into consideration the fact that a composite material is an advanced structure made from at least two distinct materials that are combined at a macroscopic scale with different mechanical properties, a composite structure with equivalent mechanical properties was considered.

Due to the specific 3D geometry of the composite, the equivalent continuous model presents open areas with predefined dimensions, and, therefore, it is important to select the position of the impactor used for low velocity impact test simulations in relation to the connecting walls, as illustrated in Figure 2. We estimated that two positions are of consequence: one illustrated in Figure 2b shows that the impactor is placed on the connecting layers, while in Figure 2c the impactor is placed between connecting layers. These two positions exemplify the possibilities of impact during composite's life cycle.

The model was designed in a DEFORM 3D software, DEFORM, Columbus, OH, USA, application and was meshed with "brick" or "tetrahedral" elements [23], as illustrated in Figure 2d. The mesh size was adjusted from fine to coarse and the number of finite elements was established at 180,000/volume.

The main steps to be taken in order to perform a finite element analysis can be grouped into a number of operations, as follows:

- Division into finite elements (discretization);
- Defining interpolation functions;
- Defining the equations of finite elements;
- Assembling elementary equations into system equations;
- Solving the obtained system of equations;
- Performing additional calculations if necessary to determine secondary unknowns.

For model calibration an initial testing was carried out on similar composite materials. A Fractovis Plus impact testing machine, Instron, Norwood, MA, USA, equipped with a round head impactor and pneumatic clamping system was used to carry out the tests.

All physical pieces involved in the impact testing were modelled. The impactor position on connection layer is presented in Figure 3a, while impactor position between connection layers is presented in Figure 3b. The model of impactor head and structure of

clamping plates is presented in Figure 4. The loading force and the processing speed were experimentally determined based on the captured data using the Fractovis Plus impact testing machine, illustrated in Table 3.

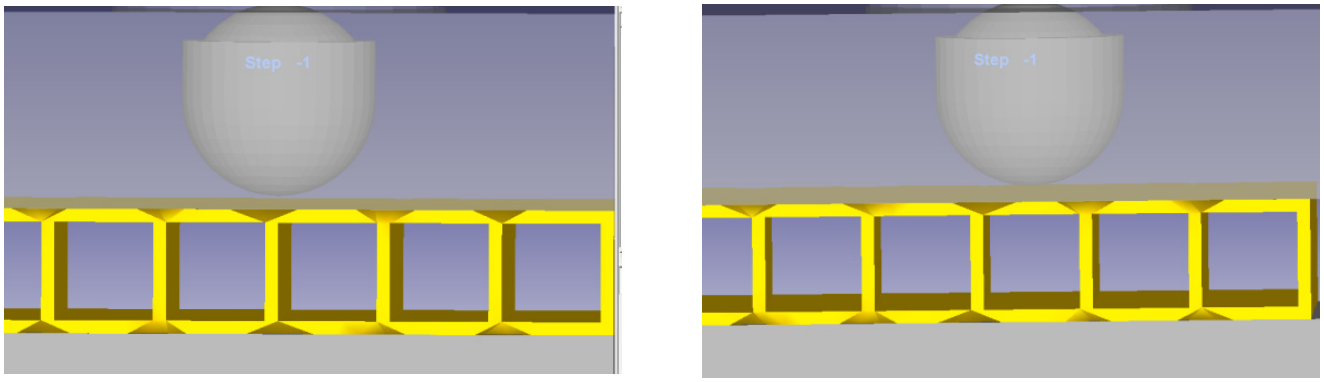

(**a**) (**b**)

Figure 3. Model of impactor head and composite structure. (**a**) On connection layer. (**b**) Between connection layers.

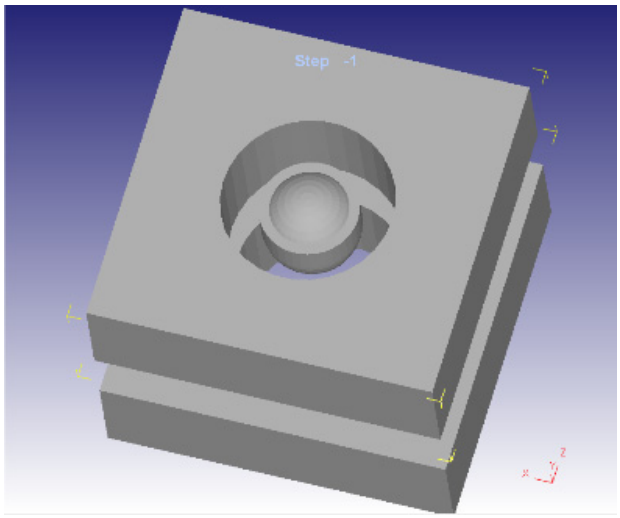

Figure 4. Mode of impactor head and structure of clamping plates.

Table 3. Working parameters.

Parameter	Value	Parameter	Value
Impact Energy [J]	37.095	Carriage Mass [kg]	4.3
Impact Velocity [m/s]	3.835	Applied Mass [kg]	0
Impact Height [mm]	750	Total mass [kg]	5.045
Impact Point Offset [mm]	0.000	Support Type	-
Extension Length [mm]	0.000	Support Diameter [mm]	20
Extension Mass [kg]	0.000		

4. Results and Discussions

4.1. Simulation of the Deformation Process

The deformation of the model was processed using DEFORM 3D. The simulation results in different steps of the action of the impactor on the 3D composite material is illustrated in Figure 5a–d.

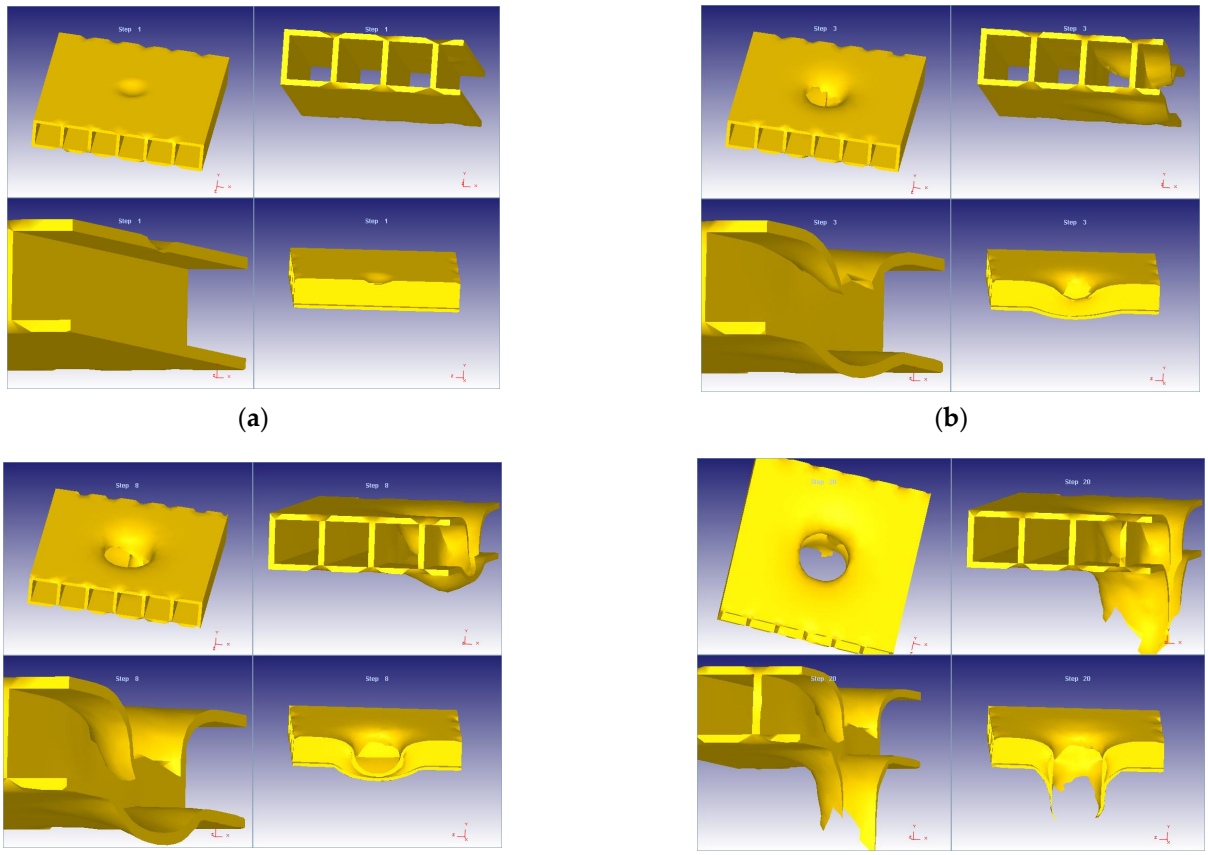

Figure 5. Impactor action. (**a**) Step 1. (**b**) Step 3. (**c**) Step 8. (**d**) Step 20.

It should be noted that in the previous figures not all the elements participating in the process appear the way the impactor head acts, being presented in Figure 6.

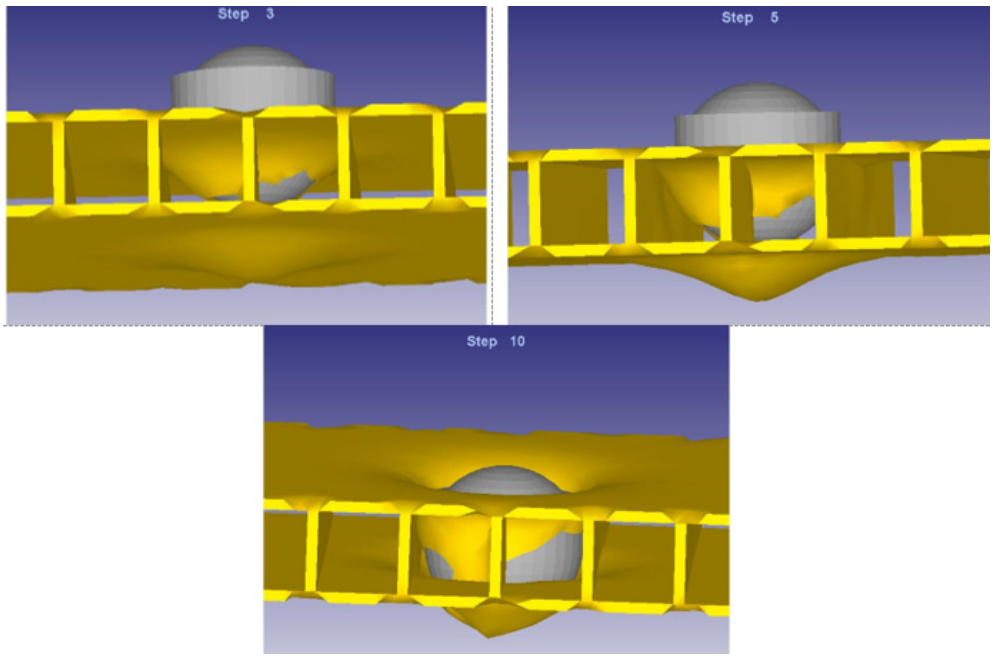

Figure 6. Impactor head action.

The simulation results were compared with those obtained after performing a real experiment, as illustrated in Figure 7.

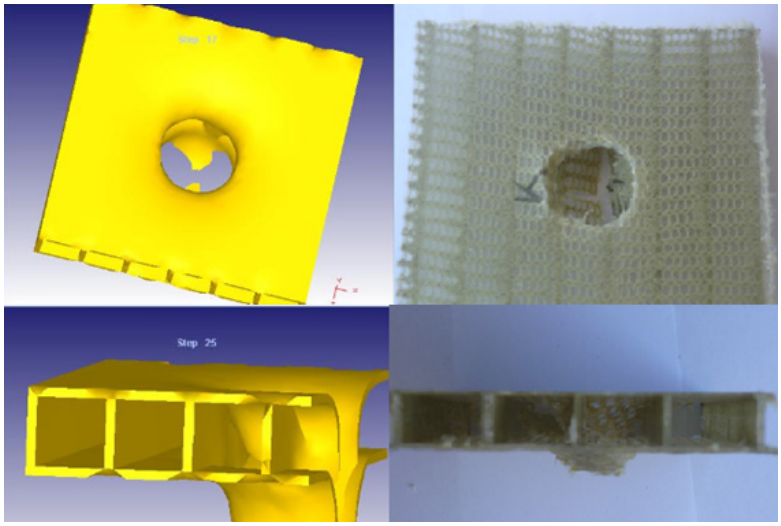

Figure 7. Comparison of the breaking area for the simulated model and impacted samples.

The program provides information on the time frames for each deformation snapshot, and about the characteristics of the process in that moment (work speed, force deformation, the value of the impactor stroke, etc.), as illustrated in Table 4.

Table 4. Extracted information obtained from finite element analysis.

Step No.	Mesh No.	Stroke	Time (s)	Load X (DaN)	Load Y (DaN)	Load Z (DaN)	Speed X (mm/s)	Speed Y (mm/s)	Speed Z (mm/s)	Volume (mm^3)
−1	1	0	0	–	–	–	0	0	0	61,478.8
5	1	0.892857	0.00357142857143	4.7649	1272.9	2.4996	0	250	0	62,600.4
10	1	1.78571	0.00714285714286	0.851317	1296.5	5.0737	0	250	0	62,600.5
15	1	2.67857	0.0107142857143	2.3586	1362.9	5.6681	0	250	0	62,600.5
20	1	3.57143	0.0142857142857	1.4461	1449.8	1.5543	0	250	0	62,600.5
25	1	4.46429	0.0178571428571	2.2943	1522.6	10.955	0	250	0	62,600.5
30	1	5.35714	0.0214285714286	101.61	1604.9	103.43	0	250	0	62,600.5
35	1	6.25	0.025	2.7895	1638	25.168	0	250	0	62,600.5
40	1	7.14286	0.0285714285714	124.62	1706.6	49.233	0	250	0	62,600.5
45	1	8.03571	0.031428571429	132.49	1830.6	47.951	0	250	0	62,600.5
50	1	8.92857	0.0357142857143	160.64	1565.8	20.883	0	250	0	62,600.5
55	1	9.82143	0.0392857142857	9.905	1932.3	4.7249	0	250	0	62,600.5
60	1	10.7143	0.0428571428571	181.59	2004.4	16.246	0	250	0	62,600.5
65	1	11.6071	0.0464285714286	149.33	2032.4	2.2658	0	250	0	62,600.5
70	1	12.5	0.05	140.42	2091.5	14.438	0	250	0	62,600.4

Figure 8 present the variation on the three axes of the displacement field on the composite structure following the impact.

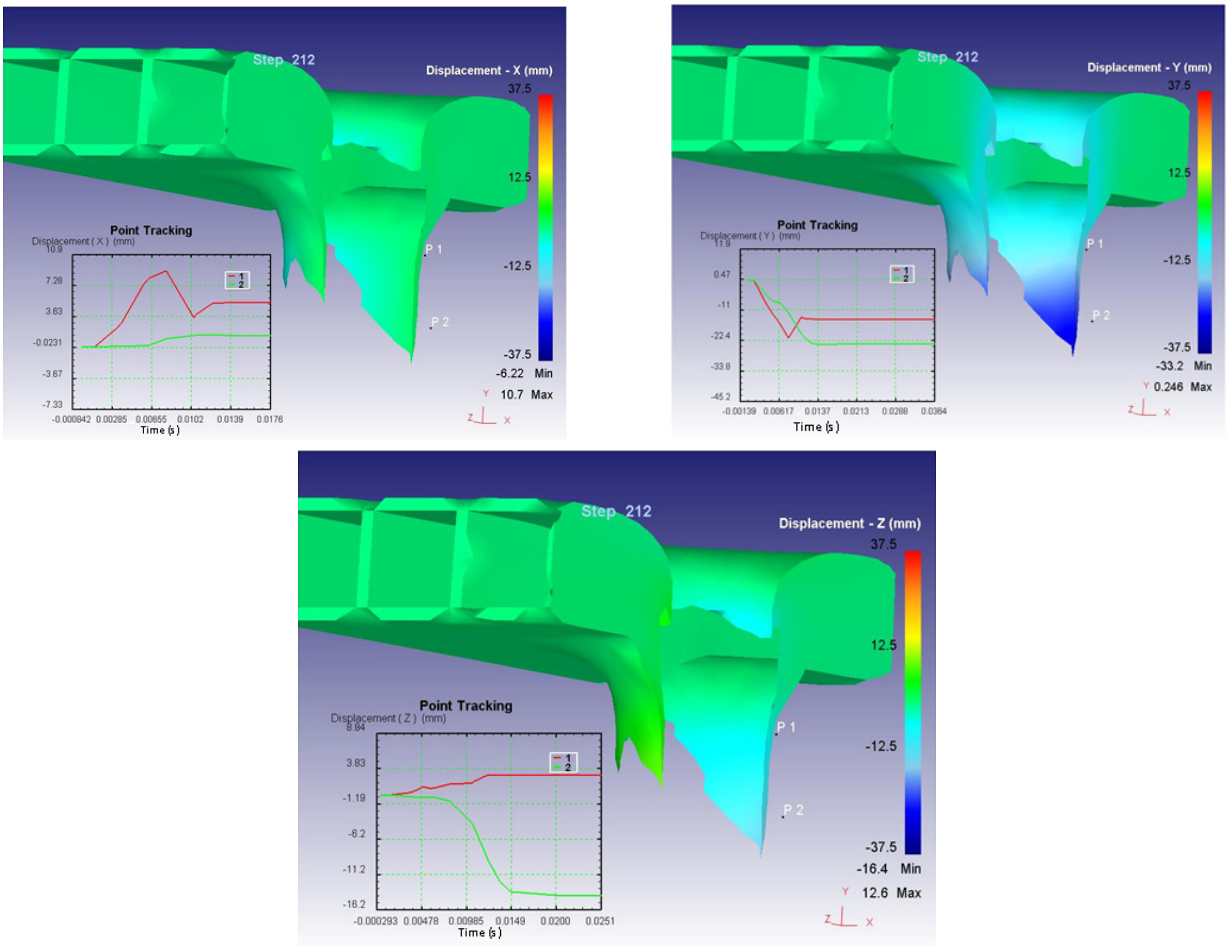

Figure 8. Variation on the 3 axes of the displacement field.

The curves in the graphs, illustrated in Figure 8, represent the evolution of the displacements in the direction of the specified axes in two points, considered P1 and P2, arranged on the surfaces (point 1 is arranged on the upper surface and point 2 on the lower surface). On the right side is the color legend of the displacements expressed in mm.

Figure 9 presents the variation on the three axes of the strain forces on the composite structure following the impact.

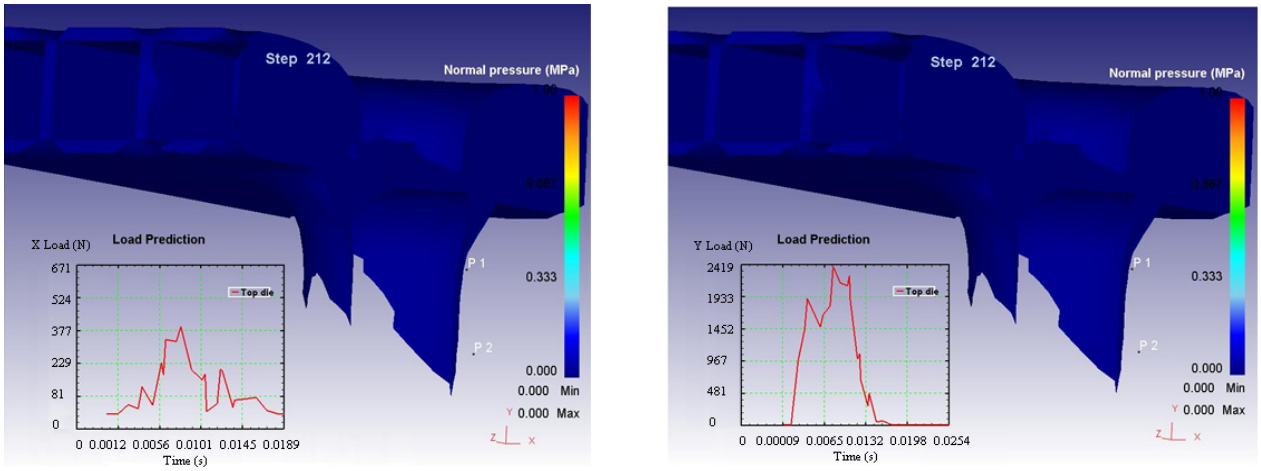

Figure 9. *Cont.*

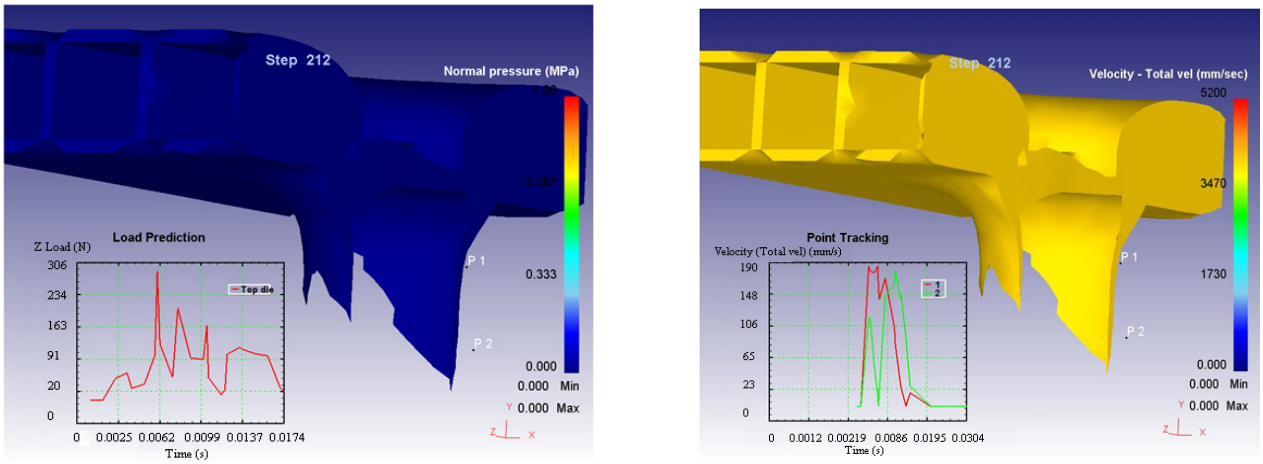

Figure 9. Variation on the 3 axes of the strain force and velocity.

Finite element modelling and analysis is particularly important in the context of the research conducted because it provides an impressive amount of information regarding the studied process, namely the impact stress of the composite structure reinforced with textile yarns. However, this information may be of no value if it is not continued and verified with one or more experimental tests performed under conditions similar to those in which the analysis was performed. These experiments will validate the finite element analysis, and once it has validated several values (e.g., the level of forces in the system, working speeds, process dynamics, etc.), it is assumed that all values, and implicitly the simulations, have been validated.

4.2. Validation—Experimental Results

The results from the simulation were compared to the results obtained for the composite materials reinforced with spacer weft knitted U-shaped structures defined in Table 1.

Considering the results of the experimental low velocity impact tests for the samples of composite materials defined in Table 1, it can be stated that the simulation with finite elements was confirmed because the level of forces in the system (shown in the figures above) at the simulation level corresponds as an order of magnitude, size, and approaches as a value, the level experimentally determined. Thus, it is observed that we have as an order of magnitude values of thousands of N (more precisely between 1200 and 2480 N, as illustrated in Figures 10 and 11) for the force measured at an experimental level, and variations from 1276 N to 2781 N in the case of the simulation performed.

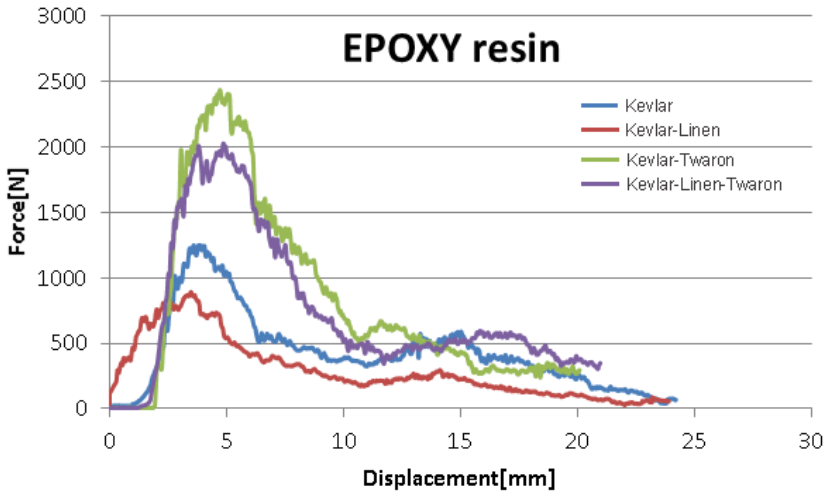

Figure 10. Force displacement curves—EPOXY resin.

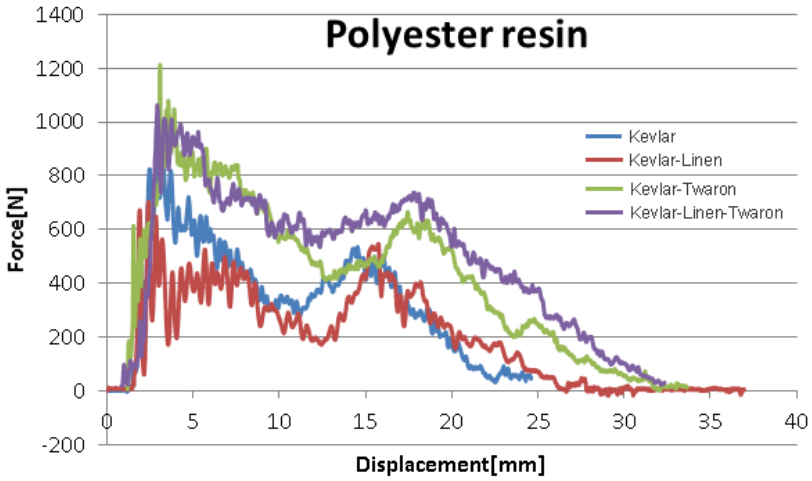

Figure 11. Force displacement curves—Polyester resin.

Furthermore, the experimental results show that the maximum level of displacement is placed between 10 and 36.56 mm, depending on the structure and the material used. In the case of the simulation, the values for virtual displacement vary between 27 and 37 mm.

It is observed that the intervals of variation of the forces in the system, and of the displacements obtained experimentally and virtually are significantly close in order of magnitude, and values which lead to the conclusion that the way the data were introduced and the conditions imposed to obtain process simulation are correct. Existing differences can be attributed to the characteristics imposed to the equivalent continuous material used for the simulation, and these characteristics can be corrected in order to improve the accuracy of the simulation.

Based on this, it can be stated that the simulation performed is confirmed by the experimental results.

4.3. Comparative Analysis

The information provided by the simulation is more detailed than the experiment itself. This information can be broken down into several areas.

A first information refers to the behavior of the structure during the impact stress. This behavior can be viewed on the simulated structure in its entirety and, in different sections, be considered relevant. Moreover, it can be seen how the structure is deformed at different moments. This is not possible in reality because the time interval in which the process takes place is very short, while the means of recording the image do not allow access inside the structure. Furthermore, the short time in which the process takes place leads to the impossibility of recording all the important phases by classical means.

From the deformation of the composite structure, two cases can be identified in which the process takes place, depending on the position between the impactor head and the composite structure:

- Case 1 results from the position of the axis of symmetry of the impactor head in relation to the partition. In this situation the impactor head passes through the partition wall (defined in Figure 2b).
- Case 2, the axis of symmetry of the impactor head passes between the partitions (defined in Figure 2c).

The deformations of the structure in the two considered cases are illustrated in Figure 12.

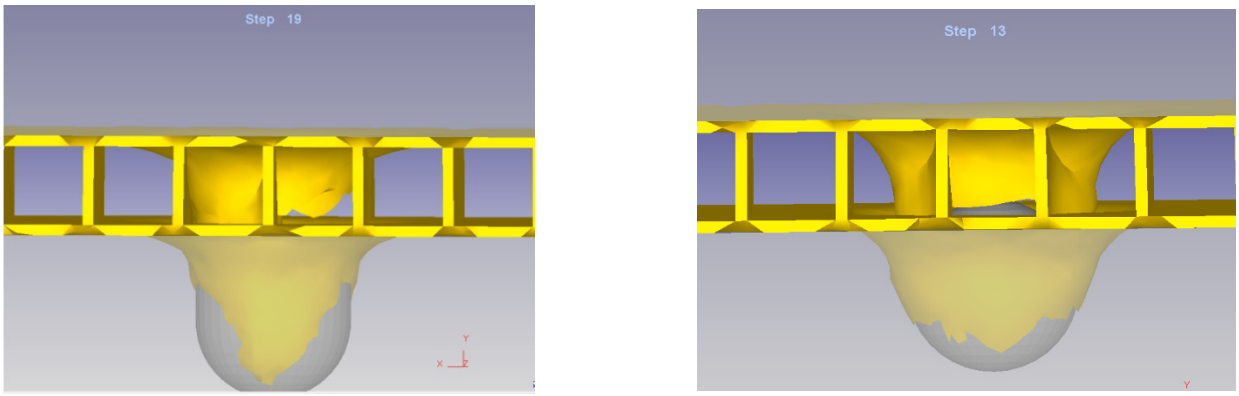

Figure 12. Deformations of the structure in the two considered cases.

It can be remarked that the penetration time in the second case is shorter and also the deformations are different in size. This phenomenon leads to the idea that the level of forces of the unitary efforts are different in the two situations.

In addition to data on the deformed structure (which can be presented as a "record" of the event), the simulation provides very important information on the field of displacement, deformation, unit effort, as well as the deformation forces in the system at any given time during the process presented in the form of a diagram. This phenomenon has been explicitly presented previously.

Figure 13 presents the stress-effective efforts for both considered cases.

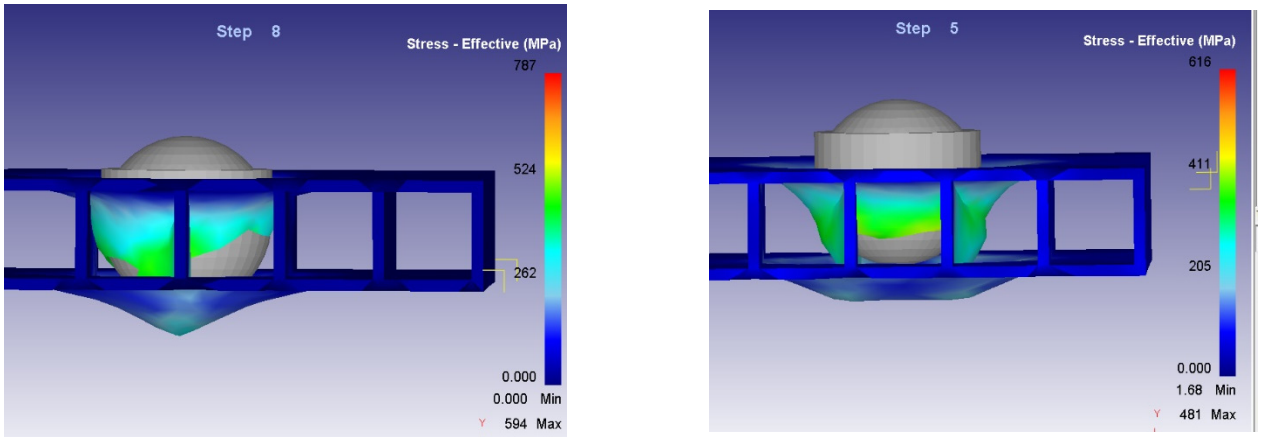

Figure 13. Stress-effective efforts of the structure in the two considered cases.

Contrary to expectations, it is observed that the level of stress-effective effort in Case 2 is lower than in Case 1. It was assumed that in the second case, due to the fact that there were two vertical walls on the direction of action, which offered a higher rigidity and resistance, the level of effort would be higher. However, this can be explained by the hemispherical shape of the impactor head. In Case 1, the first point of contact is made in the direction of the partition wall which, during the whole process, is subjected to deformation, generating great efforts. In the second case, the walls are on the sides of the impactor head. Initially, the impactor head acts on the horizontal flat surface, which has a low resistance. Subsequently, after the contact between the partition walls has been cancelled, the punch will act on the partition walls.

Based on these considerations, it can be concluded that the arrangement of the composite structure in relation to the impactor head has an influence on: the process times (a shorter time in Case 2); the forces in the system (Case 2 requiring high values for the Y axis direction, perpendicular to the structure, but much higher in the other two directions

which leads to a lower resultant force); and the variation of the deformation speed on the three axes for the two cases (presented in Figures 14–16).

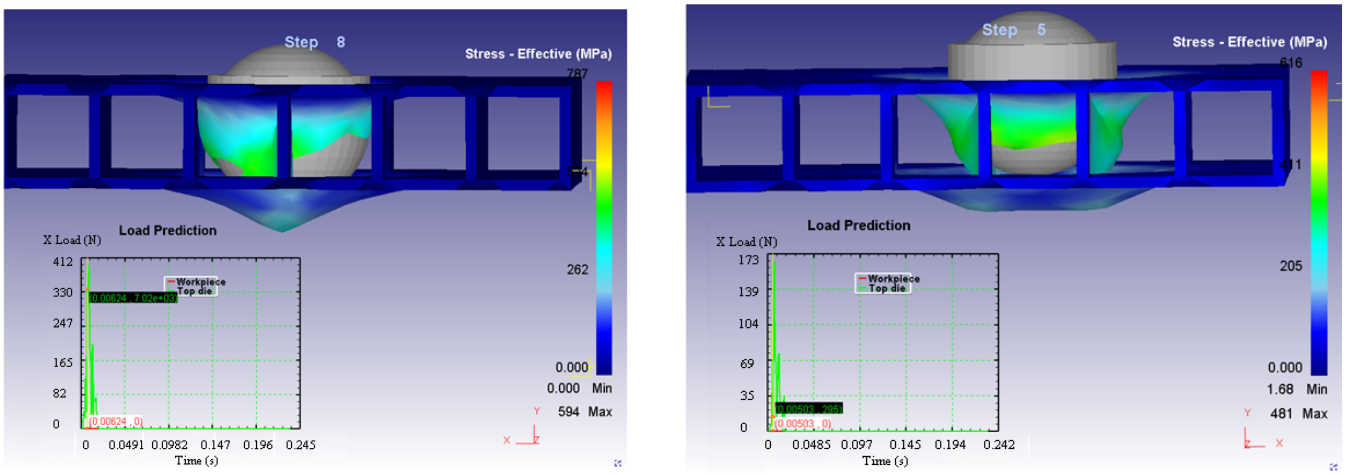

Figure 14. Stress-effective efforts—X axes in the two considered cases.

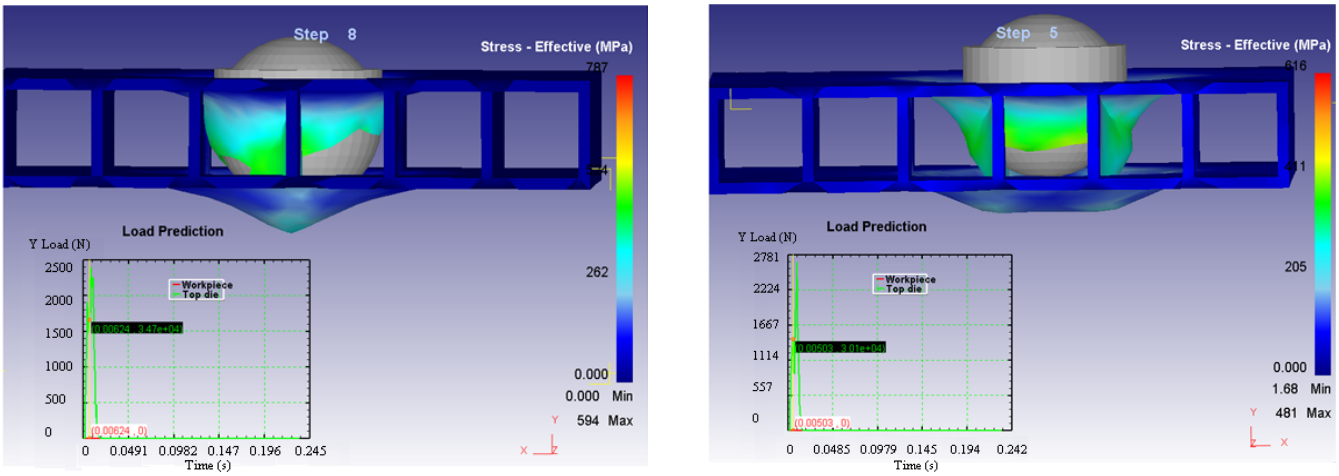

Figure 15. Stress-effective efforts—Y axes in the two considered cases.

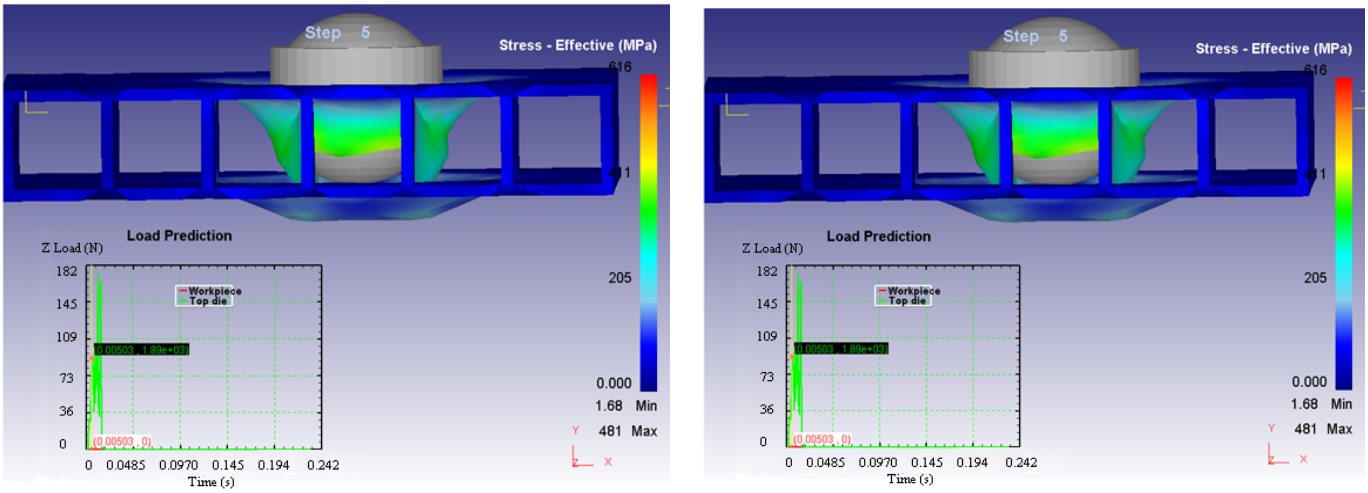

Figure 16. Stress-effective efforts—Z axes in the two considered cases.

Another variable that is influenced by the relative position between the impactor head and the composite structure is the size of the displacements of the structure, illustrated in Figure 17.

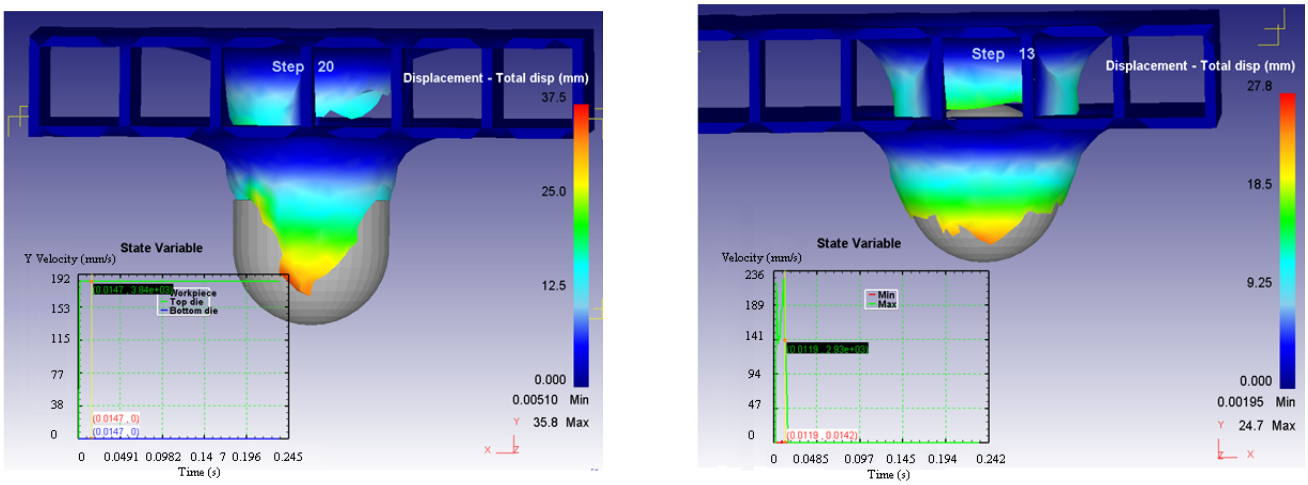

Figure 17. Displacement variation in the two considered cases.

5. Conclusions

Modelling and finite element analysis are particularly important in the present research context, providing an impressive amount of information regarding the impact behavior of polymeric composites reinforced with knitted 3D sandwich fabrics. However, this information has no value if not validated by one or more experimental tests carried out in similar conditions to those under which the analysis was performed.

An FEM model was proposed in the paper, in which the ensemble knitted reinforcement and matrix is considered a continuous material with specific properties. This equivalent material was used to build the model and to simulate low velocity impact behavior.

This is a different approach than models presented in the literature as it eliminates the complex and restrictive geometrical models of the knitted structures, especially difficult and time consuming for 3D geometries and the specific connections between layers. The model was developed using Deform 3D software, calibrated using the data from an initial test carried out for all experimental variants.

The FEM model offered important information concerning the behavior structure during impact, showing how the material reacts with the impactor, how it breaks and to which level of stress. The simulation takes into consideration both situations in which the composite can be impacted during use: the impact can occur perpendicular to a connecting wall or between two connecting walls.

The behavior can be visualized for the structure as a whole and, for different sections, be considered significant. Furthermore, the structure's strain can be visualized at any moment. This is not possible for the tests used for validation due to the very short time interval, and the impossibility to record inside the structure, as well as to record all significant stages using conventional means.

Apart from the information regarding the material deformation (that can be presented as a 'movie' about this event), important data are gained concerning the displacement/strain/stress/effort, as well as the deformation forces for single moments during the impact and a diagram of their evolution throughout the entire phenomenon.

Author Contributions: Conceptualization, S.D.I., L.C., C.D. and M.C.L.; methodology and software, C.D., M.A., I.I. and I.D.; performed the experiments S.D.I., L.C. and I.D.; validation, M.A., I.I. and L.C.; formal analysis, S.D.I. and L.C.; investigation, C.D., I.D., M.C.L. and I.I.; resources, M.C.L. and L.C.; data curation, M.C.L. and S.D.I.; writing—original draft preparation, S.D.I., M.A. and I.I.;

writing—review and editing, L.C., I.D., M.C.L. and C.D.; funding acquisition, M.C.L. and S.D.I. All authors have read and agreed to the published version of the manuscript.

Funding: This work is funded by TUIASI Internal Grants Program (GI_P17/2021) financed by the Romanian Government.

Institutional Review Board Statement: Not applicable.

Informed Consent Statement: Not applicable.

Data Availability Statement: Not applicable.

Conflicts of Interest: The authors declare no conflict of interest.

References

1. Lomov, S.; Ivanov, D.; Verpoest, I.; Zako, M.; Kurashiki, T.; Nakai, H.; Hirosawa, S. Meso-FE modelling of textile composites: Road map, data flow and algorithms. *Compos. Sci. Technol.* **2007**, *67*, 1870–1891. [CrossRef]
2. D'Amato, E. Finite element modeling of textile compozites. *Compos. Struct.* **2001**, *54*, 467–475. [CrossRef]
3. Nilakantan, G.; Keefe, M.; Bogetti, T.; Adkinson, R.; Gillespie, J. On the finite element analysis of woven fabric impact using multiscale modeling techniques. *Int. J. Solids Struct.* **2010**, *47*, 2300–2315. [CrossRef]
4. Nawafleh, M.A.; Al-Kloub, N. Plane deformation of a textile material with boundary forces using finite element method. *Jordan J. Mech. Ind. Eng.* **2009**, *3*, 222–227.
5. Zhou, Y.; Sun, Y.; Huang, T. Bird-Strike Resistance of Composite Laminates with Different Materials. *Materials* **2020**, *13*, 129. [CrossRef] [PubMed]
6. Loginov, A.U.; Grishanov, S.A.; Hardwood, R.J. Modelling the Load–Extension Behaviour of Plain-knitted Fabric: Part I: A Unit-cell Approach towards Knitted-fabric Mechanics. *J. Text. Inst.* **2002**, *93*, 218–238. [CrossRef]
7. Araújo, M.; Fangueiro, R.; Hong, H. Modelling and Simulation of the Mechanical Behaviour of Weft-Knitted Fabrics for Technical Applications. Part II: 3D model based on the elastica theory. *Autex Res. J.* **2003**, *3*, 166–172.
8. Araujo, M.; Fangueiro, R.; Soutinho, F. Improving the stiffness of unidirectionally orientated weft knitted structures for polymer matrix composite reinforcement. *J. Text. Inst.* **2009**, *100*, 715–721. [CrossRef]
9. Abounaim, M.; Hoffmann, G.; Diestel, O.; Cherif, C. High performance thermoplastic composite from flat knitted multi-layer textile perform using hybrid yarn. *Compos. Sci. Technol.* **2011**, *71*, 511–519. [CrossRef]
10. Abounaim, M.; Hoffmann, G.; Diestel, O.; Cherif, C. Termoplastic composite from innovative flat knitted 3D multi-kayer spacer fabric using hybrid yarn and the study of 2D mechanical properties. *Compos. Sci. Technol.* **2010**, *70*, 363–370.
11. Ionesi, D.; Dumitras, C.; Ciobanu, L.; Vircan, A. Analysis of low velocity impact behaviour of aramid-linen fibre reinforced compositesusing Taguchi method. *J. Optoelectron. Adv. Mater.* **2012**, *14*, 544–550.
12. Ionesi, D.; Fangueiro, R.; Ciobanu, L.; Budulan, C. Practical aspects regarding the production of composite materials with 3D textile reinforcements. In Proceedings of the 16th International Conference MODTECH 2012, Sinaia, Romania, 24–26 May 2012; pp. 477–480.
13. Liu, D.; Christe, D.; Shakibajahromi, B.; Knittel, C.; Castaneda, N.; Breen, D.; Dion, G.; Kontos, A. On the role of material architecture in the mechanical behavior of knitted textiles. *Int. J. Solids Struct.* **2017**, *109*, 101–111. [CrossRef]
14. Kyosev, Y. Survey over the mechanical modelling of weft knitted structures. In Proceedings of the 2nd International Technical Textiles Congress 2005, Istanbul, Turkey, 13–15 July 2005. [CrossRef]
15. Araújo, M.; Fangueiro, R.; Hong, H. Modeling and Simulation of the Mechanical Behavior of Weft-Knitted Fabrics for Technical Applications, Part III: 2D hexagonal FEA model with non-linear truss elements. *Autex Res. J.* **2004**, *4*, 25–32.
16. Choi, K.; Lo, T. An Energy Model of Plain Knitted Fabric. *Textile Res. J.* **2003**, *73*, 739–748. [CrossRef]
17. Aranda-Iglesias, D.; Giunta, G.; Peronnet-Paquin, A.; Sportelli, F.; Keniray, D.; Belouettar, S. Multiscale modelling of the mechanical response of 3D multi-axial knitted 3D spacer composites. *Compos. Struct.* **2021**, *257*, 1–13. [CrossRef]
18. Chen, S.; Long, H.; Liu, Y.; Hu, F. Mechanical properties of 3d-structure composites based on warp-knitted spacer fabrics. *Autex Res. J.* **2015**, *15*, 127–137. [CrossRef]
19. Orlik, J.; Krier, M.; Neusius, D.; Pietsch, K.; Sivak, O.; Steiner, K. Recent Efforts in Modeling and Simulation of Textiles. *Textiles* **2021**, *1*, 322–336. [CrossRef]
20. Omrani, E.; Hasani, H.; Dibajian, S.H. Multi-Scaled Modeling the Mechanical Properties of Tubular Composites Reinforced with Innovated 3DWeft Knitted Spacer Fabrics. *Appl. Compos. Mater.* **2018**, *25*, 145–161. [CrossRef]
21. Hamedi, S.; Hasani, H.; Dibajian, S.H. Numerical simulating the flexural properties of 3D weft-knitted spacer fabric reinforced composites. *J. Compos. Mater.* **2017**, *51*, 1887–1899. [CrossRef]
22. Vassiliadis, S.; Provatidis, C.; Kallivretaki, A. Geometrical modeling of plain weft knitted fabrics. *Indian J. Fibre Text Res.* **2007**, *32*, 62–71.
23. Dumitras, C.; Hobjila, V. *Programarea si Utilizarea Calculatorului. Elemente Finite*; Cerni Publishing House: Bucharest, Romania, 2003.

materials

MDPI

Article

New Waste-Based Composite Material for Construction Applications

Eugen Constantin Ailenei [1], Savin Dorin Ionesi [1,*], Ionut Dulgheriu [1], Maria Carmen Loghin [1,*], Dorina Nicolina Isopescu [2], Sebastian George Maxineasa [2] and Ioana-Roxana Baciu [2,*]

[1] Faculty of Industrial Design and Business Management, "Gheorghe Asachi" Technical University of Iasi, Blvd. Mangeron, No. 29, 700050 Iasi, Romania; eugen.ailenei@tuiasi.ro (E.C.A.); ionut.dulgheriu@academic.tuiasi.ro (I.D.)

[2] Faculty of Civil Engineering and Building Services, "Gheorghe Asachi" Technical University of Iasi-Romania, Blvd. Mangeron, No. 1, 700050 Iasi, Romania; isopescu@tuiasi.ro (D.N.I.); sebastian.maxineasa@tuiasi.ro (S.G.M.)

* Correspondence: dionesi@tuiasi.ro (S.D.I.); cloghin@tex.tuiasi.ro (M.C.L.); ioanaroxana.baciu@yahoo.com (I.-R.B.)

Abstract: The global demand for fiber-based products is continuously increasing. The increased consumption and fast fashion current in the global clothing market generate a significant quantity of pre-and post-production waste that ends up in landfills and incinerators. The present study aims to obtain a new waste-based composite material panel for construction applications with improved mechanical properties that can replace traditional wood-based oriented strand boards (OSB). The new composite material is formed by using textile wastes as a reinforcement structure and a combination of bi-oriented polypropylene films (BOPP) waste, polypropylene non-woven materials (TNT) waste and virgin polypropylene fibers (PP) as a matrix. The mechanical properties of waste-based composite materials are modeled using the Taguchi method based on orthogonal arrays to maximize the composite characteristics' mechanical properties. Experimental data validated the theoretical results obtained.

Keywords: waste-based composite; panel; construction applications; textile waste; mechanical properties

Citation: Ailenei, E.C.; Ionesi, S.D.; Dulgheriu, I.; Loghin, M.C.; Isopescu, D.N.; Maxineasa, S.G.; Baciu, I.-R. New Waste-Based Composite Material for Construction Applications. *Materials* **2021**, *14*, 6079. https://doi.org/10.3390/ma14206079

Academic Editor: Francisco Javier Espinach Orús

Received: 2 September 2021
Accepted: 7 October 2021
Published: 14 October 2021

1. Introduction

Nowadays, the demand for textile products is experiencing exponential growth generated by both demographic indicators and the fashion industry. By increasing consumption and fast-changing fashion trends in the global clothing market as a result of the new fast fashion current, a substantial product life cycle shortening can be remarked. These aspects generate increased amounts of post-consumer waste added to the initial pre-consumption waste, which results during all technological flows of the processing industry of fibers, fabrics, textile garments, interior textiles and technical textiles.

According to the analysis made by Boston Consulting Group [1] for the Copenhagen Summit "Pulse of the Fashion Industry 2017" out of a total of 2.1 billion tons of waste produced worldwide annually 4%, representing 92 million tons, are produced by the fashion industry. Over 35% of pre-consumption waste is generated in the primary processing phase of the raw material, of which 9% is in fiber production and 91% in technological operations of product manufacturing (spinning, weaving and manufacturing). This analysis also shows that the processing and recycling of post-consumer textile waste are limited in quantity and technology. In this case, 80% of post-consumer waste ends up in landfills and incinerators, and only 20% is recycled or reused. All these details related to raw materials are presented in graphic form in Figure 1.

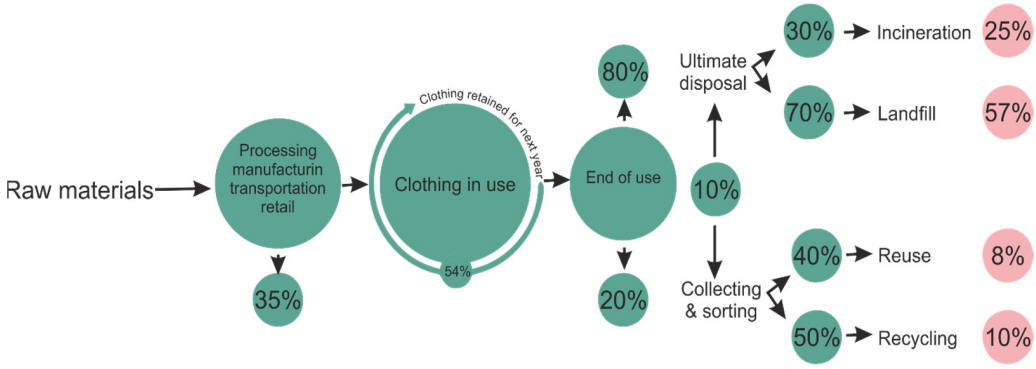

Figure 1. Pre- and post-consumer waste in the clothing industry [1].

According to demographic statistics, in 2030, the world population will be about 8.5 billion persons, and the demand for clothing products is expected to increase from 60 million tons in 2018 by 63% to 102 million tons in 2030 with a significant environmental impact [1].

From the perspective of textile products consumption per person in the industrial countries, the demand in 2010 is at an average of 28 kg/person increasing in 2020 by 10%, at 31 kg/person. Still, demand is growing by 51% in developing countries, from 7.9 to 12 kg/person [2–4].

To have a more precise image of the quantity and composition of the waste generated by the textile industry, we will analyze the demand both by type of fibers (natural and chemical) and on the proportion of each type of fibers within this industry. At the level of the 2018 year, the amount of polyester fibers worldwide consumed far exceeded the other types of chemical fibers and those of natural fibers (Figure 2). The share of synthetic fibers is 62.2% and natural fiber 37.7%. From synthetic fibers total consumption, polyester has over 51.5% of total demand. The percentage of fibers used for clothing is a significant share of over 55% [5].

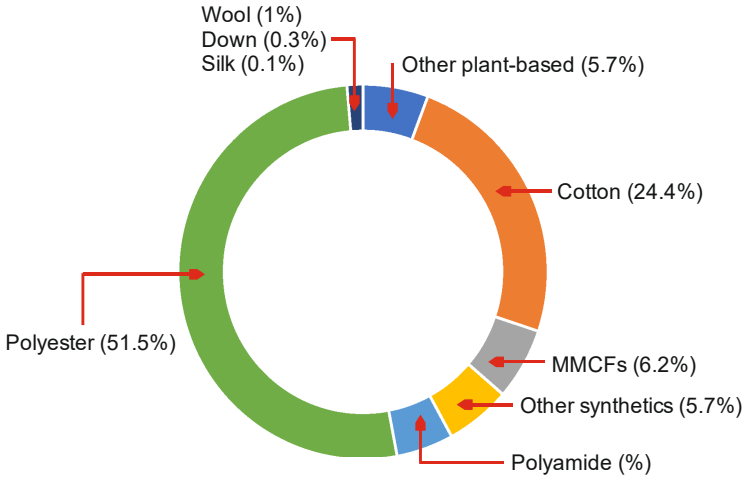

Figure 2. Fiber-type market share [5].

It can be remarked that synthetic fibers have a growing share of the textile industry market. A large part of them is directed to the fashion industry and interior products, generating significant amounts of pre-consumption and post-consumption waste with a very long degradation period. The global trend is to reduce the demand for natural cotton fibers due to the negative impact on the environment. Considering that cotton production consumes an estimated 16% of all insecticides and 7% of all herbicides [1,6], the global trend is to reduce the demand for natural cotton fibers due to the negative impact on the

environment. A significant part of this market share has been taken by eco-friendly cotton and polyester fibers with similar characteristics [6,7].

The European Council adopted on 22 May 2018 the waste management package of laws: Directive 2018/851 of the European Parliament and of the Council of 30 May 2018 amending Directive 2008/98/EC on waste, which lays down new rules on waste management and new recycling targets. According to these directives, the member states shall establish, by 1 January 2025, the separate collection of textiles and hazardous waste from households [8].

The main methods used for textile materials recycling, according to Ellen MacArthur Foundation [6,7], are classified as follows:

- Mechanical—textile waste is transformed into new products without changing the basic chemical structure by cutting, shredding and defibrating the waste to the level of fibers and transforming them into yarns and fabrics. It is closed-loop recycling with the addressability of all types of fibers (vegetable, animal and oil-based). The new products obtained are new yarns and non-woven materials. The qualities of the fibers obtained are generally inferior to the virgin fibers used in the initial products.
- Chemical—textile waste is decomposed into monomers, oligomers or basic chemicals. This form of recycling produces high-value products because they are identical to the original constituents used in obtaining the products subject to recycling. In addition, it addresses vegetable and oil-based fibers.
- Thermal—often refers to transforming PET flakes, pellets or chips into fibers by extruding the melt. It is often confused with energy recovery by burning textile waste.

The recycling process often consists of a mixture of mechanical, chemical and thermal processes in most cases. Examples are chemical recycling methods, in which, before dissolution or depolymerization, in the case of cellulosic fibers or monomers/oligomers, they are mechanically processed. This is similar to thermal recycling because the production of flakes, pellets and chips from PET waste is carried out by mechanical means. To remove paint pigments, additives and other impurities, chemical treatments are performed before mechanical recycling [9]. The recycling process can be in a closed or open cycle, according to the resulted product. For example, suppose the textile waste is converted into the same type as the initial one. In that case, it can be affirmed that it is a closed recycling cycle by recovering both components [10,11] or just the polyester polymer [12,13].

On the other hand, suppose the textile waste is converted into a new product with a different destination. In that case, the recycling cycle is open, used to make thermal insulation materials and sound-absorbing material for construction applications [14–16] or composite materials with thermoplastic matrix [17–20]. In addition, they are found with a reinforcing role in different applications for the realization of composite materials used in various sectors [19–23].

Considering the low recycling rate of waste resulting from pre-and post-consumption of textile products, the researchers are constantly looking for new environmentally friendly recycling technologies [18,24,25] and new applications for waste-based textile products [26–28]. The general direction is to upcycle, to obtain new products with increased added value and functionalities, but in general practice, the recycling of textile waste is downcycled [29,30].

The main objective of the completed research was to assess the possibility of reducing the negative impact of the textile and building industries on the natural environment by manufacturing a panel made of textile wastes that can be used for replacing the oriented strand boards (OSB) in different civil engineering applications. The 8 mm OSB is the most suitable construction product for comparison due to the fact that it is highly popular for building interior non-structural walls in houses made by using the light timer framing system. Therefore, the authors compared the analyzed textile waste product only with the 8 mm OSB, and thus, the composite product has the same thickness.

2. Materials and Methods

To complete this research have been used unsorted and underrated textile pre- and post-consumption wastes as reinforcement structure and bi-oriented polypropylene films (BOPP) waste, polypropylene non-woven materials (TNT) waste and virgin polypropylene fibers (PP) as the matrix.

The experimental work focused on producing textile-reinforced composite materials entirely made from production and technological waste for both reinforcement structures and matrices using thermoforming technology. This process is the adequate technology of the product targeted in work due to its advantages: short technological flow; low costs; no operations needed for sorting the textile wastes; elimination of the process of defibration of the textile wastes, which is an energy-intensive operation.

The investigation work has been carried out using the Taguchi Design of Experiment (DOE) method based on orthogonal arrays that use performance indicators, such as the signal-noise (S/N) ratio, that simultaneously take into consideration the desired response value (signal) and the variability thereof (noise) [31–33]. The DOE method aims to minimize the variability of the parameters reported to the noise factors and maximize the variability reported to the signal factors. The main steps that were followed to complete the experiment are:

- definition of system objectives—can be represented either by parameter optimization either by reaching a minimum or maximum value. The deviation from optimum performance is used to define the quality loss function;
- determination of parameters that influence the system and the specific levels of each;
- definition of the orthogonal array used in experimenting, according to the number of parameters and their specific levels;
- implementation of experiment and collect the experimental data;
- statistically analysis and interpretation of obtained raw data;
- results validation.

Taking into consideration the main objective of the research, the S/N ratio has been determined using the more significant, the better relation:

$$\frac{S}{N} = -10\log\left(\sum\left(\frac{1}{Y^2}\right)/n\right) \quad (1)$$

where Y = responses for the given factor level combination and n = number of responses in the factor level combination.

The main signal parameters taken into consideration are represented by matrix type, temperature, time, pressing force and matrix proportion. The specific levels of each are presented in Table 1.

Table 1. Signal parameters selection.

Level	Matrix Type	Temperature °C	Time [min]	Pressing Force [N/cm^2]	Matrix Proportion [%]
1	BOPP	180	10	68	20
2	TNT	190	15	88	30
3	PP	200	20	108	40
4	BOPP + TNT	210	25	128	50
Symbol	A	B	C	D	E

After analyzing orthogonal array models, the signal parameters and specific levels of each have been deemed adequate for the L16 orthogonal array, presented in Table 2 in coded (C) and uncoded (UNC) values.

Table 2. Orthogonal array selection.

Experiment Annotation	Matrix Type (A)		Temperature [°C] (B)		Time [min] (C)		Pressing Force [N/cm^2] (D)		Matrix Proportion [%] (E)	
	C	UNC	C	UNC	C	UNC	C	UNC	C	UNC
A1	1	BOPP	1	180	1	10	1	68	1	20
A2	1	BOPP	2	190	2	15	2	88	2	30
A3	1	BOPP	3	200	3	20	3	108	3	40
A4	1	BOPP	4	210	4	25	4	128	4	50
B5	2	TNT	1	180	2	15	3	108	4	50
B6	2	TNT	2	190	1	10	4	128	3	40
B7	2	TNT	3	200	4	25	1	68	2	30
B8	2	TNT	4	210	3	20	2	88	1	20
C9	3	PP	1	180	3	20	4	128	2	30
C10	3	PP	2	190	4	25	3	108	1	20
C11	3	PP	3	200	1	10	2	88	4	50
C12	3	PP	4	210	2	15	1	68	3	40
D13	4	BOPP + TNT	1	180	4	25	2	88	3	40
D14	4	BOPP + TNT	2	190	3	20	1	68	4	50
D15	4	BOPP + TNT	3	200	2	15	4	128	1	20
D16	4	BOPP + TNT	4	210	1	10	3	108	2	30

The waste-based composite materials panels were made using thermoforming technology, as illustrated in Figures 3 and 4. The used thermoforming press uses two plates that can be electrically heated up to 250 °C and water-cooling systems. The main parameters that can be modified are represented by temperature (0–250 °C) and pressing force (0–196 N/cm^2).

(**a**) (**b**) (**c**) (**d**)

Figure 3. The stages of the technological thermoforming process: (**a**) pre-and post-production waste; (**b**) cutting; (**c**) mixing, thermoforming and cooling; (**d**) waste-based composite panel.

(**a**) (**b**)

Figure 4. The waste-based composite materials panels: (**a**) pre-and (**b**) post-the technological thermoforming process.

The mechanical properties of the obtained waste-based composite materials were evaluated from a tensile and flexural point of view using the LBG TC10 testing machine equipped with a 10kN load cell, taking into consideration the specifications of SR EN 300:2006 [34] and SR EN ISO 527-4:2000 standards [35]. For each sample, a series of five tests were performed according to the standards mentioned above. In addition, the SR EN 300:2006 standard has been used to compare with 8 mm OSB boards.

The reduction by 20% of the distance between supports has been decided because the samples subjected to flexure did not break. To record the maximum bending force in 60 ± 30 s, the speed test was set at 20 mm/min.

According to SR EN 310-1996, the bending strength of composite samples is calculated as a ratio between the bending moment (at the maximum load F_{max}) to the moment of its full cross-section:

$$f_m = \frac{3F_{max}}{2bt^2} \quad (2)$$

where:

f_m = bending strength [N/mm^2];
F_{max} = maximum load [N];
l_1 = distance between the supports [mm];
b = width of the test sample [mm];
t = thickness of the test sample [mm].

According to SR EN 310-1996, Young's modulus has been determined for each sample using the following relation:

$$E_m = \frac{l_1^3 x(F_2 - F_1)}{4br^2 x(a_2 - a_1)} \quad (3)$$

where:

l_1 = distance between the supports [mm]
b = width of the test sample [mm];
t = thickness of the test sample [mm];
$F_2 - F_1$ = increasing the force, in newtons, on the straight portion of the load-deformation curve. F_1 is 10% of the breaking load, and F_2 is 40% of the breaking load.
$a_2 - a_1$ = the increase of the arrow at the middle of the sample (corresponding to $F_2 - F_1$)

According to SR EN ISO 527-4:2000, the tensile strength has been automatically determined using testing samples type 2, as illustrated in Figure 5.

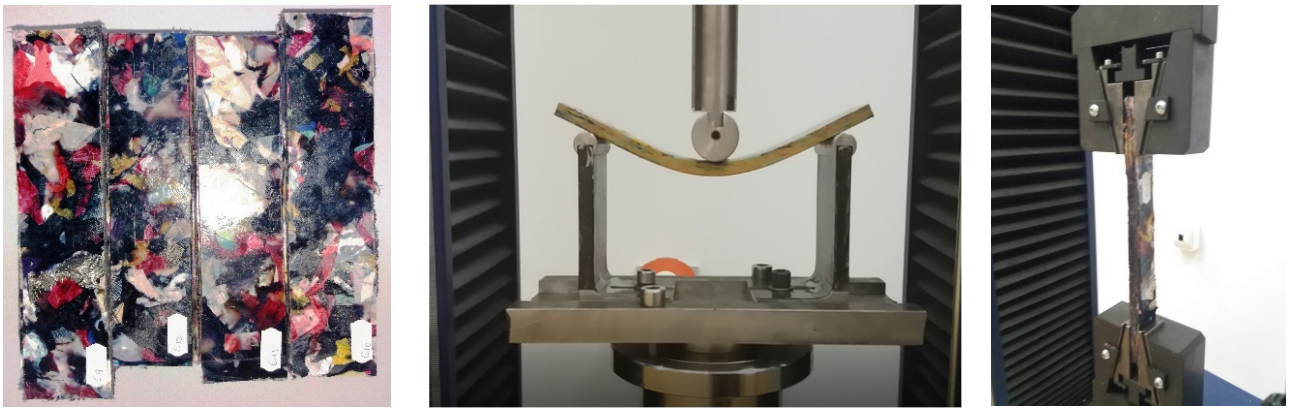

(**a**) (**b**) (**c**)

Figure 5. Mechanical properties testing (C9, C10, C11, C12): (**a**) tested samples; (**b**) compression testing; (**c**) stretch testing.

3. Results

The samples were produced according to the proposed experimental matrix, and the density, bending, Young's modulus and tensile strength were determined. The definition of the signal and noise factors is followed by statistical analysis. The results are presented in Table 3.

Table 3. Experimental design using L16 array and experimental results.

No.	A	B	C	D	E	Density [kg/m^3]	Bending [N/mm^2]	Young Modulus [N/mm^2]	Tensile Strength [N/mm^2]	SNRA	STDE	MEAN	CV
A1	1	1	1	1	1	936	4.7	239.0	3.95	15.66	440.89	295.95	1.49
A2	1	2	2	2	2	1104	19.8	865.9	12.04	26.27	567.89	500.47	1.13
A3	1	3	3	3	3	1283	33.0	1183.7	19.98	30.68	697.89	629.86	1.11
A4	1	4	4	4	4	1075	31.0	1253.1	20.19	30.59	661.27	594.78	1.11
B5	2	1	2	3	4	1065	32.4	1264.2	21.74	31.15	661.68	595.73	1.11
B6	2	2	1	4	3	1118	32.5	1256.9	19.25	30.40	673.04	606.65	1.11
B7	2	3	4	1	2	1220	31.4	1437.4	14.22	28.27	759.10	675.64	1.12
B8	2	4	3	2	1	1136	18.1	1333.8	8.45	23.70	710.05	624.21	1.14
C9	3	1	3	4	2	1024	14.7	948.6	10.56	24.69	562.93	499.42	1.13
C10	3	2	4	3	1	1051	15.6	1137.0	8.65	23.59	625.61	553.03	1.13
C11	3	3	1	2	4	1115	25.9	966.4	15.14	28.34	592.12	530.60	1.12
C12	3	4	2	1	3	1111	22.4	1079.7	12.28	26.66	622.47	556.28	1.12
D13	4	1	4	2	3	1216	35.2	1350.7	20.73	31.06	726.99	655.74	1.11
D14	4	2	3	1	4	1042	35.1	1397.5	23.19	31.75	702.65	624.53	1.13
D15	4	3	2	4	1	1106	21.2	1048.9	9.98	25.14	613.59	546.59	1.12
D16	4	4	1	3	2	1092	27.7	1257.3	13.78	27.85	669.76	597.83	1.12

The response resulting from Taguchi analysis revealed the significance of the signal factors reported to the S/N ratio and the mean. The obtained regression results are presented in Table 4, for the S/N ratio and in Table 5, for means. Combining the obtained results from S/N ratio analysis and means analysis results in the classification of influence level of the factors over the proposed model, presented in Table 6.

Table 4. Regression Information—S/N ratio.

Term	Coefficient	Standard Error	Low Confidence	High Confidence	T [Value]	*p* [Value]
Intercept	27.24	0.52	26.27	28.20	52.59	0.00
A [1]	−1.44	0.90	−3.11	0.23	−1.60	0.15
A [2]	1.14	0.90	−0.52	2.81	1.27	0.24
A [3]	−1.42	0.90	−3.08	0.25	−1.58	0.15
B: Factor 2	0.72	0.69	−0.58	2.01	1.03	0.33
C: Factor 3	1.33	0.69	0.03	2.62	1.91	0.09
D: Factor 4	1.10	0.69	−0.19	2.39	1.58	0.15
E: Factor 5	4.23	0.69	2.94	5.53	6.09	0.00

Table 5. Regression Information—Means.

Term	Coefficient	Standard Error	Low Confidence	High Confidence	T [Value]	*p* [Value]
Intercept	567.96	11.84	545.93	589.98	47.95	0.00
A [1]	−62.69	20.51	−100.84	−24.54	−3.06	0.02
A [2]	57.60	20.51	19.45	95.75	2.81	0.02
A [3]	−33.12	20.51	−71.27	5.02	−1.61	0.15
B: Factor 2	40.38	15.89	10.83	69.93	2.54	0.03
C: Factor 3	57.13	15.89	27.58	86.68	3.60	0.01
D: Factor 4	13.15	15.89	−16.40	42.70	0.83	0.43
E: Factor 5	43.23	15.89	13.68	72.78	2.72	0.03

Table 6. Classification of influence level.

Level	Matrix Type (A)	Temperature [°C] (B)	Time [min] €	Pressing Force [N/cm^2] (D)	Matrix Proportion [%] €
1	25.8	25.64	25.56	25.58	22.02
2	28.38	28	27.3	27.34	26.77
3	25.82	28.11	27.7	28.32	29.7
4	28.95	27.2	28.38	27.7	30.46
Delta	3.15	2.74	2.81	2.73	8.43
Rank	2	5	3	4	1

By analyzing the regression results for S/N ratio and means, illustrated in Tables 4 and 5 and the response resulting from Taguchi analysis, presented in Table 6, the significance of the signal factors reported to S/N ratio, and the means is:

- Maximum influence—factor E (matrix proportion);
- High influence—factor A (matrix type);
- High influence—factor C (time);
- Low influence—factor D (pressing force);
- Low influence—factor B (temperature).

The values obtained for the S/N ratio and means from Table 3 are graphically represented in Figures 6 and 7, and the interactions between factors are graphically represented in Figures 8 and 9.

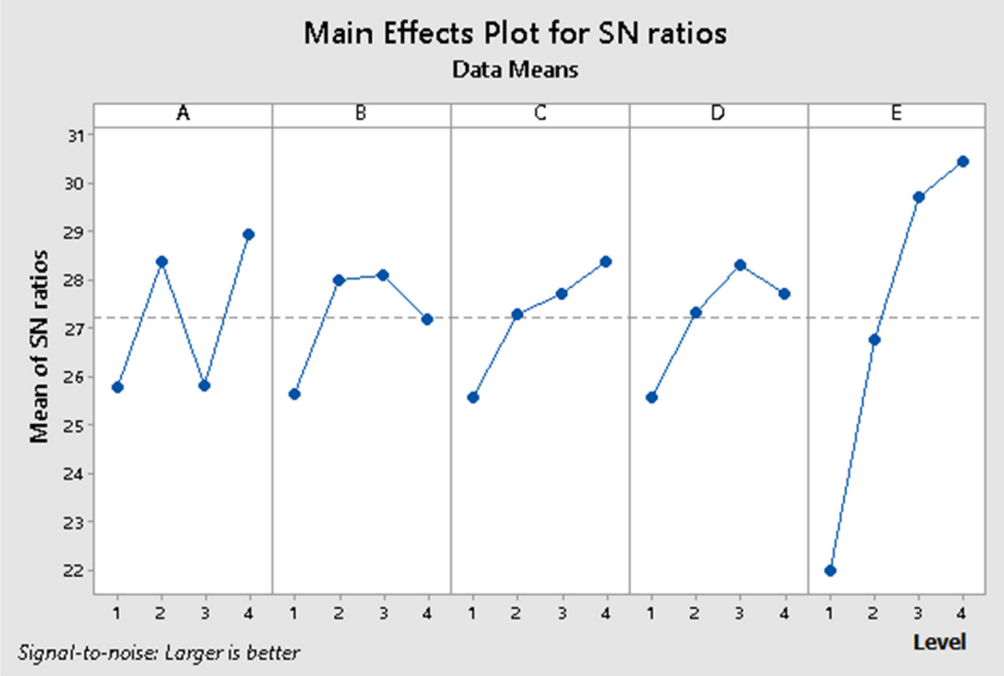

Figure 6. The values obtained for the main effects plot for S/N ratio.

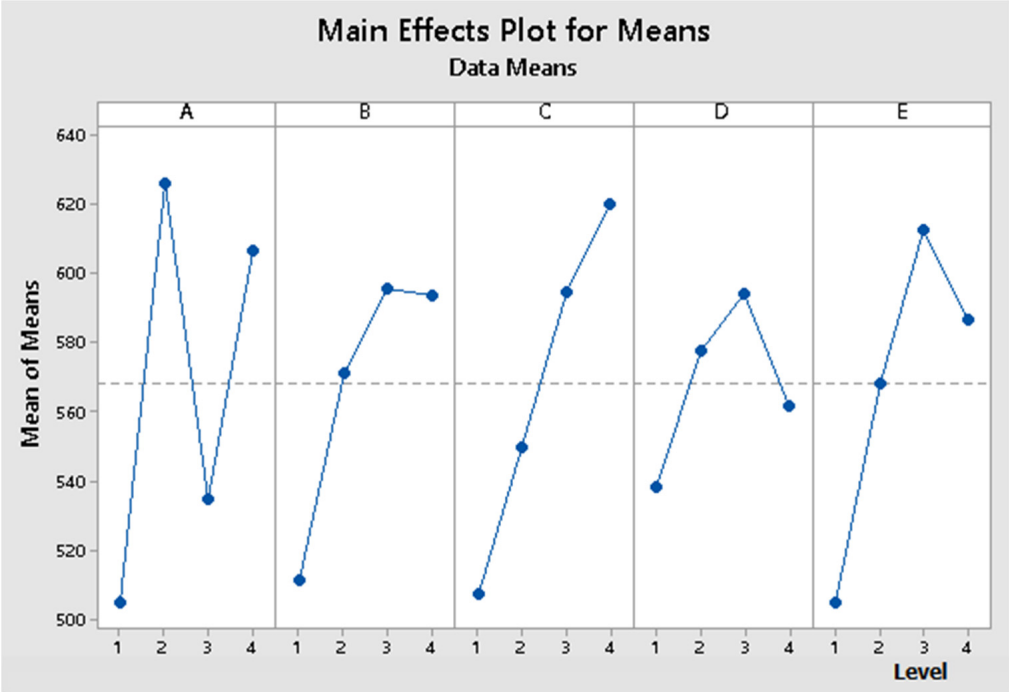

Figure 7. The values obtained for the main effects plot for means.

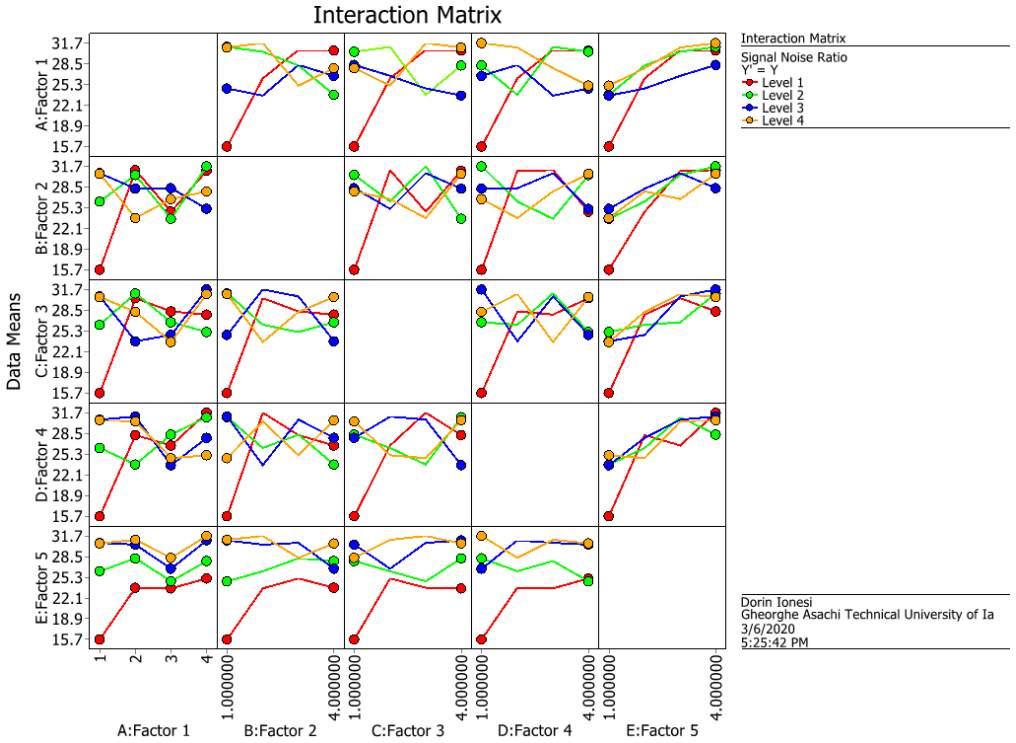

Figure 8. The interactions between factors for S/N ratio.

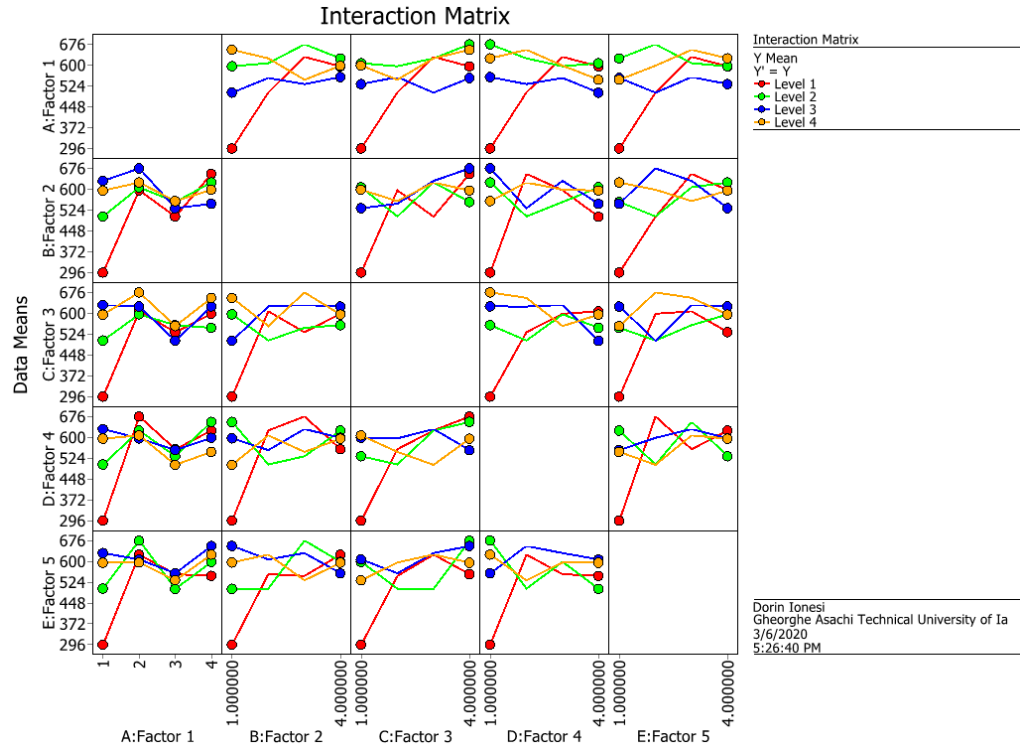

Figure 9. The interactions between factors for means.

The values obtained for the S/N ratio and Table 3 are graphically represented in Figures 6 and 7. The interaction matrix for the S/N ratio and means are illustrated in Figures 8 and 9. The S/N ratio has been calculated using the formula defined for larger, the better case.

By analyzing the results obtained for the S/N ratio, the optimal combination of signal parameters is A4 B2 C4 D3 E4, representing a composite material that uses the BOPP + TNT

as matrix, a temperature of 190 °C, thermic treatment time of 25 min, 108 N/cm^2 and 50% Matrix proportion. By analyzing the results obtained for means, the optimal combination of signal parameters is A4 B3 C4 D3 E3, representing a composite material that uses the BOPP + TNT as the matrix, a temperature of 180 °C, thermic treatment time of 25 min, pressing force 108 N/cm^2 and 40% Matrix proportion.

From the S/N ratio point of view, it can be remarked that factor E has a low variation on the 3rd and 4th levels. Still, according to means analysis made across the same levels, the 3rd one has a high influence over the properties of the designed composite material. Therefore, by combing the obtained results for S/N ratio and means analysis, the optimum signal factors combination is A4 B2 C4 D3 E3, representing a composite material that uses the BOPP + TNT as a matrix, a temperature of 190 °C, thermic treatment time of 25 min, pressing force 108 N/cm^2 and 40% Matrix proportion.

As shown in Figure 10, after applying the prediction method for the optimal model, the S/N ratio is maximal reported to the S/N ratio obtained from statistical processing of experimental data according to the Taguchi experiment matrix.

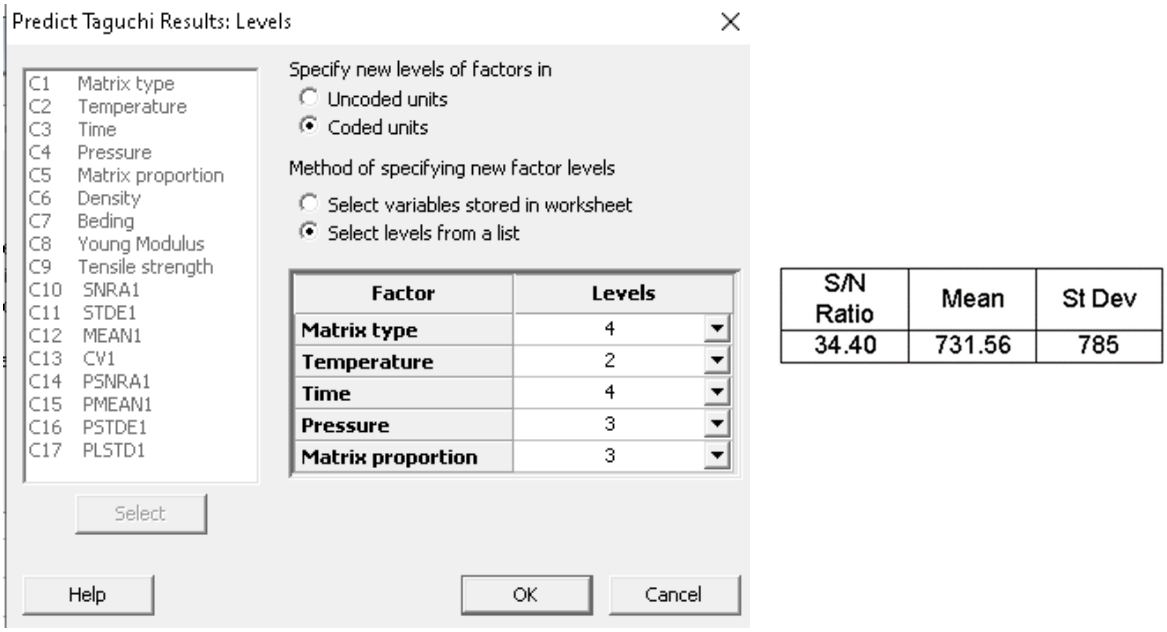

(**a**) (**b**)

Figure 10. Definition of the levels of the parameters for (**a**) result prediction; (**b**) predicted values.

This method can be used for predicting results characterized by different combinations of the considered signal parameters.

4. Model Validation

For the determination of the accuracy of Taguchi analysis, model validation has been made. In this case, model validation was made by performing several tests, taking into account the optimum levels previously determined of the defined signal parameters (Table 7).

Table 7. Mechanical properties of the obtained optimum model of the waste based composite material.

A	B	C	D	E	Density [kg/m^3]	Bending [N/mm^2]	Young Modulus [N/mm^2]	Tensile Strength [N/mm^2]
4	2	4	3	3	1112	34.8	1385.6	23.3

The mechanical properties of the obtained optimum model of the waste-based composite material were evaluated from the tensile and flexural point, considering the specifications of SR EN 300:2006 and SR EN ISO 527-4:2000 standards.

It can be remarked that the obtained results are maximum from a tensile strength point of view, and lower with 5% from Young Modulus point of view (reported to A7 sample) and with 1% from Bending point of view (reported to A13 sample), but with a density lower with 13% reported to the maximum value (A3 sample).

Considering that the waste-based composite material has been designed as an alternative for 8 mm OSB boards, the obtained mechanical properties were compared to the mechanical properties of the 8 mm OSB boards (Table 8). Therefore, the OSB board's mechanical properties, presented in Table 8, were determined according to SR EN 300:2006 and SR EN ISO 527-4:2000 standard specifications.

Table 8. Mechanical properties of the 8 mm OSB boards.

Testing Direction	Density [kg/m^3]	Bending [N/mm^2]	Young Modulus [N/mm^2]	Tensile Strength [N/mm^2]
Transversal	643	9.9	1499	2.26
Longitudinal	643	23.2	3427.7	5.68

The reinforcement structure into the designed waste-based composite material was randomly arranged. Due to this fact, the mechanical properties are isotropic.

By comparing the mechanical properties of the designed waste-based composite material to the ones of the 8 mm OSB boards, it can be remarked that:

- the tensile strength of waste-based composite material is higher with 1030.97% on the transversal direction and 410.21% on longitudinal direction;
- the bending resistance of waste-based composite material is higher with 351.92% on the transversal direction and 150% on longitudinal direction;
- the rigidity of waste-based composite material is lower with 8% on the transversal direction and with 60% on longitudinal direction;
- the density of waste-based composite is higher at 173%.

5. Conclusions

The present paper aims at assessing the opportunity of improving the overall environmental performances of the construction and textile industries by using various textile wastes for manufacturing a panel that can be used as an OSB board replacement, with a thickness of 8 mm, for assembling the interior non-structural walls in light timber frame building. The novelty of this study resides in the combination of pre-and post-production textile wastes used as reinforcement structure and bi-oriented polypropylene films waste and polypropylene non-woven materials waste used as matrix.

The obtained results reveal that developing composite material panels for construction applications made from pre-and post-production textile material wastes to replace traditional wood-based oriented strand boards is an efficient solution. In addition, the mechanical properties of the new material are significantly higher than those of traditional 8 mm OSB boards.

The use of virgin polypropylene fibers as a matrix brings no advantage compared to bi-oriented polypropylene films waste and polypropylene non-woven materials waste. Therefore, the new waste-based composite material was validated based on experimental results obtained by testing the resulting optimal model in similar conditions and comparing the obtained results with the initial model and 8mm OSB board mechanical characteristics.

Author Contributions: Conceptualization, E.C.A., I.D. and M.C.L.; methodology and software, S.D.I., D.N.I. and S.G.M.; performed the experiments E.C.A., I.-R.B. and S.G.M.; validation, M.C.L., S.D.I. and D.N.I.; formal analysis, E.C.A., S.D.I. and I.D.; investigation, S.D.I., M.C.L. and D.N.I.; resources, M.C.L. and I.D.; data curation, M.C.L. and D.N.I.; writing—original draft preparation, E.C.A., S.D.I. and I.-R.B.; writing—review and editing, M.C.L., D.N.I. and S.G.M.; funding acquisition, M.C.L. All authors have read and agreed to the published version of the manuscript.

Funding: This work is funded by TUIASI Internal Grants Program (GI_P17/2021), financed by the Romanian Government.

Institutional Review Board Statement: Not applicable.

Informed Consent Statement: Not applicable.

Data Availability Statement: Not applicable.

Acknowledgments: This paper was realized with the support of COMPETE project nr.9PFE/2018, financed by the Romanian Government.

Conflicts of Interest: The authors declare no conflict of interest.

References

1. Eder-Hansen, J.; Chalmer, C.; Tärneberg, S.; Tochtermann, T.; Sebastian Boger Theelen, G.; Global Fashion Agenda & The Boston Consulting Group. Pulse-of-the-Fashion-Industry_2017. 2017, pp. 9–61. Available online: https://globalfashionagenda.com/?x=0&y=0&s=Pulse-of-the-Fashion-Industry_2017 (accessed on 5 March 2019).
2. Pepper, R.; Opperskalski, S.; Evonne, S.; Truscott, T. Textile-Exchange. Preferred-Fiber-Material-Market-Report_2016. *Text. Exch.* **2016**, *19*. Available online: https://textileexchange.org/wp-content/uploads/2017/02/TE-Preferred-Fiber-Market-Report-Oct2016-1.pdf (accessed on 15 March 2020).
3. Beton, A.; Dias, D.; Farrant, L.; Gibon, T.; Le Guern, T. Environmental Improvement Potential of textiles (IMPRO Textiles). *Publ. Off. Eur. Union* **2014**, *9*. Available online: https://ec.europa.eu/jrc/en/publication/eur-scientific-and-technical-research-reports/environmental-improvement-potential-textiles-impro-textiles (accessed on 5 March 2020).
4. Šajn, N.; EPRS—European Parliamentary Research Service. Environ. *Impact Text. Cloth. Ind.* 2019. Available online: https://www.europarl.europa.eu/thinktank/en/document.html?reference=EPRS_BRI(2019)633143 (accessed on 15 May 2020).
5. Opperskalski, S.; Evonne, S.; Truscott, T. Textile-Exchange_Preferred-Fiber-Material-Market-Report_201. *Text. Exch.* **2019**, *6*. Available online: https://textileexchange.org/wp-content/uploads/2019/11/Textile-Exchange_Preferred-Fiber-Material-Market-Report_2019.pdf (accessed on 15 March 2020).
6. Ellen MacArthur Foundation. A New Textiles Economy: Redesigning Fashion's Future. 2017. Available online: http://www.ellenmacarthurfoundation.org/publications (accessed on 15 March 2020).
7. Ailenei, E.C.; Loghin, C.; Ichim, M.; Hoblea, A. New composite materials using polyester woven fabric scraps as reinforcement and thermoplastic matrix. *Ind. Text.* **2021**, *72*, 62–67. [CrossRef]
8. Directive (EU) 2018/851 of the European Parliament and of the Council of 30 May 2018 amending Directive 2008/98/EC on waste. 2018. Available online: https://eur-lex.europa.eu/ (accessed on 10 May 2020).
9. Yousef, S.; Tatariants, M.; Tichonovas, M.; Kliucininkas, L.; Lukosiute, I.; Yan, L. Sustainable green technology for recovery of cotton fibers and polyester from textile waste. *J. Clean. Prod.* **2020**, *254*, 120078. [CrossRef]
10. Ling, C.; Sheng, S.; Hou, W.; Yan, Z. Separation of waste polyester/cotton blended fabrics by phosphotungstic acid and preparation of terephthalic acid. *Polym. Degrad. Stab.* **2019**, *161*, 157–165. [CrossRef]
11. Sun, X.; Lu, C.; Zhang, W.; Tian, D.; Zhang, X. Acetone-soluble cellulose acetate extracted from waste blended fabrics via ionic liquid catalyzed acetylation. *Carbohydr. Polym.* **2013**, *98*, 405–411. [CrossRef] [PubMed]
12. Gholamzad, E.; Karimi, K.; Masoomi, M. Effective conversion of waste polyester–cotton textile to ethanol and recovery of polyester by alkaline pretreatment. *Chem. Eng. J.* **2014**, *253*, 40–45. [CrossRef]
13. Navone, L.; Moffitt, K.; Hansen, K.; Blinco, J.; Payne, A.; Speight, R. Closing the textile loop: Enzymatic fibre separation and recycling of wool/polyester fabric blends. *Waste Manag.* **2019**, *102*, 149–160. [CrossRef]
14. Echeverria, C.; Pahlevani, F.; Handoko, W.; Jiang, C.; Doolan, C.; Sahajwalla, V. Engineered hybrid fibre reinforced composites for sound absorption building applications. *Resour. Conserv. Recycl.* **2018**, *143*, 1–14. [CrossRef]
15. Tiuc, A.E.; Vermesan, H.; Gabor, T.; Vasile, O. Improved Sound Absorption Properties of Polyurethane Foam Mixed with Textile Waste. *Energy Procedia* **2016**, *85*, 559–565. [CrossRef]
16. Drochytka, R.; Dvorakova, M.; Hodna, J. Performance Evaluation and Research of Alternative Thermal Insulation Based on Waste Polyester Fibers. *Procedia Eng.* **2017**, *195*, 236–243. [CrossRef]
17. Zou, Y.; Reddy, N.; Yang, Y. Reusing polyester/cotton blend fabrics for composites. *Compos. Part B Eng.* **2011**, *42*, 763–770. [CrossRef]
18. Barbero-Barrera, M.; Pombo, O.; Navacerrada, M. Textile Fibre Waste Bindered With Natural Hydraulic Lime. *Compos. Part B Eng.* **2016**, *94*, 26–33. [CrossRef]
19. Echeverria, C.; Pahlevani, F.; Sahajwalla, V. Valorisation of discarded nonwoven polypropylene as potential matrix-phase for thermoplastic-lignocellulose hybrid material engineered for building applications. *J. Clean. Prod.* **2020**, *258*, 120730. [CrossRef]
20. Petrucci, R.; Nisini, E.; Puglia, D.; Sarasini, F.; Rallini, M.; Santulli, C. Tensile and fatigue characterisation of textile cotton waste/polypropylene laminates. *Compos. Part B Eng.* **2015**, *81*, 84–90. [CrossRef]

21. Gómez, J.; Madariaga, F.; Sierra, A.; León, R.; Abt, T. Scrap denim-PP composites as a material for new product design. In *IFDP'16—Systems & Design: Beyond Processes and Thinking*; Editorial Universitat Politècnica de València: Valencia, Spain, 2016; pp. 819–828. [CrossRef]
22. Mishra, R.; Behera, B.; Militky, J. Recycling of Textile Waste into Green Composites: Performance Characterization. *Polym. Compos.* **2014**, *35*, 1960–1967. [CrossRef]
23. Zonatti, W.; Guimarães, B.; Duleba, W.; Baruque-Ramos, J. Thermoset composites reinforced with recycled cotton textile residues. *Text. Cloth. Sustain.* **2015**, *1*, 1–12. [CrossRef]
24. Zhang, Z.; Wang, C.; Mai, K. Reinforcement of Recycled PET for Mechanical Properties of Isotactic Polypropylene. *Adv. Ind. Eng. Polym. Res.* **2019**, *2*, 69–76. [CrossRef]
25. Popa, N.; Timofte, D.; Voicu, G.; Durbaca, I.; Toma, L. Aspects Regarding Valorification of Natural Fibrous Materials from Textile and Leather Industry for Composite Materials. *J. Eng. Stud. Res.* **2017**, *20*, 77. [CrossRef]
26. Müller, M. Hybrid composite materials on basis of reactoplastic matrix reinforced with textile fibres from process of tyres recyclation. *Agron. Res.* **2015**, *13*, 700–708.
27. Aghaee, K.; Foroughi, M. Mechanical Properties of Lightweight Concrete Partition with a Core of Textile Waste. *Adv. Civ. Eng.* **2013**, *2013*. [CrossRef]
28. Lacoste, C.; El Hage, R.; Bergeret, A.; Corn, S.; Lacroix, P. Sodium alginate adhesives as binders in wood fibers/textile waste fibers biocomposites for building insulation. *Carbohydr. Polym.* **2017**, *184*, 1–8. [CrossRef] [PubMed]
29. Sandin, G.; Peters, G. Environmental impact of textile reuse and recycling—A review. *J. Clean. Prod.* **2018**, *184*, 353–365. [CrossRef]
30. Elander, M.; Ljungkvist, H. Critical Aspects in Design for Fiber-to-Fiber Recycling of Textiles. A Mistra Future Fashion Report Phase 2. 2016. Available online: http://mistrafuturefashion.com/wp-content/uploads/2016/06/MFF-report-2016-1-Critical-aspects.pdf (accessed on 15 March 2020).
31. Taguchi, G.; Chowdhury, S.; Wu, Y. *Taguchi's Quality Engineering Handbook*; Wiley: New York, NY, USA, 2005.
32. Taguchi, G. *Introduction to Quality Engineering*; Asian Productivity: Tokyo, Japan, 1986.
33. Titu, M. (Ed.) *Statistica Tehnica si Proiectarea Experimentelor*; Universitatii "L. Blaga": Sibiu, Romania, 2005.
34. EN; Oriented strand boards (OSB). *Definitions, Classification and Specifications (Standard Roman—SR EN 300: 2006/SR EN 310)*; European Committee for Standardization: Brussels, Belgium, 2006.
35. EN; Plastics. *Determination of Tensile Properties. Part 4: Test Conditions for Composites of Plastics Reinforced with Isotropic and Orthotropic Fibres, in Romanian (Standard Roman—SR EN ISO 527-4:2000)*; Romanian Standardization Association: Bucuresti, Romania, 2000.

Available online at www.sciencedirect.com

jmr&t Journal of Materials Research and Technology

www.jmrt.com.br

Original Article

Influence of silane coupling agent on shear thickening fluids (STF) for personal protection

T.F. Santos[a,*], C.M.S. Santos[a], M.S. Aquino[b], Dorin Ionesi[c], J.I. Medeiros[a,*]

[a] Textile Engineering Post Graduate Program (PPGET), Federal University of Rio Grande do Norte, Natal, Rio Grande do Norte, Brazil
[b] Textile Engineering Department (DET), Federal University of Rio Grande do Norte, Natal, Rio Grande do Norte, Brazil
[c] Gheorghe Asachi Technical University of Iasi, Faculty of Textile Leather and Industrial Management, Iaşi, Romania

ARTICLE INFO

Article history:
Received 15 March 2019
Accepted 9 July 2019
Available online 25 July 2019

Keywords:
Impact
Adhesion
Shear thickening fluids

ABSTRACT

The present work studied the influence of silane coupling agent in non-Newtonian fluid, in the impact resistance, adhesion and flexibility results. The results of stab performance for Kevlar samples impregnated with silane agent showed results significantly higher than others samples non impregnated, such results are closely associated with the formation of siloxane bonds due to the coupling agent. The impact resistance properties of all samples were tested using drop tower testing, and the flexibility was testes beyond bending angle test. SEM and FTIR analyses were used to verify the chemicals compositions and to evaluate qualitatively the presence of nanoparticles samples. Abrasion test were realized to verify the influence of silane agent of the resistance adhesive of non-Newtonian fluid under samples. The Kevlar samples impregnated with STF and coupling silane presented best flexibility (angle of bending = 30.33°), a significant increase on the dissipation kinetic (penetration depth) in comparing to the others and resistance adhesive of non-Newtonian fluid under samples. Therefore, practically this property remained unalterable in relation to Kevlar samples with STF and Kevlar control.

1. Introduction

A fluid is considered non-Newtonian when its viscosity is not constant at a given temperature and pressure [1–3]. Instead, the value depends on flow conditions such as the geometry, rate and shear time, and the kinematic history of the sample. The behavior of non-Newtonian fluid can be classified into three categories: viscoelastic fluids, time dependent and time independent. Non-Newtonian fluids non-time dependent are the field of this work. Those can be classified in Shear-thinning or pseudoplastics, viscoplastics, and shear-thickening (STF) [4]. STF's are also known as dilatant materials and their apparent viscosity increases proportionally to the shear rate. This behavior can be explained as follows: when the fluid is at rest, the liquid present in it, is sufficient only to fill the voids. As the shear rate increases, the dense form of the solids breaks

* *Corresponding authors.*
E-mails: thiagotextilufrn@hotmail.com (T. Santos), ivanmedeiros.portugal@gmail.com (J. Medeiros).
https://doi.org/10.1016/j.jmrt.2019.07.013

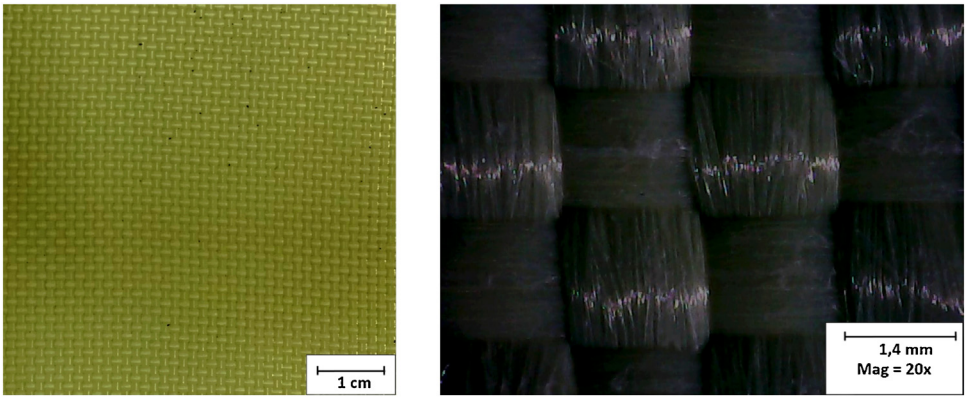

Fig. 1 – (a) Kevlar woven samples used in the study and (b) shows the optic microscopy Kevlar® 29 woven structure.

down and the material expands slightly causing an increase in the void. Therefore, the available liquid is no longer sufficient to lubricate the solid particles movement and the resulting solid-solid friction causes the stresses to increase rapidly, also increasing the apparent viscosity [5]. The properties of SFT's has been taken in several studies on their use as reinforcement of textile fibers applied to ballistic protection [6]. Wilson and Jacob also used silica nanoparticles and verified the formation of siloxane bonds during functionalization process, in addition to a significant improvement in the shear rigidity, penetration resistance and a slight increase in tensile strength. In spite of this advance, fiber/STF adhesion, as in the case of Kevlar®, was shown to be weak, requiring the use of a coupling agent that allows a better adhesion between organic and inorganic compounds. The silane compound is a type of coupling agent that can act on this adhesion because it increases the friction between the particles [7]. This work aims to study the influence of silane agent on shear thickening fluid (STF) under mechanical properties of the composite for ballistic protection.

2. Materials and methods

For all experiments was used Kevlar 29 high-performance woven fabrics, compound of Aramid (poly ρ-phenylene terephthalamide), taffeta 1 × 1 plain weave structure, 7 weft/cm and 7 warp/cm density, 375.0 ± 16 Tex count in both direction yarns, and 497 ± 25 g/m^2 weight, as shown in Fig. 1.

The methodology applied was that as described in literature, with some adaptations. Shear Thickening Fluid (STF) was prepared using 88% of ethanol, 6% of polyethylene glycol 300 (by ISOFAR) and 6% of silica in size of 7 nm (AEROSIL 300 by EVONICK), underweight in constant stirring on a magnetic stirrer during 40 min. Initially, the solution was prepared using alcohol 99% purity (by ATRIOM), nanosilica and coupling agent (3-Metacriloxipropiltrimetoxisilano by PROSIL) in 1.29% concentration by weight in a Becker under constant stirring on a magnetic stirrer during 20 min. Followed by addiction of polyethylene glycol and stirring for further 30 min. Finally, the impregnation process was made in a foulard using 0.5 bar at room temperature. Thereafter, the impregnated samples were dried using an oven under 78 °C during 1 h.

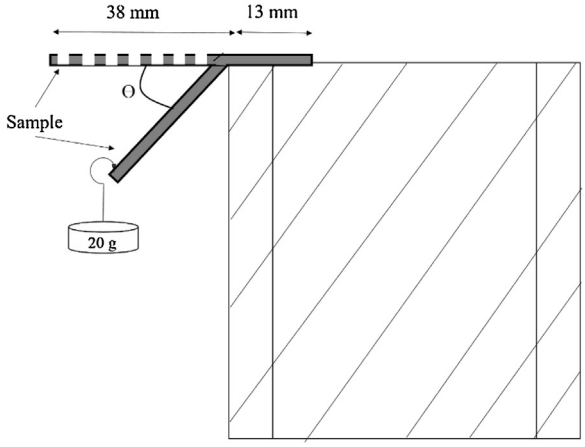

Fig. 2 – Bending test setup.

2.1. *Bending test*

This test consists to deform the material at a midpoint (13 mm), causing a curvature or bending form on the surface without fracture occurrence. This test is usually employed to determine the flexibility of materials as shown in Fig.2. At first, the sample tested (51 mm) was loaded with a mass of 20 g, in which it gave rise to an angle of curvature that in turn is mentioned in the literature as a measure of sample flexibility [8], higher the angle, it indicates more flexibility.

2.2. *Drop tower test*

It was carried out in objective to measure the stab resistance of the composite. Penetration tests were carried out using a S̈1″ knife blade, based on NIJ-0115.00 [9], specifying the minimum performance requirements for a material resistant to attack by pointed and edged weapons [10]. The samples had been placed in multilayer foam as described in Fig. 3a. To perform the knife test, the knife blade S̈1″ was assembled on a support, and then, loaded with a mass of 3.34 kg corresponding to 13 Joule Fig. 3b. The depth penetration in the sample was calculated leading to consider the length knife cut in the witness papers in each layer penetrated by the knife blade S̈1″.

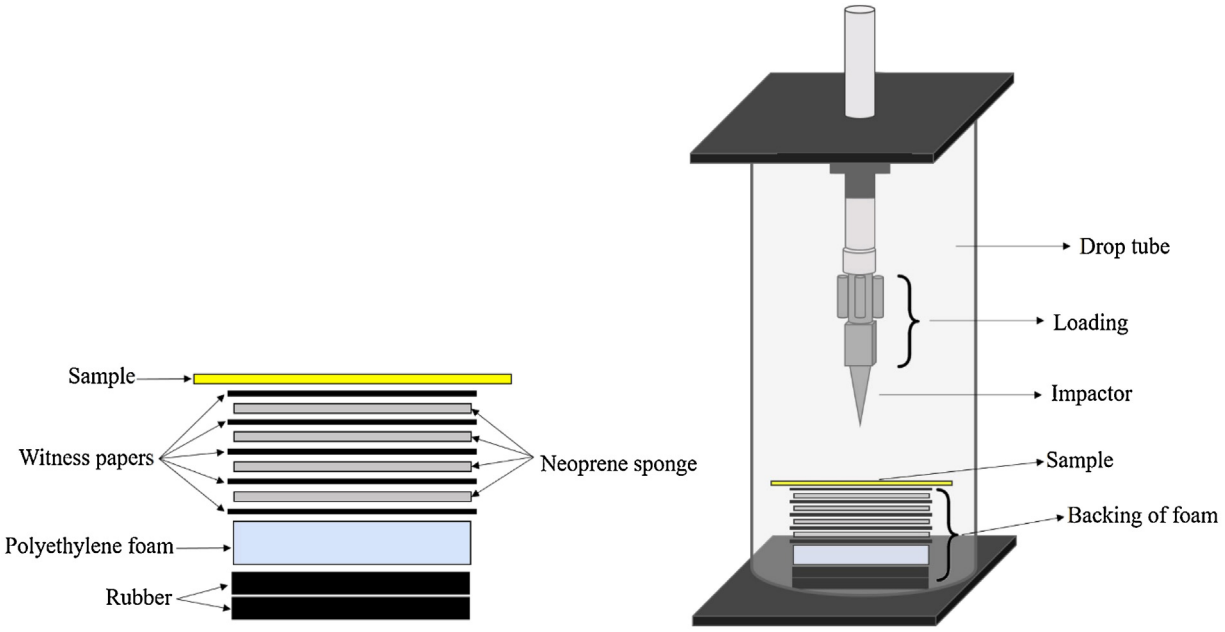

Fig. 3 – (a) Multilayer foam representation and (b) drop tower test.

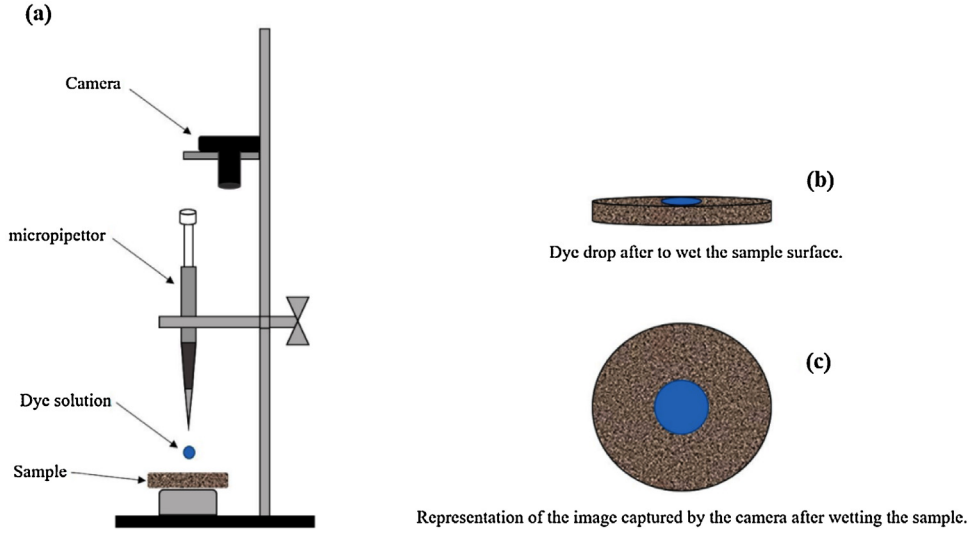

Fig. 4 – Adhesion test illustration. (a) Apparatus (b) horizontal wettability (c) wettability image.

2.3. *Adhesion test (Martindale)*

For adhesion test, were used a process similar to "Martindale" method ISO 12947. The tests were carried out, applying 2000 cycles of Lissajour movements, with 0,5 Kpa pressure on the samples (Kevlar control, Kevlar with STF and Kevlar with STF and coupling agent) [11]. However, the tests were stopped every 1000 cycles, in order to measure the adhesion. The adhesion of samples was calculated using a solution of methylene blue dye (1 g/L) and a micropipette (10 μl). Every stop, the samples were subjected to the apparatus shown in Fig. 4a, that consists in to qualify, by horizontal wettability (Fig. 4b) according to the adhesion of the STF under the fabric surface samples, after friction cycles. Therefore, it will have greater adhesion the sample that presents wettability with

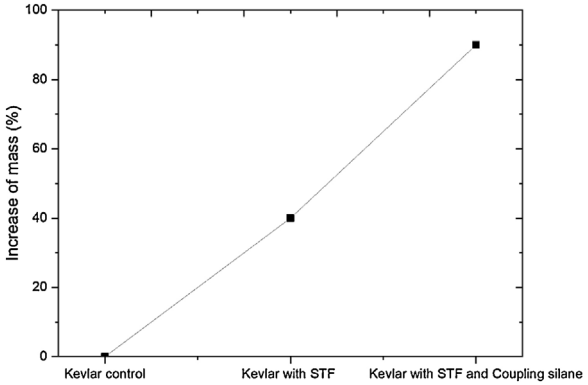

Fig. 5 – Increase mass of the samples after impregnation.

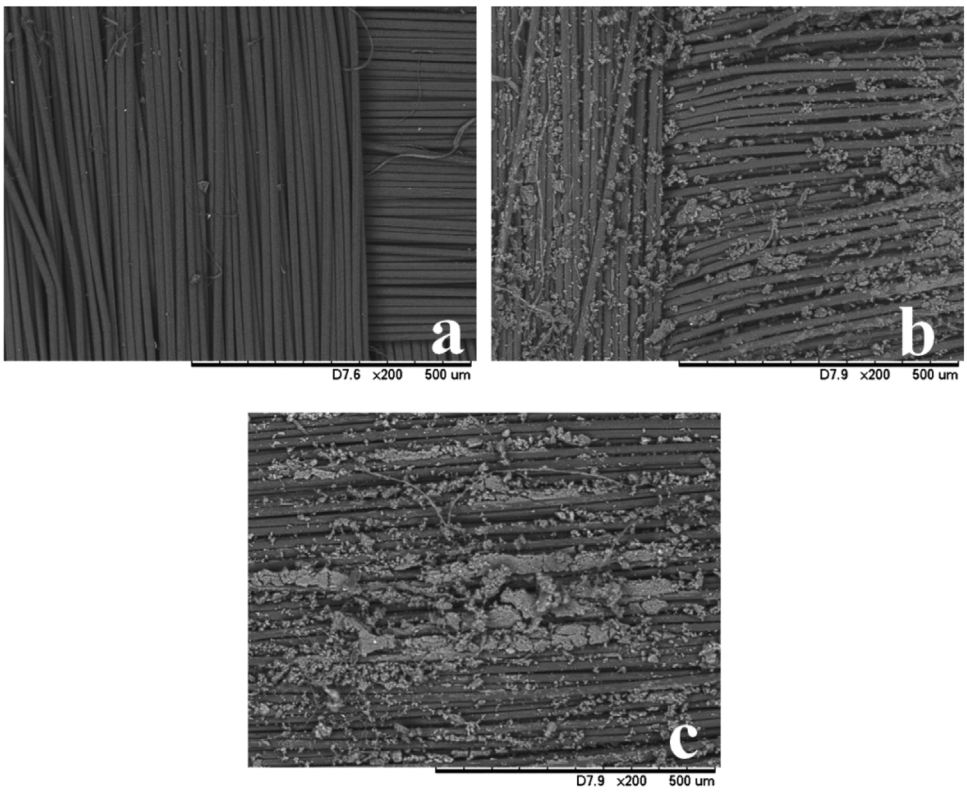

Fig. 6 – SEM analyses for the samples studied. (a) Kevlar control; (b) Kevlar with STF; and (c) Kevlar with STF and coupling agent.

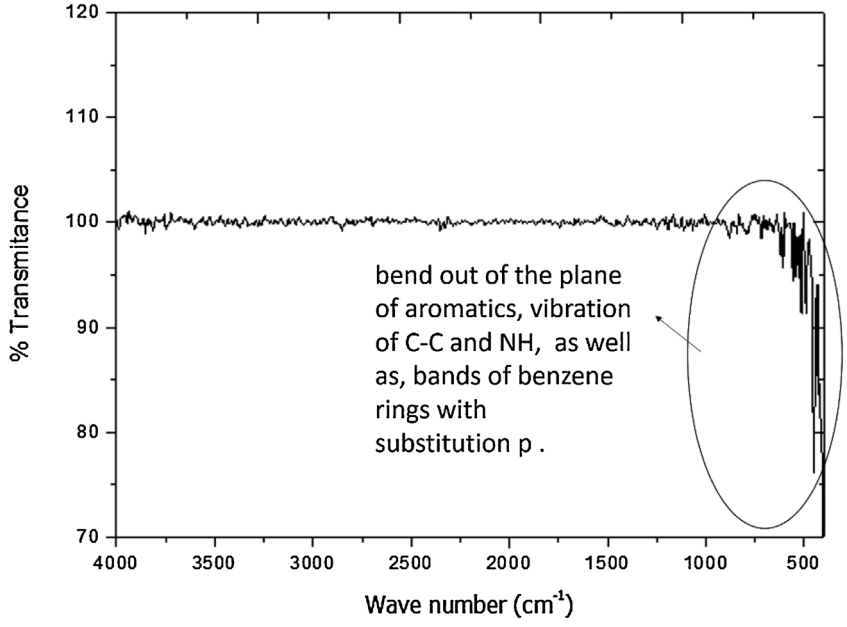

Fig. 7 – FTIR results for unmodified STF (Kevlar control).

greater stability throughout the cycles (the wettability of each sample was calculated using a photography and the software Image J as shown on Fig. 4c).

3. Results and discussions

Results obtained for samples with STF and coupling agent shows higher increase of mass on surface in comparison to others, as shown on Fig. 5. This evidenced that the use of silane agent favours the greater quantitative efficiency of non-Newtonian fluid in the samples.

The samples were analysed by SEM as shown on Fig. 6. The results show higher concentration of silica on surface on the samples with STF and coupling agent when in comparison to others.

Fig. 7 shows obtained FTIR curves for pure Kevlar control sample without any treatment, while the curves shown in Figs. 8 and 9 show high energy transmittance peaks, especially for the sample modified with non-Newtonian fluid STF and coupling agent silane (Fig. 9) respectively. The increase of siloxane bands and the presence of new functional groups were perceptible for both samples studied.

As shown in Fig. 9, the peaks shown at 1720 and 1637 cm^{-1} are attributed to carbon stretch vibrations C=O and vinyl stretch vibrations C=C, respectively, indicating high frequency bonds belonging to the silane bond groups [12–14]. The peaks shown at 2957 cm^{-1} and 2894 cm^{-1} correspond to bands of stretching vibrations of alkyl groups (CH_2 and CH_3) which can be attributed to polyethylene glycol and silane agent. These peaks occur due to the functionalization of the silica particles and indicate the formation of new bonds [15,16].

The peak between 1073 cm^{-1} at 1380 cm^{-1} represents siloxane (Si—O—Si and Si—OC vibrations) which occurring naturally on silica. The samples modified with silane agent showed waves number on a larger scale and with greater intensity,

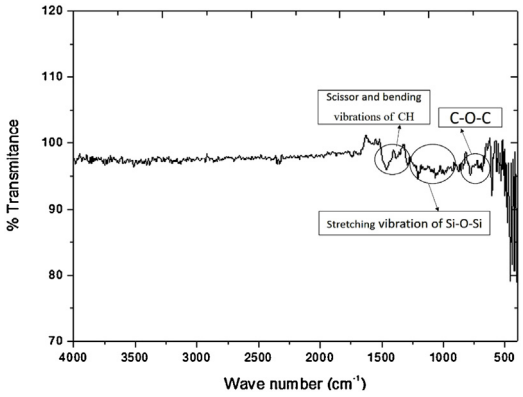

Fig. 8 – FTIR results for samples with STF only (Kevlar + STF).

indicating stronger links [17,18]. Thus, Kevlar samples with STF and silane agent, exhibited high siloxane binding peak, as shown in Fig. 9, promoting a significant increase in siloxane bonds and higher concentrations when in presence of higher amount of nanoparticles in the sample as shown in Fig. 6c, in addition, adhesion (Fig. 10) and best flexibility (Fig. 11) results, as well as depth of penetration results as shown in Fig. 12.

The wettability analysis shows that the more STF fluid on the surface sample is the more wettable. This analysis was carried out according to the different cycles in the martindale (1000 and 2000 cycles), in order to observe if Kevlar control, Kevlar with STF and Kevlar with STF + coupling silane presented a difference in FTS adhesion on the surface fabric. Curves shown on Fig. 10 show that the samples with STF and coupling agent showed higher adhesion of the STF on fiber surface when in comparison to others. The increase in the number of strong siloxane chemical bonds due to addition of the silane agent promoted a significant increase in adhesion,

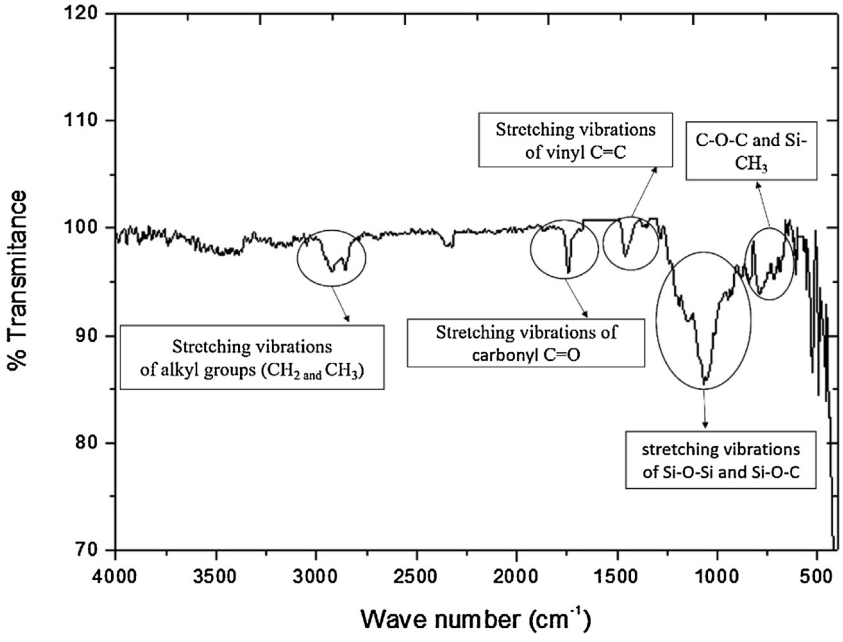

Fig. 9 – FTIR results of modified STF with coupling silane (Kevlar + STF and Coupling silane).

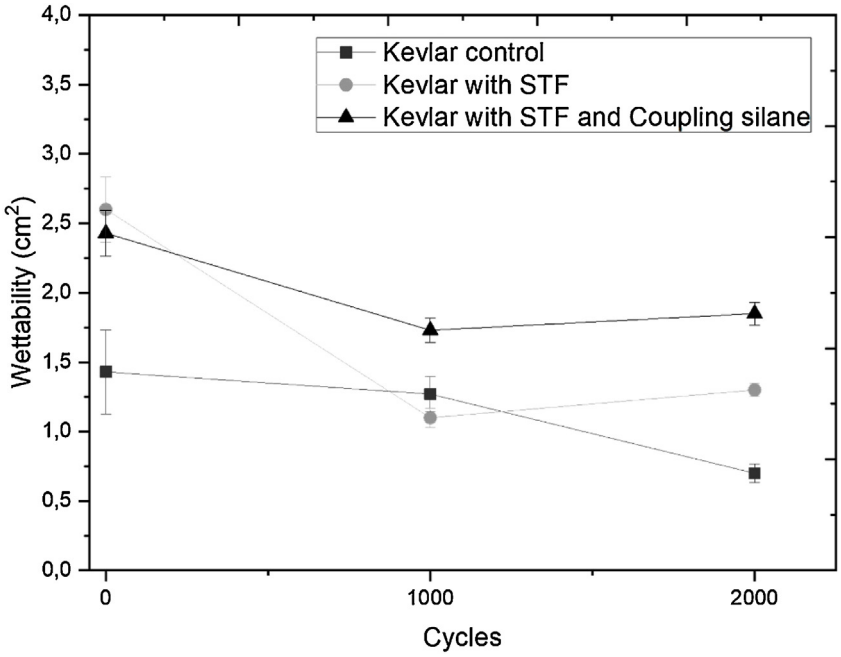

Fig. 10 – Adhesion test (Martindale) for all samples studied.

this is directly associated to the durability and efficiency of surface modification.

Results for bending and drop tower tests were taken and shown in Figs. 11 and 12, respectively. The Fig. 12, shows clearly the samples of Kevlar with STF presented low flexibility (angle of bending = 20°) in comparing to the others (Kevlar control and Kevlar with STF and coupling silane), it shows clearly that the coupling agent stabilized the flexibility samples. The Fig. 12 shows the penetration depth test results for all samples studied the flexibility of the sampled samples was modified Kevlar control, Kevlar with STF and Kevlar with STF + coupling silane. Thus, the bending angle of the Kevlar with STF + coupling silane samples was higher when compared to the Kevlar with STF sample. Showing that the Kevlar sample with STF + coupling silane Kevlar control were more flexible than Kevlar with STF.

According to the results taken, we could conclude that the Kevlar with STF and coupling silane showed significantly less penetration depth (mm) than those Kevlar control (49%) and Kevlar with STF (32%) samples. This can be explained because the sample that presents the use of silane agent, has a greater distribution of impact kinetic energy, dissipating it layer by layer in a gradual behavior. This also shows that upon receiving the impact the sample dissipates the energy over the layers, propagating the smallest portion of the impact to the ballistic panel user, as shown in Fig. 12. The depth of penetra-

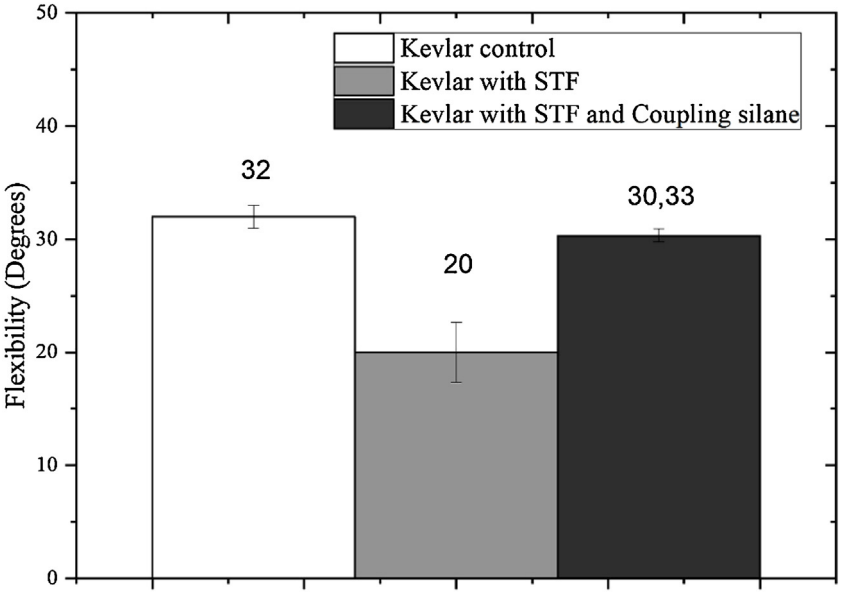

Fig. 11 – Bending for all samples studied.

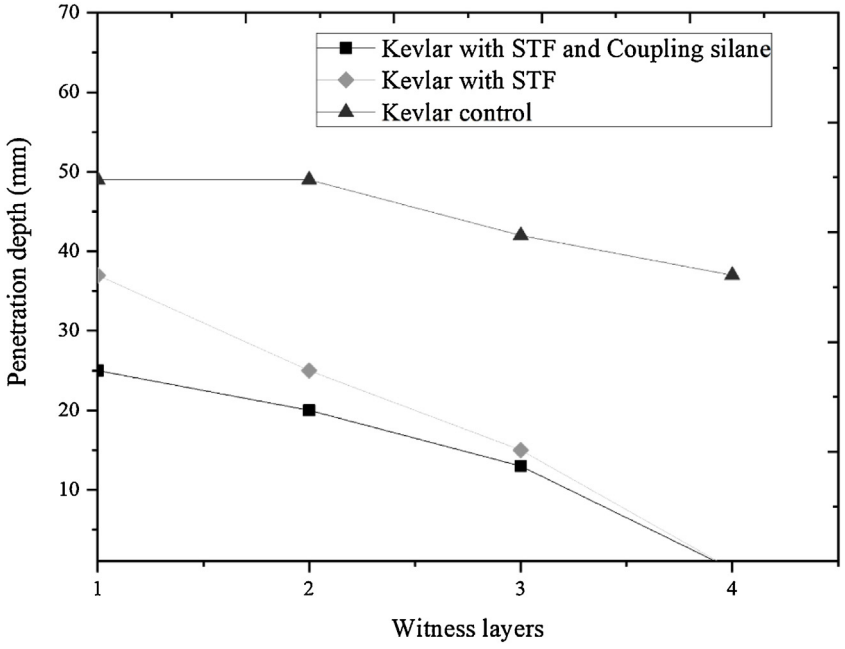

Fig. 12 – Penetration depth tests for all samples studied.

tion of drop tower test as a function of layers of witness paper. It was obtained that all the samples impregnated with STF (Kevlar control, Kevlar with STF and Kevlar with STF + coupling silane) were compared with the standard sample. In this way, they exhibited significant penetration depth performance and in the behavior of absorption and dissipation (layer to layer of witness paper) of impact energy.

4. Conclusions

In this study, STF was prepared using submicron SiO_2 particles spherical of silica dispersed into Polyethylene Glycol (PEG) and prepared with the addition silane agent. The silane coupling agent addition provided strength increase in the shear thickening response. It reveals improvement in the impact energy absorption, significant increase in adhesion, promotes an increase in the number of chemical bonds, as well as, higher peaks, indicating stronger bonds of siloxane, thereby reducing penetration depth, increasing the flexibility in relation to the other samples (Kevlar control and Kevlar with STF). This demonstrates that the use of Silane Coupling agent promotes greater improvement of performance of ballistic penetration resistance of personal protective composites panels.

Conflicts of interest

The authors declare no conflicts of interest.

Acknowledgments

Authors acknowledge to the support of CAPES—Grant for this research and Evonik industries for cooperation in acquiring materials for this research.

REFERENCES

[1] Chhabra RP. Group, and particles in non-newtonian fluids. 2nd ed; 2007, http://dx.doi.org/10.1002/cjce.5450850216.
[2] Chhabra RP. Non-newtonian fluids: an introduction. In: Rheology of complex fluids; 2010. p. 3–34, http://dx.doi.org/10.1007/978-1-4419-6494-6_1.
[3] Hassan TA, Jeelani S, Mahfuz H, Rangari VK. Synthesis of shear thickening fluid using sonochemical method. NSTI-Nanotech 2006;2(2006):637–40, http://dx.doi.org/10.1002/(SICI)1097-4628(19980822)69:8%3C1557::AID-APP10%3E3.0.CO;2-S.
[4] Barman PC, Kairi RR, Das A, Islam R. An overview of non-newtonian fluid. Int J Appl Sci Eng 2016;4:97, http://dx.doi.org/10.5958/2322-0465.2016.00011.3.
[5] Wetzel ED. The effect of rheological parameters on the ballistic properties of shear thickening fluid (STF)-kevlar composites. AIP Conference Proceedings, AIP 2004:288–93, http://dx.doi.org/10.1063/1.1766538.
[6] Joselin R, Jacob Wilson W. Investigation on impact strength properties of Kevlar fabric using different shear thickening fluid composition. Def Sci J 2014;64:236–43, http://dx.doi.org/10.14429/dsj.64.7322.
[7] Clements FE, Mahfuz H. Enhancing the stab resistance of flexible body armor using functionalized SiO_2 nanoparticles. In: International Conference on Composite Materials; 2007. p. 1–11.
[8] Lee YS, Wetzel ED, Wagner NJ. The ballistic impact characteristics of Kevlar R woven fabrics impregnated with a colloidal shear thickening fluid. J Mater Sci 2003;38:2825–33, http://dx.doi.org/10.1023/A:1024424200221.
[9] National Institute of Justice. https://ezp.lib.unimelb.edu.au/login?url=https://search.ebscohost.com/login.aspx?direct=true&db=ncj&AN=SM183652&scope=site, 2000.
[10] Decker MJ, Halbach CJ, Nam CH, Wagner NJ, Wetzel ED. Stab resistance of shear thickening fluid (STF)-treated fabrics. Compos Sci Technol 2007, http://dx.doi.org/10.1016/j.compscitech.2006.08.007.

[11] Gürgen S, Kuşhan MC. The stab resistance of fabrics impregnated with shear thickening fluids including various particle size of additives. Compos A Appl Sci Manuf 2017;94:50–60, http://dx.doi.org/10.1016/j.compositesa.2016.12.019.
[12] Hooshmand T, Van Noort R, Keshvad A. Storage effect of a pre-activated silane on the resin to ceramic bond. Dent Mater 2004;20:635–42, http://dx.doi.org/10.1016/j.dental.2003.08.005.
[13] Rodriguez MA, Liso MJ, Rubio F, Rubio J, Oteo JL. Study of the reaction of γ-methacryloxypropyltrimethoxysilane (γ-MPS) with slate surfaces. J Mater Sci 1999;34:3867–73, http://dx.doi.org/10.1023/A:1004666621479.
[14] Lin M, Xu P, Zhong W. Preparation, characterization, and release behavior of aspirin-loaded poly(2-hydroxyethyl acrylate)/silica hydrogels. J Biomed Mater Res B Appl Biomater 2012;100B:1114–20, http://dx.doi.org/10.1002/jbm.b.32678.
[15] Ravarian R, Wei H, Rawal A, Hook J, Chrzanowski W, Dehghani F. Molecular interactions in coupled PMMA–bioglass hybrid networks. J Mater Chem B 2013;1:1835, http://dx.doi.org/10.1039/c2tb00251e.
[16] Huang FH, Chang CC, Oyang TY, Chen CC, Cheng LP. Preparation of almost dispersant-free colloidal silica with superb dispersiblility in organic solvents and monomers. J Nanoparticle Res 2011;13:3885–97, http://dx.doi.org/10.1007/s11051-011-0342-y.
[17] Choi W-K, Kim H-I, Kang S-J, Lee YS, Han JH, Kim B-J. Mechanical interfacial adhesion of carbon fibers-reinforced polarized-polypropylene matrix composites: effects of silane coupling agents. Carbon Lett 2016;17:79–84, http://dx.doi.org/10.5714/CL.2016.17.1.079.
[18] Li S, Wang J, Zhao S, Cai W, Wang Z, Wang S. Effect of surface modification and medium on the rheological properties of silica nanoparticle suspensions. Ceram Int 2016;42:7767–73, http://dx.doi.org/10.1016/j.ceramint.2016.01.199.

Mathematical correlation between section lines in 3D shapes and fashioning lines in 3D knitted fabrics

SAVIN DORIN IONESI
LUMINITA CIOBANU
MARIANA URSACHE

REZUMAT – ABSTRACT

Corelații matematice între liniile de secțiune ale corpurilor 3D și liniile de conturare din tricoturile cu geometrie tridimensională

Tricoturile 3D prezintă un potențial deosebit pentru aplicații tehnice complexe, cunoscând în ultimele decenii o dezvoltare semnificativă. Prima etapă în proiectarea tricoturilor conturate spațial este reprezentată de trecerea de la planul de secțiune al corpului 3D la planul tricotului. Din punct de vedere matematic, liniile de secțiune ale oricărui corp 3D sunt continue, astfel putând fi definite cu precizie. Tricoturile însă sunt alcătuite din ochiuri cu anumite dimensiuni, care trebuie avute în vedere atunci când se definește modelul matematic al segmentelor din liniile de conturare drepte sau curbe. Lucrarea prezintă o metodă de definire a incrementului vertical, respectiv orizontal ale liniilor de conturare, bazată pe aproximarea erorilor dintre liniile de secțiune continue și liniile segmentate din planul tricotului.

Cuvinte-cheie: model matematic, linii de secțiune, linii de conturare, aproximarea erorilor

Mathematical correlation between section lines in 3D shapes and fashioning lines in 3D knitted fabrics

3D shaped knitted fabrics present a very good potential for complex technical applications and have known a significant development in the last two decades. In order to design a 3D-shaped knitted fabric, the first step to be followed is represented by the transition from the 2D solid evolutes of the geometric shape to the fabric plan. Mathematically, the section lines for each type of 3D shapes are continuous and they can be accurately defined. However, knitted fabrics are made of stitches of certain dimensions that must be taken into consideration when defining the mathematical models of the straight or curved fashioning line segments. The paper presents a method to define the vertical and horizontal increment of a fashioning line, based on the error approximation between the continuous section lines and the segmented lines in the fabric plan.

Keywords: mathematical model, section lines, fashioning lines, error approximation

INTRODUCTION

A 3D shaped knitted fabric is produced using the spatial fashioning technique. These kind of fabrics are characterised by a 3D geometry that is based on a 3D solid with regular or irregular shape. Until now, the researchers focused more on the shape modelling than on the modelling of the section and fashioning lines [1]. To ensure a proper definition of the 3D knitted fabrics, both section lines of the 3D body and the fashioning lines of the 3D shaped knitted fabric must be defined [2, 3, 4]. Fashioning lines have usually two components: one with a decreasing direction and one with increasing direction. The final 3D shape is obtained through the union of these lines according to their specific parameters (line increment and stitch dimension). Taking into account the particularities of the knitted fabrics, the fashioning lines are formed by varying the number of stitches knitted in each row.
Section lines, given by the 2D develop of the 3D solid are represented by continuous lines: straight (with constant increment) or curved (with variable increment). A fashioning line, given by the 2D develop of the fabric plan is segmented, being compounded by multiple line segments [1], as illustrated in figure 1.
Because the fashioning lines are not continuous lines, as it is the case with the section lines, they are quantified using the line increment Δr and Δa, representing the number of rows, respectively needles by which the line varies at each step. The basic element is the knitted stitch and its dimensions – the stitch pitch and height. The fashioning line can be therefore considered as a polygonal line that follows the stitches in the knitted fabric. Due to the nature of these lines (the section line is continuous while the fashioning line is segmented) the equations that define them will differ.

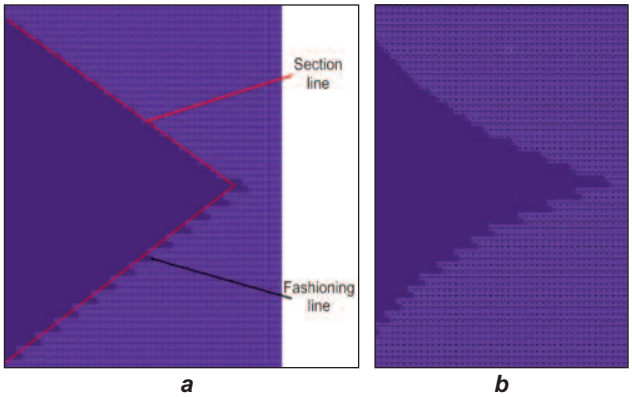

Fig. 1. Aspect of fashioning lines: *a* – straight and *b* – curved

In order to ensure a correct definition of the narrowing and widening steps, which are given by the line increment Δr and Δa, a strictly correlation between section lines in 3D shapes and fashioning lines in 3D knitted fabrics must be made. When this correlation is made, between these lines occur differences that influence the number of stitches that must be produced in a row in order to obtain a certain dimension. To solve this problem the surface of the 3D shape develops bordered by the fashioning line must be determined.

For rectangular knitted panels (when the length and width of the panel are known) the surface and the necessary number of stitches can be easily determined. For knitted fabrics with irregular shape (figure 2) that are defined by a curved fashioning line (as illustrated in figure 1b) a difference or error will occur between fashioning and section lines. Initially this error can be practically approximated but if an exactly shape is required rigorous solutions, represented by the integral calculus and approximation, must be applied. The integral calculus consists in finding the numerical approximation for the surface S [5].

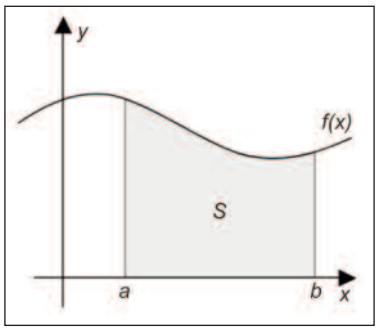

Fig. 2. Numerical integration

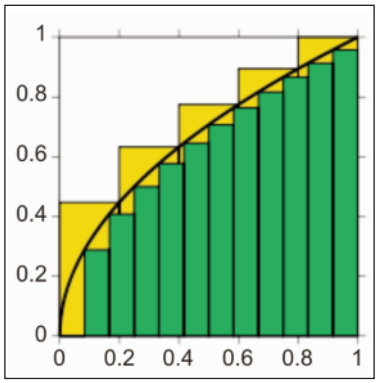

Fig. 3. Error approximation for $y = f(x)$ function with 5 and 12 steps

If the $y = f(x)$ section line curve is consider on [0,1] interval the integral surface of the $f(x)$ function on the given interval is represented by the integral area of f and is noted $\int_0^1 \sqrt{x}\,dx$. The error approximation has been carried out using 5 and 12 steps, as illustrated in figure 3. It can be remarked that if a higher number of approximation steps is used the error between the section and fashioning line is smaller.

ERROR APROXIMATION METHODS

Several techniques for approximating the definite integral can be used [4] to approximate the errors that occur between the fashioning and section lines, so that the surface of the knitted fabric, the number of stitches, the narrowing and widening steps are accurately determined:

- Rectangle rule (also called midpoint rule);
- Trapezoidal rule;
- Simpson's rule.

Rectangle rule

The rectangle method (also called the *midpoint* or *mid-ordinate rule*) computes an approximation to a definite integral, made by finding the area of a collection of rectangles whose heights are determined by the values of the function. The rectangle rule offers three possible solutions, as illustrated in figure 4:

- The left rule uses the left endpoint of each subinterval;
- The right rule uses the right endpoint of each subinterval;
- The midpoint rule uses the midpoint of each subinterval.

For the error approximation of a knitted fabric fashioning line specific geometry the best suitable method is represented by the right rule, which use the endpoint of each interval. For the y_i=f(x_i) function, with $\Delta Dx_i = h_i = \Delta a_i$, the error approximation is given by the following relations:

- Left rule

$$\int_a^b f(x)dx = \Delta a_1 h_1 y_0 + \Delta a_2 y_1 + ... + \Delta a_n y_{n-1} + R_n \quad (1)$$

- Right rule

$$\int_a^b f(x)dx = \Delta a_1 y_1 + \Delta a_2 y_2 + ... + \Delta a_n y_n + R_n \quad (2)$$

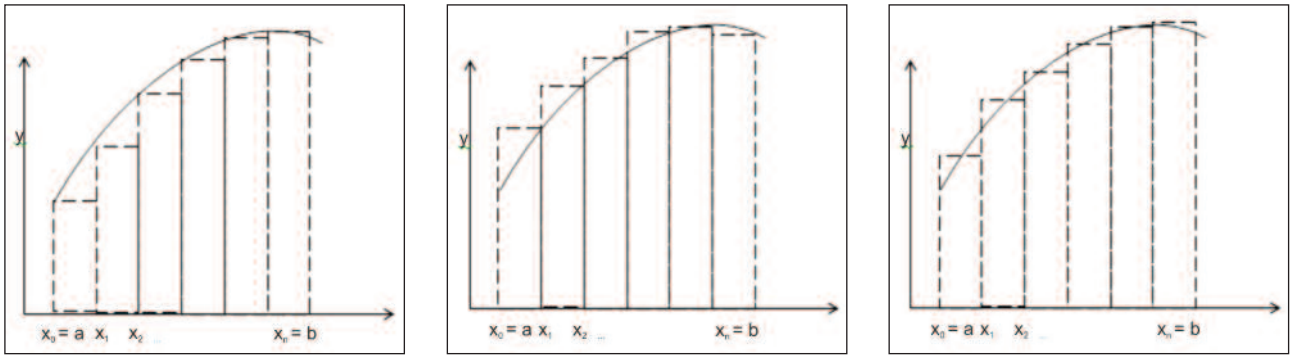

Fig. 4. Error approximation using the rectangle rule

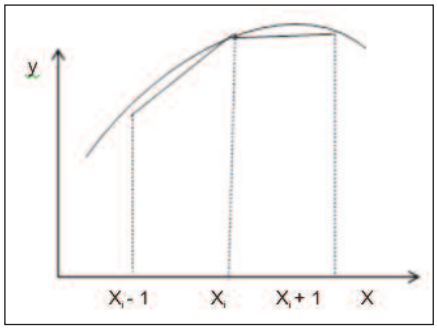

Fig. 5. Error approximation using the trapezoidal rule

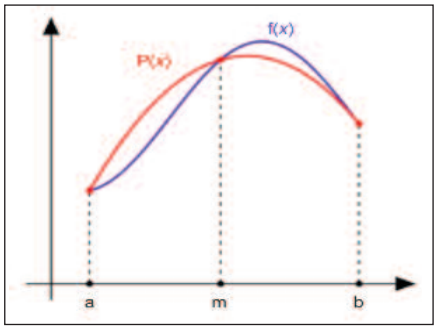

Fig. 6. Error approximation using the Simpson's rule

- Midpoint rule

$$\int_a^b f(x)\mathrm{d}x = \sum_{i=1}^{n} \Delta a_i f\left(\frac{\Delta a_{i-1} + \Delta a_i}{2}\right) + R_n \qquad (3)$$

where: Δa is the horizontal increment, h – the horizontal step and R_n – error approximation.
The vertical increment Δr must be defined in order to complete the calculus of the fashioning line. Generally, the vertical increment can be 1, 2 or 3 courses. When the vertical increment is set up the technical limitations of the knitting process should be considered.

Trapezoidal rule

The trapezoidal rule works by approximating the region under the graph of the function $f(x)$ as a trapezoid and calculating its area, as illustrated in figure 5. On $[x_i, x_{i+1}] = [\Delta a_i, \Delta a_{i+1}]$ segment the trapeze is determined by the $(\Delta a_i, 0)$ $(\Delta a_{i+1}, 0)$ extremities of the segment on OX axis and by the $(\Delta a_i, f(\Delta a_i))$ $(\Delta a_{i+1}, f(\Delta a_{i+1}))$ $f(x)$ function values in the extremities. The error approximation is given by the following relations:

$$\int_a^b f(x)\mathrm{d}x = \sum_{i=1}^{n} h_i \frac{f(\Delta a_{i-1}) + f(\Delta a_i)}{2} + R_n \qquad (4)$$

$$h = \frac{b-a}{n} = \Delta a, \quad x_i = a + ih, \quad i = 0...n \qquad (5)$$

Where: Δa is the horizontal increment, h – the horizontal step and R_n – error approximation.

Simpson's rule

In contrast to the trapezoidal rule, which uses the linear interpolation method (the approximation is made using straight), the Simpson's rule use quadratic polynomial parabolic interpolation (figure 6). One derivation replaces the integrand $f(x)$ by the quadratic polynomial $P(x)$ which takes the same values as $f(x)$ at the end points a and b and the midpoint $m = (a + b)/2$. Due to this reason the precision of this method is superior to rectangle or trapezoidal rule.
The error approximation is given by the following relations:

$$\int_a^b f(x)\mathrm{d}x \approx \frac{\Delta a}{3}\left[f(\Delta a_0) + 4\,f(\Delta a_1) + 2\,f(\Delta a_2) + \ldots + 2\,f(\Delta a_{n-2}) + 4\,f(\Delta a_{n-1}) + f(\Delta a_n)\right] + R_n \qquad (6)$$

where: Δa is the horizontal increment and R_n – error approximation.

ERROR APROXIMATION USING SIMPSON'S RULE

When considering the correspondence between section lines and fashioning lines, equivalence between the continuous surface of the 3D body and the discontinuous fabric made of stitches must be made. The most suitable method used to determine the error between the section and fashioning lines is represented by the Simpson's rule.
An application has been developed using different browser – supported programming languages in order to define fashioning lines of a 3D fabric. The interface and computations was carried out in PHP and JavaScript combined with a mark-up language (HTML). The designed application allow the users to determine the errors using the Simpson's method and the line increment Δr and Δa, according to the bordering function.

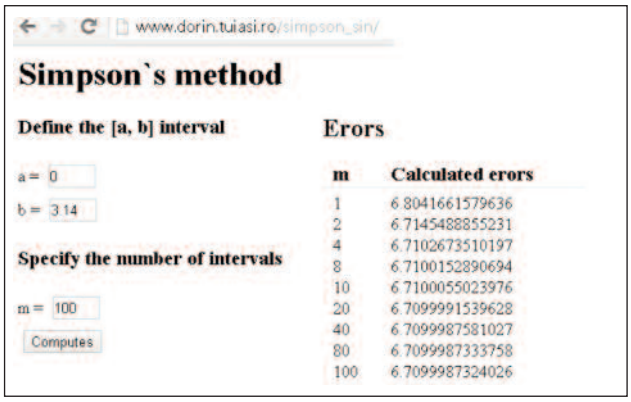

Fig. 7. Error determination for the first example $f(x) = \sin(x) + 1.5$

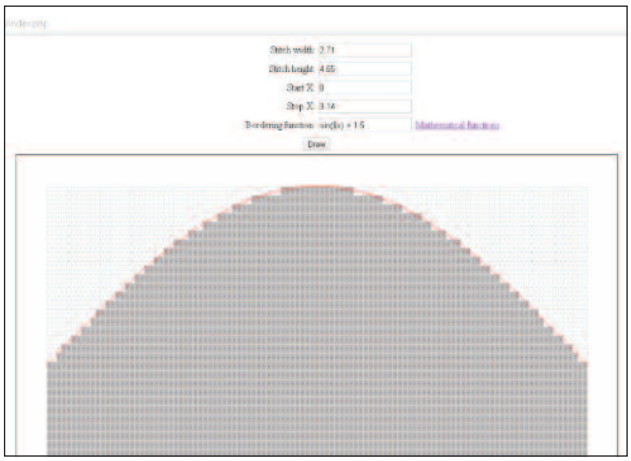

Fig. 8. Narrowing and widening steps for $f(x) = \sin(x) + 1.5$

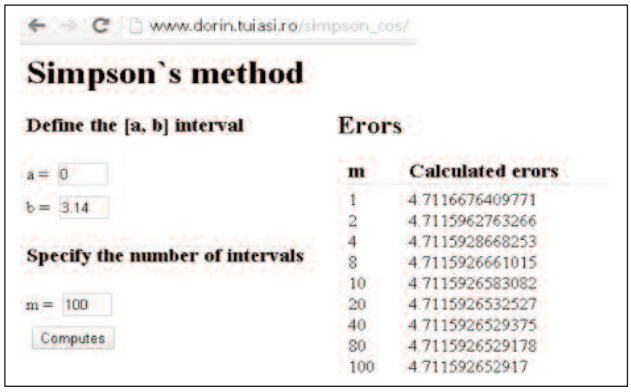

Fig. 9. Error determination for the second example $f(x) = \cos(x) + 1.5$

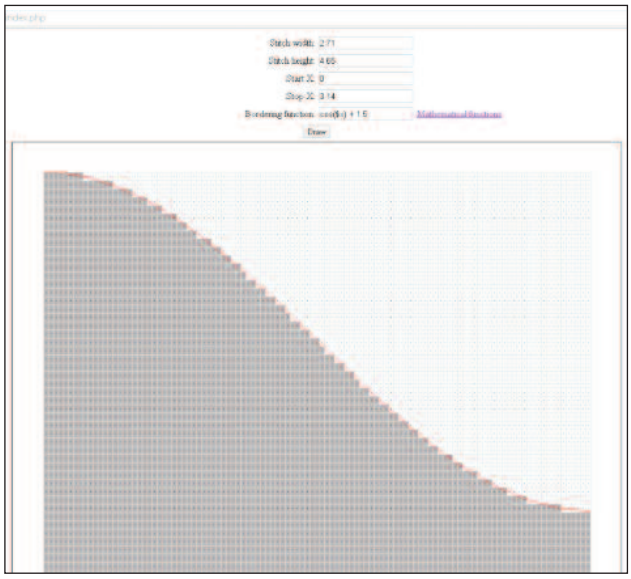

Fig. 10. Narrowing and widening steps for $f(x) = \cos(x) + 1.5$

Two cases have been illustrated for two different functions corresponding to fashioning lines with variable increment: $f(x) = \sin(x) + 1.5$ and $f(x) = \cos(x) + 1.5$. The program calculates the error based on Simpson's rule (figures 7 and 9) and it determines the distribution of stitches along the fashioning lines within the knitted fabric (figures 8 and 10). The stitch distribution is determined based on the stitch dimension (height and width) according to the intended fabric density. In figures 8 and 10, the lighter areas correspond to needles not working in the knitting programme.

CONCLUSIONS

The 3D shaped knitted fabrics that are produced using the spatial fashioning technique have a good potential for technical applications. In order to produce such a fabric it is necessary to ensure the correlation between the 3D shape of the solid and the 2D develop of the knitted fabric. Also the errors that occur between the section and fashioning lines must be determined in order to define the widening and narrowing steps specific for the fashioning technique. The most suitable method that can be used for error determination is represented by Simpson's rule because it allows a smooth approximation between section and fashioning lines.

An application was developed to determine the distribution of stitches along the fashioning lines with variable increment corresponding to the section lines of 3D solids. In both cases that were presented ($f(x) = \sin(x) + 1.5$ and $f(x) = \cos(x) + 1.5$) it must be emphasised that the errors decrease with the increase of the number of intervals considered.

BIBLIOGRAPHY

[1] Ciobanu, L., Ionesi, D., Ciobanu, R., *Design of fashioning lines in 3D knitted fabrics*, In: Industria Textila, 2011, vol. 62, issue 4, pp. 198–201

[2] Dias, T., Fernando, A., Choy, P.K., Xie, P., *Knitting seamless three-dimensional shell structures on modern electronic flat bed knitting machines*, In: Medical Textiles, 1999, pp. 36–43

[3] Power, J., *Knitting shells in the third dimension*, In: JTATM, 2004, vol. 4, nr. 4, pp. 1–12

[4] Dulgheriu,I., Matenciuc, C., Ionesi, D., Moricz, J., *The optimisation of sealing parameters of assembling intended for products made of composite materials*, In: Industria Textila, 2011, vol. 62, issue 4, pp. 209–213

[5] Nicolescu, M., Dinculeanu, N., Marcus, S., *Analiza matematica, I+II*, EDP, 1963

Authors:

IONESI SAVIN DORIN
CIOBANU LUMINITA
URSACHE MARIANA
Faculty of Textiles, Leather and Industrial Management
"Gheorghe Asachi" Technical University of Iasi

Corresponding author:

URSACHE MARIANA
e-mail: ursache@tex.tuiasi.ro

Study regarding the optimization of the mechanical behaviour of glass fibre reinforced concrete

E. MARIN, M. BARBUTA, L. CIOBANU, S. D. IONESI, I. CIOARA, C. DUMITRAS
Technical University"Gheorghe Asachi" of Iasi, Romania

The use of fibre reinforced concrete is well documented and the advantages of such materials in civil engineering refer to improved mechanical strength, improved concrete ductility and increased durability. The literature presents numerous studies concerning the subject. Some of them reveal the ecological trend of replacing cement with waste by-products such as silica, fly ash and slag. In this context it is of interest to study how the fibre reinforcement contributes to the mechanical behaviour of these recyclable composites. It is also important to see how the fibre characteristics affect the mechanical properties of the concrete. The paper presents an optimization study that considers the fibre length and the fibre percentage in the mix as independent variables. The output variable is the flexural strength. The experiment was carried out according to the experimental matrix and the data was processed using DOE++. A mathematical model for the flexural strength was obtained based on the ANOVA analysis. The model was validated. The response surfaces indicate that the optimum areas (maximum flexural strength) correspond to the maximum values of the input variables. The position of the area of maximum in the response surfaces indicate that the output variable can be further increased. Due to processing problems related especially with the percentage of fibres in the mix, only the fibre length was increased, while maintaining the fibre percentage to 1%. The results confirm the improvement of the flexural strength over the limit suggested by the experimental matrix.

(Received June 23, 2014; accepted November 13, 2014)

Keywords: Fibre reinforced concrete, Fly ash, Fibre characteristics, Flexural strength, and optimization

1. Introduction

The use of glass as reinforcement material for concrete started in the 1960s. Researches up to date showed that the reinforcement of concrete with fibres leads to the absorption of the internal strains caused by the local variation in temperature, the drying and the initial contractions of the concrete element [6, 9, 10, and 11].

In Romania, the study of the fibre reinforced concrete is well developed by the civil engineering specialists, as it was recognised as an efficient way of improving mechanical behaviour.

The glass fibre reinforced concrete has numerous applications, such as: ornamental structures, wells, decorative elements, prefabricated panels, façade elements, domes, prefabricated elements, etc.

Further researches on the fibre reinforced concrete refer not only to the improvement of static strength, but also to the control of the cracking process, the improvement of concrete ductility, energy absorption characteristics and resistance to impact and to temperature variations [5, 7, 8]. Currently, the R&D trend is the production of concrete with elements that partially replace the cement, such as fly ash and slag. Such materials satisfy the increasing need for environment protection by adopting the so called no waste technologies [12, 13, 15, and 16]. Mineral components such as silica, slag and fly ash are commonly used as additives or cement replacements. They increase the density of the composite, reduce its porosity and improve the durability of the element. The partial replacement of the Portland cement was initiated in the 1960s and in the following decades [12, 13, 14, 15, and 16]. It cuts down the production costs and also the level of pollution caused by its processing

Almost all studies in the literature concerning this subject are not considering the possibilities offered by the fibre characteristics and the influence these characteristics can present on the concrete composites. Glass fibres (filaments) are not introduced as such in the composite. They are obtained by cutting glass yarns to preset length and therefore the properties of these yarns are very important as well as the knowledge of how the yarn segments are distributed within the concrete composite.

The paper has two objectives: the characterisation of the influence of the glass fibres in a composite with concrete with fly ash matrix and the optimization of the characteristics of these fibres – fibre length and fibre percentage in the mix – so that the material reaches the maximum its mechanical behaviour. The paper considers the flexural strength as the output variable reflecting the mechanical behaviour. It shows a part of a larger research that includes other mechanical properties of the glass fibre reinforced concrete materials.

2. Materials and methods

2.1. Experimental matrix

In order to solve the problem considered for the study – optimization of the use of glass fibres in composites with concrete and fly ash matrix – the advantages and disadvantages of the existing methods for the experiment design were reviewed. The nature of the problem lead to the selection of a central composite design that allows the identification of the optimum areas by generating response surfaces using the experimental data. This type of experiment guaranties the precision of the results and the validity of the conclusions drawn from these results.

The experiment has two input variables: the fibre length (x1) and the percentage of glass fibre in the mix (x2). These variables were identified as significant to the mechanical strength of reinforced concrete. The output variable is the flexural strength of the concrete composite. In this experiment the optimum areas for the output variable correspond to the maximization of the flexural strength.

The coded and natural values for the input variables in the experiment are presented in Table 1.

Table 1. Coded and natural values for the input variables

No.	**Variables**	**Coded variable**		-1.414	-1	0	1	1.414
1.	Fibre length [mm]	x_1	**Natural variable**	5	10	20	30	35
2.	Fibre percentage [%]	x_2		0.25	0.5	1	1.5	1.75

The variation of each variable was carefully considered; the selection of the variation interval is based on the review of literature and on practical experience in producing concrete mixes. Table 2 presents the resulting experimental matrix. According to this matrix, a number of 13 runs are carried out randomly, on samples of glass fibre reinforced concrete, with different combinations of fibre length and fibre percentage in the mix.

Table 2 Experimental matrix

Run	Input variables				Mass of cut fibre [g]
	Coded variables		Natural variables		
	x_1	x_2	Fibre length [mm]	Fibre percentage [%]	
1	-1	-1	10	0.5	319
2	-1	+1	10	1.5	956
3	+1	-1	30	0.5	319
4	+1	+1	30	1.5	956
5	+1.414	0	35	1	637
6	-1.414	0	5	1	637
7	0	+1.414	20	1.75	1116
8	0	-1.414	20	0.25	159
9	0	0	20	1	637
10	0	0	20	1	637
11	0	0	20	1	637
12	0	0	20	1	637
13	0	0	20	1	637

2.2. Characterisation of the glass fibres

The study was carried out using glass fibres rovings, linear density 2400 tex. The yarns were tested to determine their tensile behaviour, the experimental data being presented in Table 3. The tests were carried out on a SATRA STM 466 testing machine, according to ASTM D2256 [3]. For the calculus of the Young's modulus and strength, the cross section of the glass roving was considered to be rectangular.

Table 3. Mechanical characteristics of the glass roving.

Yarn	Breaking force [N]	Breaking elongation [%]	Young's modulus [N/mm^2]	Strength [N/mm^2]
Glass 2400 tex	704.1	3.02	16058.61	201.17

The glass rovings were cut to the specified dimensions, according to the experimental matrix. The corresponding values of the mass of the cut fibres were calculated based on the mass of the testing samples and the value of the second variable (x2).

The introduction of the fibres in the mix made for the concrete with fly ash created some problems related to processing. These problems referred to the phenomena of fibre floating (when mixing), fibre clogging and fibre snagging (in the concrete composite) [2]. These problems affected the uniformity of the fibre distribution in the concrete samples and measures were taken to eliminate them, by modifying the mixing process.

2.3 Testing of the glass reinforced concrete samples

The tests were conducted according to SR EN 12390-4: 2005 [4], on 550x50x50 mm prisms of glass fibre reinforced concrete. The samples were tested using a hydraulic press. The force required for complete breaking was measured. Fig. 1 shows how the samples were tested and their aspect after breaking.

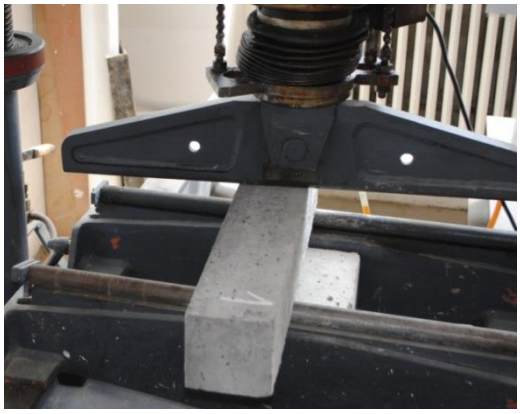

a) while testing

b) after testing

Fig. 1. Testing for flexural strength.

The test results showed that the presence of glass fibres improves the way the reinforced concrete samples break. If for the samples of concrete the breaking is sudden (the so called catastrophic breaking), the reinforcement with glass fibres slows down the fracture process by generating cracks in the concrete before the destruction of the sample. These cracks determine a gradual breaking process, indicating an improved behaviour for the reinforced concrete element.

The analysis of the cross section of the samples of glass fibre reinforced concrete offered information on the degree of dispersion of the fibres in the concrete mix. The first observation is that the fibres are distributed uniformly and without preset directions in the matrix, as exemplified in Fig. 1.b.

Another observation is that the cut fibres do not lose their integrity, maintaining the initial bundle, even if the concrete penetrates between individual fibres, as illustrated in Fig. 2. Therefore, the dimensions of bundle of fibres (reflected by the yarn/roving fineness) influence the distribution of the glass fibre in the concrete mix.

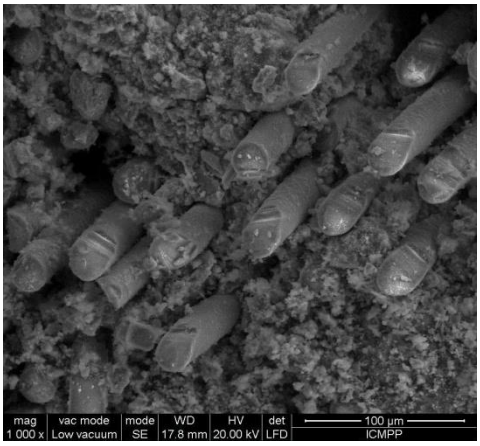

Fig. 2. Cross section of the concrete prism after testing.

3. Results and discussions

The experimental results regarding the flexural strength of the glass reinforced composites with concrete and fly ash matrix are presented in Table 4.

Table 4. The values of the flexural strength according to the experimental matrix.

	Variables		Flexural strength [N/mm^2]
	x_1	x_2	
1	-1	-1	3.54
2	-1	+1	3.36
3	+1	-1	2.74
4	+1	+1	4.18
5	+1.414	0	3.91
6	-1.414	0	3.98
7	0	+1.414	4.32
8	0	-1.414	3.89
9	0	0	3.95
10	0	0	4.12
11	0	0	3.92
12	0	0	3.97
13	0	0	3.93

3.1. Statistical processing of the experimental data

The statistical processing of the experimental data was carried out using DOE++ that allows the plotting of the 2D and 3D response surfaces and the determination of the areas of maximum for the output variable (flexural strength). The interactions of the two input variables were determined based on the extreme and average experimental values. The relevance of the model was considered for two levels of confidence - L1 (90%) and L2 (70%).

An ANOVA analysis was carried out using the experimental data. It shows that the linear and quadratic effects have a significant influence on the model for both levels of confidence. The regression equation giving the mathematical model for the flexural strength is:

$$Y = 3.932 + 0.2737x_1 + 0.5738x_2 - 0.1575x_1x_2 - 0.2954x_2^2 \quad (1)$$

The response curves obtained for the output variable have as optimum value (the point of absolute maximum) the point corresponding to the coordinates: x1= 30 mm and x2 = 1.5% representing the highest values considered for both variables. In this case, the maximum corresponds to a combinations of factors considered in the experimental matrix. The flexural strength for this point is 4.18 N/mm^2, representing an increase of 33.3% in reference to the witness sample (concrete with fly ash).

The positions of the response curves in Fig. 3 suggest the importance of the second parameter – the percentage of fibres in the mix. This fact is also confirmed by the interactions matrix presented in Fig. 4. The matrix shows that the effect of the first independent variable (the length of the fibres) is not as strong as the effect of the second variable on the flexural strength.

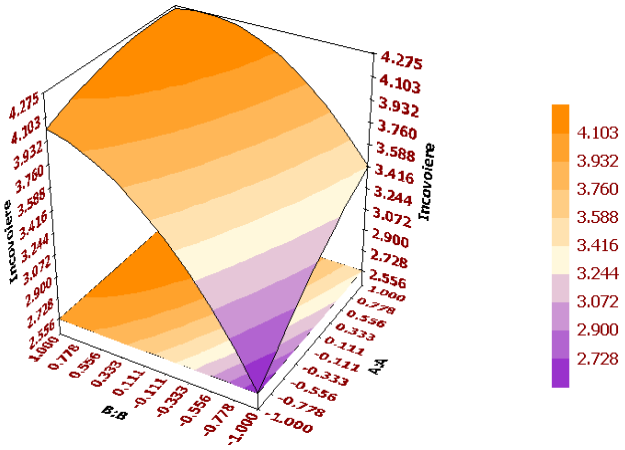

Fig. 3. 3D response surfaces for the flexural strength.

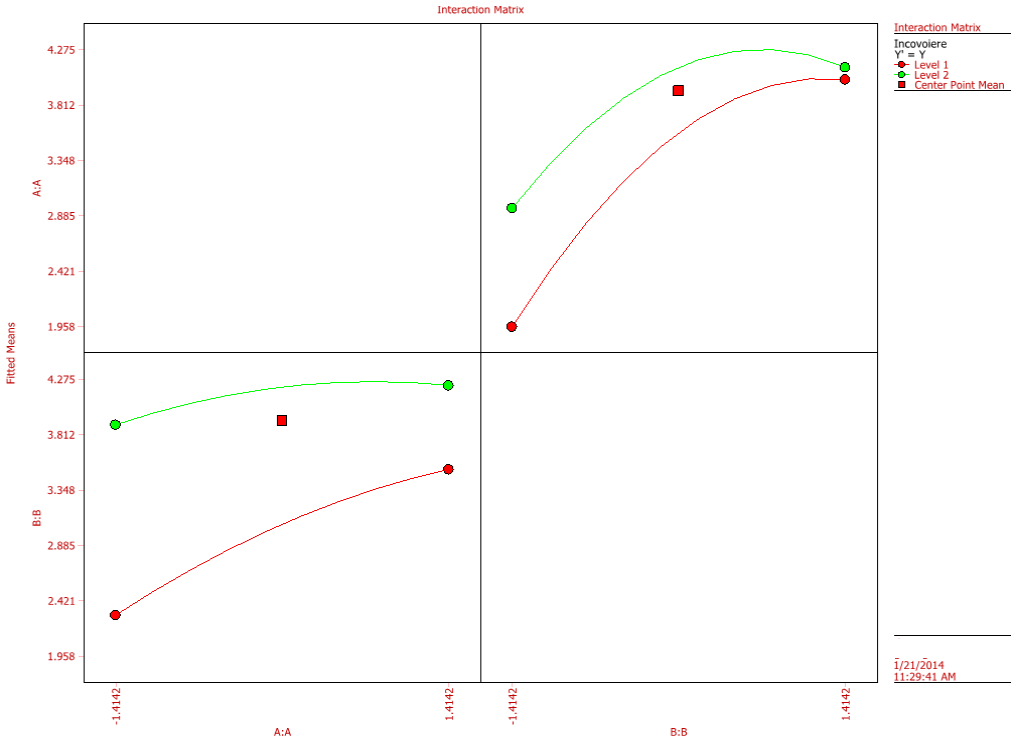

Fig. 4. Interactions of the experimental matrix.

The 2D response surface illustrated in Fig. 5 indicates more clear the position of the point of maximum. Furthermore, this graphic show that the plot area of maximum is not completely placed inside the surface defined by the experimental matrix.

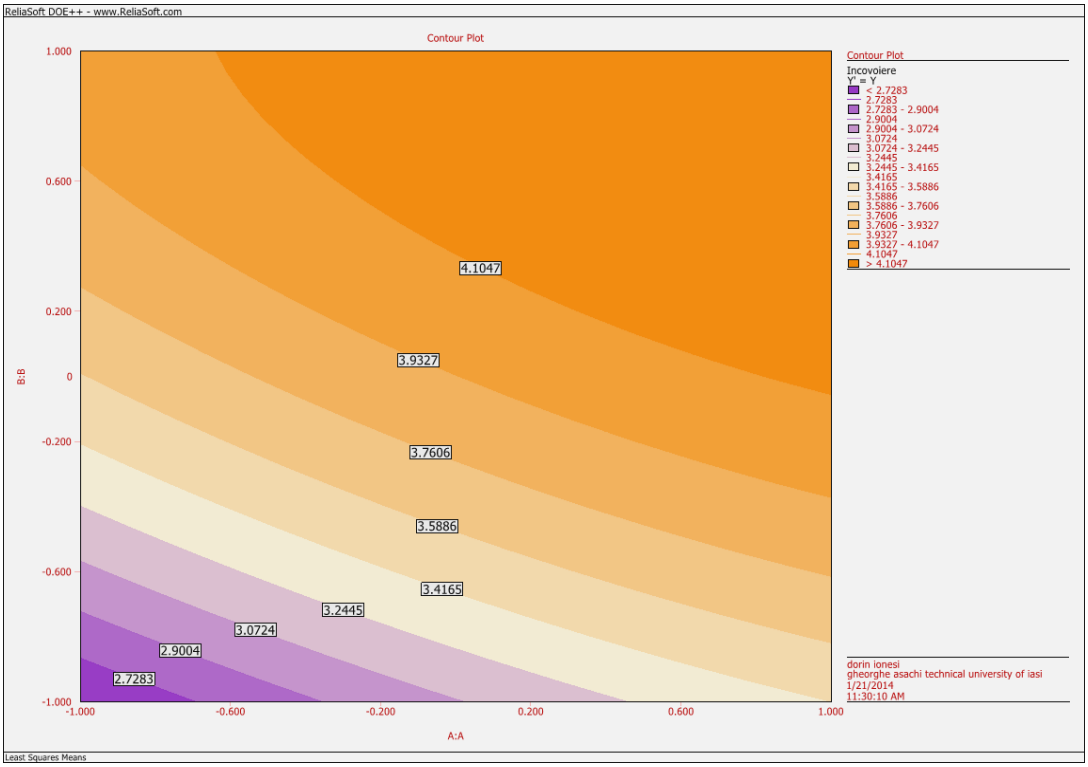

Fig. 5. 2D response surfaces for the flexural strength.

Considering the influence of the length of the fibre on the flexural strength of the composite with concrete matrix, this can be seen for all values of the second variable (fibre percentage in the mix), but it grows for fibre percentages higher than 1%. The graphs suggest that an increase of the fibre length could be beneficial for the mechanical behaviour of the concrete elements (flexural strength).

For the lower fibre percentages (0.25% and 0.5%), the strength is decreased in reference to the witness - approx. 25% less for the concrete variant corresponding to Run 8 (x1 = 20 mm and x2 = 0.25%) and approx. 12% for the concrete variant corresponding to Run 1 (x1 = 10 mm and x2 = 0. 5%). It is interesting to emphasise that in the case of 0.5% fibre in the mix, when increasing the fibre length to x1 = 30 mm, the flexural strength improves in reference to the witness with approx. 15%.

Of course, the increase of the two variables must be considered taking into view the problems related to the processability of the concrete mix that were mentioned above [2]. This means that there will be certain limits to the fibre length and fibre percentage due to the difficulties related to the mixing of the glass fibres with the concrete.

It can be concluded that the flexural strength is controllable through a combination of both factors. The strength can be increased either by the use of higher length for the fibres and a lower percentage in the mix, or by maintaining lower values for the cut fibres (20 mm seems to be the inferior limit) and increasing the fibre percentage.

3.2. Validation of the mathematical model

The mathematical model resulting from the experimental data must be validated. As mentioned above, the point of maximum was determined for a pair of input variables from the experimental matrix, in natural values x1 = 30 mm and x2 = 1.5%. The experiment (run 4) was repeated and the experimental data obtained were similar to the calculated data.

Furthermore, the possibility of improving the flexural strength by increasing the fibre length over the range considered in the experimental matrix was studied. Other three length values for the cut glass fibres were used to determine the flexural strength, namely 45, 50 and 60 mm, while the percentage of fibres in the mix was kept at 1%. This way, the problems related to processability were eliminated. Table 5 shows the values obtained for the flexural strength in the case of the higher values for the fibre length.

Table 5. Flexural strength for the chosen fibre lengths.

Caracteristici fibră		Rezistența la încovoiere (N/mm^2)
Lungime de fibră (mm)	Procent de fibră (%)	
35	1	4.29
45	1	4.35
50	1	4.41
60	1	4.5

The experimental data confirms that the point of maximum in the experimental matrix was correctly

determined, but also that the flexural strength of the glass fibre reinforced concrete with fly ash can be further improved by using higher length for the cut fibres. The graph from Fig. 6 presents the variation of the flexural strength with the fibre length, considered for the extended interval, from 5 mm to 60 mm. For all values, the fibre percentage was maintained constant to 1%. For comparative purposes, the graph also shows the flexural strength of the witness - concrete with fly ash.

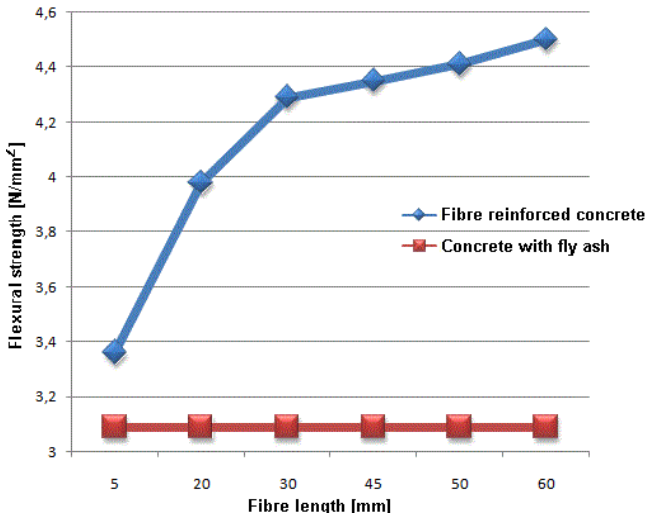

Fig. 6. Variation of flexural strength with the fibre length, for 1% percentage of glass fibre in the mix.

The flexural strength can be improved up to 50%. The possibility of increasing the fibre percentage must also be considered, but such high values for the fibre length presented the risk of processing problems that can affect the uniformity of the composite.

The graph also shows that the strength increases significantly in the range included in the experimental matrix (up to 35 mm). The increase of strength from 35 mm up to 60 mm fibre length is not as steeped and suggests that this length approaches the limit of its practical interval.

4. Conclusions

The paper presents the modelling of the mechanical behaviour of glass reinforced concrete with fly ash, in view of the recent researches for improving the strength of the building elements made with waste materials.

The paper aims at optimizing the characteristics of the glass fibres used in the concrete mix, considering the fibre length and the fibre percentage in the mix as the independent variables. An experimental matrix based on a composite experimental design was defined. The output variable is the flexural strength.

The experimental study allowed drawing practical conclusions on the way the glass fibres influence the processability of the composite with concrete and fly ash matrix. The observations made during processing confirmed the variation intervals chosen for the two variables. It was observed that a higher fibre percentage, combined with higher fibre length caused problems regarding the distribution of the fibres in the composite and its strength.

The experimental data was processed and response surfaces were obtained. These surfaces indicate the followings:

- The optimum value (the point of maximum) is obtained for the maximum values of the input variables (code values x1 = +1 and x2 = +1)
- The second variable x2 (percentage of fibres in the mix) presents the strongest influence on the flexural strength; the influence of the first variable (fibre length) is more visible when the fibre percentage increases.
- For both variables, the lower part of their variation intervals are not improving the flexural strength. The strength is significantly improved starting with 20 mm length and 1% fibre in the mix.

The experiment was validated by testing in the point of maximum (that coincided with a run from the experimental matrix). The practical results confirmed the model. Furthermore, the position of the area of maximum shown by the response surfaces suggests that another increase in both variables can further improve the flexural strength of the concrete composite. Considering the processing problems encountered while producing the samples, it was preferred to increase the fibre length, while maintaining the fibre percentage to 1%, a value that ensured optimum processing. The experimental results confirm the improved flexural strength and suggest that a length of 60 mm approaches the limit to which the mechanical behaviour can be increased.

The tests also showed the importance of the yarn fineness on the distribution in the concrete mix and subsequently on its strength.

References

[1] E. Marin, I. Cioara, L. Ciobanu **S**tudy regarding the mechanical behaviour of high performance fibres, ISKA, Iași, p.21, June, 2013.

[2] E. Marin, M. Bărbuță, L. Ciobanu, I. Cioară, Practical aspects related to the testing of FRC, Technical Textiles. Present and Future Symposium, Iași, 2013.

[3] ASTM D2256 Standard Test Method for Tensile Properties of Yarns by the Single-Strand Method, ASTM collection, vol. 7.1, 2008, on CD.

[4] SR EN 12390-5:2005 Încercare pe beton întărit. Partea 5: Rezistența la întindere prin încovoiere a epruvetelor (http://www.mdrl.ro/_documente/constructii/reglementari_tehnice/lista_standarde.pdf, accessed 15.12.2013).

[5] C.D. Johnston, Fibre Reinforced Cement and Concrete - Advances in Concrete Technology, Canada, 1992.

[6] C. Avram, C. Bob, New types of special concrete – Faculty of Civil Engineering, Technical Publishing House Buc. 1980.

[7] S. Price, Fibre-Reinforced Polymer –

Reinforcement for Concrete Structures, Proceedings of the 6th International Symposium on Fibre-Reinforced Polymer (FRP) Reinforcement for Concrete Structures (FRPRCS-6), Singapore, edited by Kiang Hwee Tan, Singapore, vol. I, 2003.

[8] K. Laoubi, E.F. El-Salakawy, B. Benmokrane and M. Pigeon, Durability of Concrete Beams Reinforced with GFRP Bars under Different Environmental and Loading Conditions, Proceedings of the 6th Symposium regarding the reinforcement of concrete structures, edited by Kiang Hwee Tan, Singapore, vol. I, 2003.

[9] G. Nawy Edward, Fundamentals of High-Performance Concrete, State University New Jersey, second edition, 2001.

[10] J.E. Bolander, S. Choi, S.R. Duddukuri, Internațional Journal of Fracture, Springer, **154** (1-2), 73 (2008).

[11] H. Oucief, M.F. Habita, B. Redjel, International Journal of Civil Engineering, **4** (2), 77 (2006).

[12] M.L. Berndt, Construction and Building Materials, Elsevier, **23**, 2606 (2009).

[13] M. Bărbuță, M. Harja, D. Babor, Romanian Journal of Materials, 40, 3 (2010).

[14] A. Marmandiu, R. Popescu, Environmental impacts of using fly ash, Bulletin of the Polytechnic Institute Iaşi, p. 1453, 2009.

[15] J.W. David, Properties and Construction Guidelines, London, **1**, 2005.

[16] F.Q. Zhao, W. Ni, Conservation and Recycling, **52**, 303 (2007).

*Correspondent author: dumitrascata@yahoo.com
lciobanu@easynet.ro

Evaluation of impact behaviour of composite materials using Taguchi method

SAVIN DORIN IONESI
RAUL FANGUEIRO
LUMINIȚA CIOBANU

CĂTĂLIN DUMITRAȘ
MARIANA URSACHE
IONUȚ DULGHERIU

REZUMAT – ABSTRACT

Evaluarea comportamentului la impact al materialelor compozite, utilizând metoda Taguchi

Studierea comportamentului la impact al materialelor compozite este mare importanță, având în vedere solicitările dinamice la care sunt supuse acestea pentru diverse aplicații. Materialele compozite ranforsate cu structuri tricotate tridimensionale au o largă utilizare în domeniul articolelor tehnice. Principalele lor avantaje sunt reprezentate de formabilitatea foarte bună, anizotropia controlată și un raport optim între masă și rezistență. În lucrare sunt analizate materiale compozite avansate, ranforsate cu structuri tricotate tip sandwich, cu diferite dimensiuni ale celulei, realizate din Kevlar și Twaron, fire de in și o matrice termorigidă. Comportamentul la impact de intensitate redusă al materialelor compozite ranforsate cu structuri tridimensionale, tricotate din bătătură, a fost modelat prin metoda Taguchi, în scopul optimizării caracteristicilor semnificative pentru acest tip de impact. Rezultatele obținute în urma modelării au fost validate prin studii experimentale.

Cuvinte-cheie: materiale compozite, impact de intensitate redusă, metoda Taguchi

Evaluation of impact behaviour of composite materials using Taguchi method

Impact behaviour is a major target in designing advanced composite materials because composites are often used in applications which imply dynamic loads. Composite materials reinforced with 3D knitted fabrics present a wide range of applications in the technical field. Their main advantages refer to excellent formability, controlled anisotropy and good mass/strength ratio. The paper considers advanced composite materials reinforced with sandwich fabrics with various cell sizes, made of Kevlar, Twaron and linen yarns, and thermoset matrix. Low velocity impact behaviour of composite materials reinforced with 3D weft knitted fabrics is modelled using the Taguchi method based on orthogonal arrays, in order to maximize the composite characteristics significant for this type of impact. The results obtained through Taguchi analysis are validated by experimental data.

Key-words: composite materials, low level impact, Taguchi method

Technical textiles are high performance textiles with increased functionality that are produced primarily for their functional characteristics and technical performance rather than for their aesthetic or decorative properties which are less or not important.
The applicability of composite materials reinforced with technical textile structures in engineering has grown exponentially in recent decades. A composite material is an advanced structure made from at least two distinct materials that are combined at macroscopic scale. The applications where textile reinforced composites are suitable cover an extremely wide range of domains – from buildings [1], to industrial applications [3], [7], to protective equipment [6] or even medical products.
Composite materials are primarily a suitable choice for producing light-weight structures due to their excellent weight/stiffness and weight/ ratio properties. The mechanical properties of composite materials are influenced by the mechanical properties of matrix, producing technology, properties of reinforcement preforms, adhesion between matrix and reinforcement preforms and fibre volume fraction.
Composite preforms refer to textile materials that can be obtained by knitting, weaving, braiding and nonwoven technologies. In order to select the optimal technological process for producing composite performs both strengths and weaknesses of each must be taken into account. The potential and the use of 3D knitted fabrics for technical applications are documented throughout literature [4]. Knitted preforms present the advantages of a superior mass/resistance ratio, low implementation time, low amount of resulting wastes and better control of the final shape and the quality of the product.
The sandwich fabrics with connection through knitted layers (single or double) are characterized by a complex geometry, for which the shape and dimensions of the cross section depend on the connecting layer [4]. The shape of the connecting layer can be different, varying from rectangular to elliptic, *V* shaped, trapeze etc.

The principle of producing sandwich fabrics requires knitting the two independent layers, and then the connecting layers while the outer layers production is stopped. The recommended needle selection for knitting the outer and connecting layers is 1:1.
In order to obtain composite materials different techniques can be used:

– embedding of reinforcement material in a matrix, that can be represented by a macromolecularsubstance or a colloidal solution or suspension with coagulation properties;
– reinforcing the matrix with layers of reinforcement materials, resulting a laminate composite.

In the last decades a significant research effort has been made to study the impact behaviour of composite materials with textile reinforcements. Several researchers [2], [8], [9] have studied the problem by examining the material properties before and after the impact. Impact load can be classified [9] in low, medium, high and hyper velocity, according to the impactor speed, as presented in figure 1. The effects of low impact velocity have gained importance in real life situations, such as bird hits, tool drop or contact with other materials that can cause internal invisible damage, irremediably affecting the mechanical properties of composites.

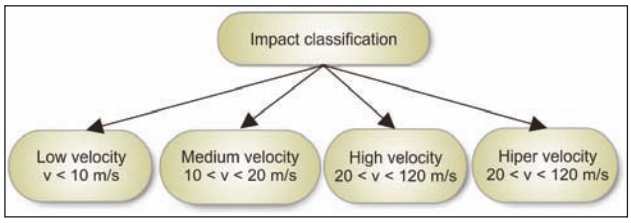

Fig. 1. Impact classification

Up to now, the evaluation of impact behaviour of composite materials reinforced with sandwich weft knitted fabrics has been made through the classical methods that involve varying one parameter at a time and keeps the rest of them constant. These methods require a large number of experimental samples, are time consuming and do not provide information regarding the interactions between parameters. In order to solve these problems, Taguchi method was designed based on the concept of orthogonal arrays. Although Taguchi method was successfully applied in many fields, such as chemical engineering, electronics, genetic algorithm, so far it has not been widely used in textile areas.
The statistically based Taguchi method was used to identify the importance of factor designs and to suggest an optimized design that can produce the optimal impact resistance for composite materials reinforced with 3D sandwich knitted fabrics.

DEVELOPMENT OF 3D COMPOSITE MATERIALS

The experimental work focused on the production of *U* shaped sandwich knitted preforms, presented in figure 2. The 3D knitted fabrics were programmed on a Sirix station and produced on Stoll CMS 320 TC weft flat knitting machine, gauge 10E.
The outer layers are knitted independently on selected needles. When initiating the connecting layer the even needles are inactive, when knitting the outer layer the uneven needles receive a tuck loop that binds the outer and connecting layer together. After finishing the final row in the connecting layer, the stitches are transferred on the uneven needles of the opposite bed, ensuring the sandwich fabric integrity. The knitting of the outer layers restarts. The cell height depends on the number of rows in the outer layers, while the cell width is determined by the number of rows in the connecting layer.
The outer layers were made using Kevlar-Inox and Twaron yarns and for connecting layers linen and Kevlar-Inox yarns were used. The fabric compactness, required to increase the volume fraction of the composites, was improved by inserting Twaron yarns, as illustrated in figure 3.
The 3D composite materials studied in this paper were produced using epoxy EPICURE 04908 resin as matrix and Vacuum Assisted Resin Transfer Moulding Technology (VARTM). The composites were cured at room temperature (23ºC). The mixing ratio of the matrix had 30% EPIKURE Curing Agent 04908 and 5% Dearing agent BYK A535. Table 1 presents the main characteristics of the resin used.
The final aspect of composite materials reinforced with weft knitted sandwich preforms is exemplified in figure 4. All knitted fabrics and composite materials were produced at University of Minho, Portugal.

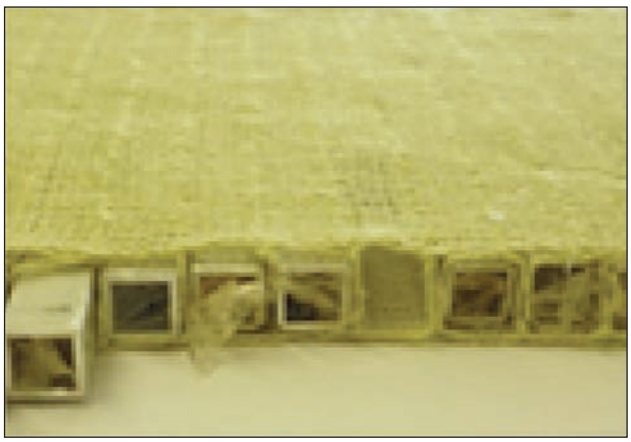

Fig. 2. *U* shaped sandwich knitted fabric

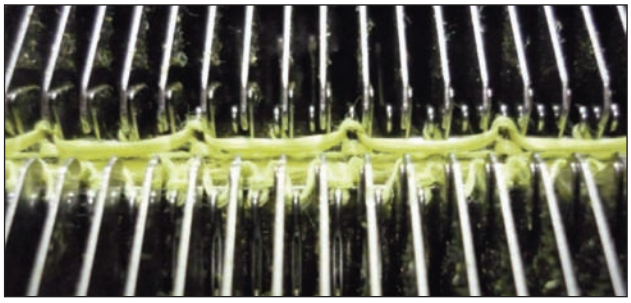

Fig. 3. Production of sandwich fabric

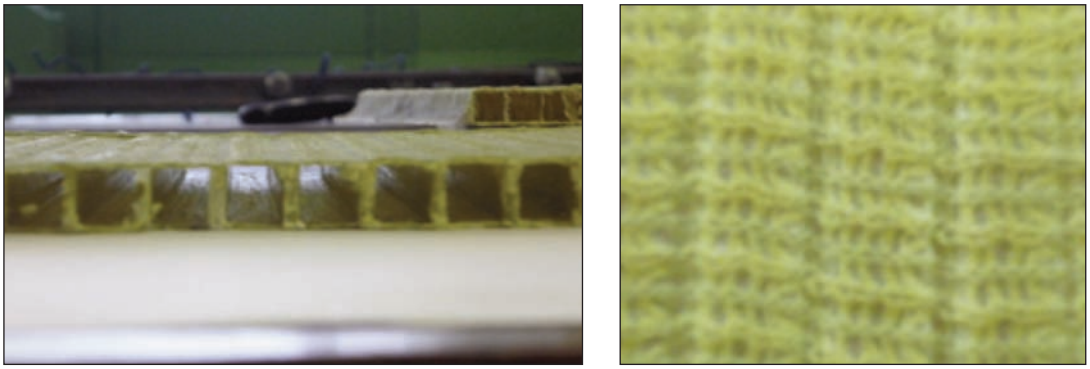

a *b*

Fig. 4. Composite material with 3D textile reinforcements – aspect of outer and connecting layers

Table 1

PRINCIPAL CHARACTERISTICS OF EPOXY EPICURE 04908 RESIN		
Properties	**Unit**	**Epoxy Epicure 04908**
Viscosity at 25°C	Mpa.s	10
Density	g/cm^3	1.15
Tensile strength	MPa	74
Tensile strain	%	9.4
Tensile modulus	MPa	2 900
Flexural strength	MPa	112
Modulus in flexure	MPa	3 100
Water absorption after 24 hours, 23°C	pbw	0.18
Water absorption after 168 hours, 23°C	pbw	0.432

EVALUATION OF IMPACT BEHAVIOUR USING TAGUCHI METHOD

The experimental matrix contains two input variables, one at four levels and the other at two levels, as presented in table 2. The selection of the signal factors was carried out so that the studied process can achieve the expected performance and have a minimum sensitivity to noises. The current study targeted the influence of signal parameters on the impact resistance of advanced composite materials.

Table 2

SIGNAL FACTORS SELECTION		
Levels	**Structure**	**Cell dimension**
1	Kevlar	10 x 10 mm
2	Kevlar/Linen	10 x 15 mm
3	Kevlar/Twaron	-
4	Kevlar/Twaron/Linen	-
Symbol	*A*	*B*

The first two columns of table 3, noted *A* and *B* represent the signal factors (structure and cell dimension), while the following two, noted N_1 and N_2 are the noise factors (impact resistance of composite materials). Signal to noise ratio (noted *S/N* ratio) is a measure used in science and engineering that compares the level of desired signal parameters to the level of background noise parameters.

The main purpose in applying the *S/N* ratio is to find the optimum combination of signal parameters that influence the system so that the *S/N* ratio is maximized. This way, these parameters become system control factors [5]. The *S/N* ratio can be determined for the following cases:

Table 3

EXPERIMENTAL DESIGN USING L_8 ARRAY AND EXPERIMENTAL RESULTS							
Experiment	***A***	***B***	N_1	N_2	**Mean**	**Standard deviation**	***S/N* ratio**
1	2	2	1 419.35	1 395.68	1 407.515	16.7372	62.9681
2	3	1	891.22	964.08	927.65	51.5198	59.3276
3	3	2	1 161.28	1 076.5	1 118.89	59.9485	60.957
4	4	2	1 170.29	1 054.69	1 112.49	81.7415	60.8907
5	2	1	2 430.59	2 385.23	2 407.91	32.0744	67.6316
6	1	2	1 181.29	1 225.12	1 203.205	30.9925	61.6025
7	1	1	1 245.3	1 287.35	1 266.325	29.7338	62.0473
8	4	1	2 024.49	1 998.21	2 011.35	18.5828	66.0692

- smaller the better

$$\frac{S}{N} = -10 \log (s^2 + \overline{y}^2) \quad (1)$$

- nominal is the best

$$\frac{S}{N} = 10 \log \left[\left(\frac{\overline{y}^2}{s^2} \right) - \frac{1}{n} \right] \quad (2)$$

- larger the better

$$\frac{S}{N} = -10 \log \left[\sqrt{\overline{y}^2} \left(1 + 3s^2 \cdot \sqrt{\overline{y}^2} \right) \right] \quad (2)$$

where:
s is standard deviation;
y – nominal value;
$\overline{y}$ – average of determined values;
n – number of runs.

After the analysis of orthogonal array models, the signal parameters and their specific levels, L_8 orthogonal array has been considered adequate. After defining the signal and the noise factors, the statistical analysis and determination of the mean, standard deviation and *S/N* ratio can be carried out, as shown in table 3. The *S/N* ratio has been calculated using the formula defined for larger the better case.

The significance of the signal factors reported to *S/N* ratio is given after performing the Taguchi analysis. The classification of influence level, presented in table 4, is: maximum influence – the factor *A* (knitted structure) and minimum influence – the factor *C* (cell dimension).

The results that were obtained after the statistical analysis for *S/N* ratio and mean was performed are graphically represented in figure 5 and figure 6.

Table 4

RESPONSE TABLE FOR *S/N* RATIOS
LARGER IS BETTER FORMULA

Level	A	B
1	61.82	63.77
2	65.3	61.60
3	60.14	-
4	63.48	-
Delta	5.16	2.16
R_5 ank	1	2

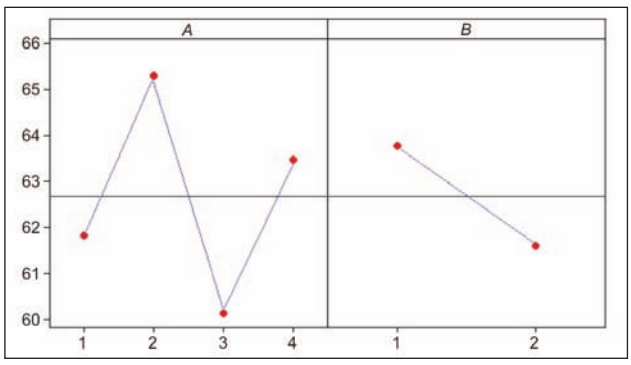

Fig. 5. Main effects plot for *S/N* ratio

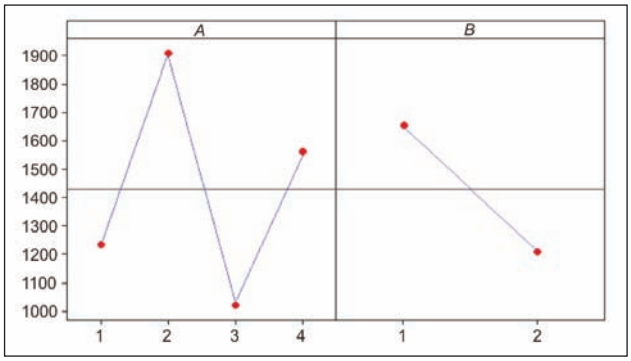

Fig. 6. Main effects plot for means

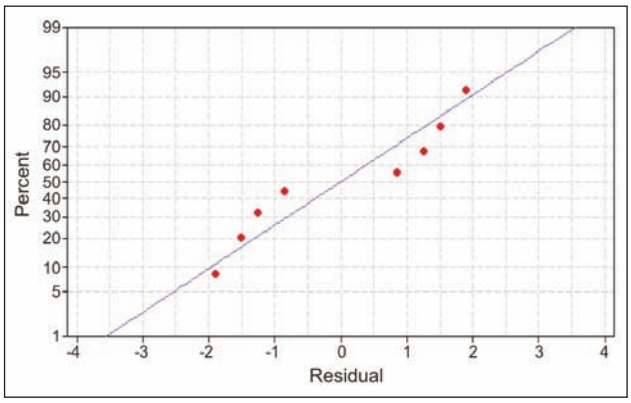

Fig. 7. Normal probability plot

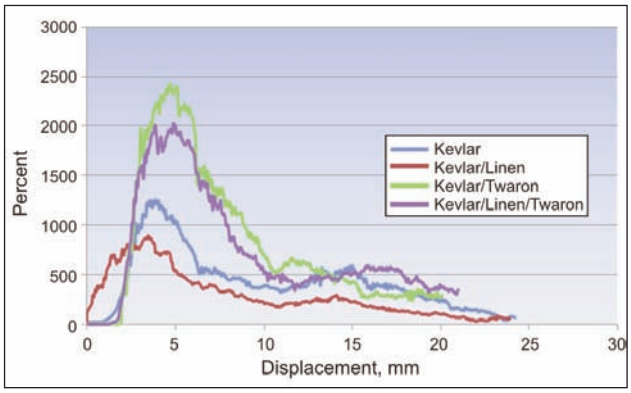

Fig. 8. Force displacement curves

The optimal combination of signal parameter in order to obtain the higher value for *S/N* ratio is A_2B_1, meaning a composite material reinforced with Kevlar-Inox and Twaron yarns and a cell dimension of 10 x 10 mm.

MODEL VALIDATION

In order to determine the accuracy of Taguchi model that was presented normal probability plot was drawn (fig. 7). It can be noted that the residual values distribution reported to the median is normal.

The reliability of presented model was also confirmed by performing a number of experimental tests taking into account the intervals for the defined signal parameters. Samples have been tested at low velocity impact using an Ceast Fractovis Plus 2 000 testing machine, an impactor with hemispherical head

with diameter of 20 mm and an impact height point of 750 mm according to ISO 6603 and ISO 7765 standards. The more significant results are graphically exemplified in figure 8.

From the graphical analysis of the experimental samples, Taguchi results correspond to the experimental results. The level of forces in the system determined through testing corresponds to variant A_2B_1, defined in the Taguchi analysis and presents the maximum value – 2 430.59 N.

CONCLUSIONS

Composite materials reinforced with sandwich *U* shaped knitted fabrics with various cell dimensions and epoxy resin were manufactured using VARTM technique. The low velocity impact behaviour has been evaluated.

The orthogonal array was defined based on structure composition and cell dimension as signal parameters an impact resistance of composite materials as noise factors. The best results have been obtained for a composite material reinforced with Kevlar-Inox and Twaron yarns and a cell dimension of 10 x 10 mm.

The model was validated based on experimental results obtained by testing sandwich composites produced with similar parameters in similar technical conditions.

BIBLIOGRAPHY

[1] Fangueiro, R., Sousa, G., Araujo, M.D., Pereira, C. *Core reinforced composite armour as a substitute to steel in concrete reinforcement*. International Symposium Polymers, in Concrete, Guimaraes, Portugal, Aprilie 2006

[2] Akin, C., Senel, M. *An experimental study of low velocity impact response for composite laminated plates*. Proceedings of Fen Bilimeleri Enstitusu Dergisi, Nissan 2010, ISSN 1302 3055

[3] Cristian, I., Nauman, S., Boussu, F., Koncar, V. *A study of strength transfer from tow to textile composite using different reinforcement architectures*. In: Applied Composite Materials, June 2012, vol. 19, issue 3–4, pp. 427–442

[4] Abounaim, Md., Hoffmann, G., Diestel, O., Cherif, C. *High performance thermoplastic composite from flat knitted multi-layer textile perform using hybrid yarn*. In: Composite Science and Technology, 2011, vol. 71, pp. 511–519

[5] Pamuk, G., Ceken, F. *Comparison of the mechanical behavior spacer knit cotton and flax fabric reinforced composites.* In: Industria Textilă, 2013, vol. 64, issue 1, pp. 3–7

[6] Fangueiro, R., Sousa, G., Araujo, M. D., Pereira, C. *Core reinforced composite armour as a substitute to steel in concrete reinforcement.* International Symposium Polymers, in Concrete, Guimaraes, Portugal, Aprilie 2006

[7] Kishore, R. A., Tiwari, R., Dvivedi, A., Singh, I. *Taguchi analysis of the residual tensile strength after drilling in glass fiber reinforced epoxy composites*. In: Materials and Design, 2009, vol. 30, pp. 2 186–2 190

[8] Loghin, C., Ionescu, I., Hanganu, L. et all. *Functional design of protective clothes with intelligent elements*. Annals of DAAAM for 2009 & Proceedings of the 20th International DAAAM Symposium, 2009, vol. 20, p. 435

[9] Loghin, C., Ursache, M., Ionescu, I. *Experimental research on the sewability of ferromagnetic micro-wires*. In: Tekstil ve Konfeksiyon, October – December 2010, vol. 20, issue 4, pp. 373–378

[10] Mathivanan, N. R., Jerald, J. *Experimental investigation on woven E-glass composites laminates subjected to low – velocity impact at different energy levels*. In: Journal of Minerals and Materials Characterization and Energy, 2010, issue 9, pp. 643–652

[11] Padaki, N. V., Alagirusamy, R., Deopura, B. I., Sugun, B. S., Fangueiro, R. *Low velocity impact behaviour of textile reinforced composites.* In: Indian Journal of Fibre and Textile Research, 2008, vol. 33, pp. 189–202

Authors:

Asist. dr. eng. SAVIN DORIN IONESI
Conf. dr. eng. LUMINIȚA CIOBANU
Conf. dr. eng. MARIANA URSACHE
Asist. dr. eng. IONUȚ DULGHERIU
Gheorghe Asachi Technical University
Faculty of Textiles, Leather and Industrial Management
Bd. D. Mangeron nr. 53, 700050 Iaşi
e-mail: dionesi@tex.tuiasi.ro

Prof. dr. eng. CĂTĂLIN DUMITRAȘ
Gheorghe Asachi Technical University
Faculty of Machine Manufacturing and Industrial Management
Bd. D. Mangeron nr. 59 A, 700050 Iaşi

Prof. dr. eng. RAUL FANGUEIRO
University of Minho, School of Engineering
Guimaraes, Portugal

Analysis of low velocity impact behaviour of aramid-linen fibre reinforced composites using Taguchi method

D. IONESI, C. DUMITRAS*, L. CIOBANU, A. VIRCAN
„Gheorghe Asachi" Technical University of Iasi

Impact damage is a major target in designing advanced composite materials reinforced with 3D knitted structures because composites are often used in applications which imply dynamic loads. 3D knitted fabrics present a large range of applications in the technical field, including advanced composites. Textile reinforcements are known for their unique combination of light weight, controlled anisotropy, formability and flexibility, as well as their strength and toughness. Epoxy and polyester composite materials reinforced with sandwich knitted fabrics made of Kevlar®, Twaron® and linen yarns are developed in the paper. Low velocity impact behaviour of composite materials reinforced with 3D weft knitted fabrics is modelled using the Taguchi method based on orthogonal arrays, in order to maximize the composite characteristics significant for this type of impact. The theoretical results obtained were validated by experimental data.

(Received April 9, 2012; accepted June 6, 2012)

Keywords:

1. Introduction

A composite material is an advanced material compound from two or more distinct materials that are combined at macroscopic scale. Composites are materials that are choice for designing light-weight structures due to their excellent weight/strength and weight/stiffness properties and may be subjected to low velocity impacts.

The applicability of textiles in engineering has grown exponentially in the recent decades. These materials are known as technical textiles and they are used for: transport, geotextiles, civil engineering, road construction, aerospace, military, medical, sports equipment, protective clothing, etc. Composite materials with textile reinforcements represent one of the most significant domains of use [8].

Advanced composite materials are based on textile fabrics with complex forms that are very different from the traditional ones, being used together with plastics, glass, films, and paper [2].

In the last decades a significant research effort has been made to study the impact behaviour of composite materials with textile reinforcements. Several researchers [11] [16] [17] have studied the problem by examining the material properties before and after impact.

According to Padaki et. all [16] impact phenomena has been classified into low velocity impact, if the impactor speed is under 0.25 km/s, medium velocity impact, if the impactor speed is between 0.25 and 2 km/s, ballistic impact if the impactor speed is between 2 and 12 km/s and hyper velocity impacts when impactor speed is higher than 12 km/s.

Carbon – graphite reinforced composites materials are widely used due to their high specific stiffness and strength. Vulnerability of carbon – epoxy composites to low velocity impact has been proved by the significant reduction of mechanical properties.

Hosur [10] reported that carbon – epoxy composites failed under impact loading through partial penetration. Gustin [9] studied the carbon and Kevlar woven sandwich composites. He observed that carbon fibre composites have relatively low impact properties but these can be improved by adding Kevlar fibres on face sheet. The addition of Kevlar fibres increases the impact forces by approximately 10%. Akin [5] and Mahapatra [14] and Mathivanan [15] have documented efforts over the past years in order to study the behaviour of glass fibres reinforced composites and notes that the system response depends on the elastic properties of the fibre material. At an impact velocity lower than 0.1 km/s there was a catastrophic failure of composites and perforation of laminates has been observed.

Textile sandwich fabrics are used as 3D performs for advanced composite materials. A sandwich fabric, woven or knitted, represents a three-dimensional construction made of two independent layers connected together through other connecting layers. The sandwich fabrics with connection through knitted layers (single or double) are characterized by a complex geometry, for which the shape and dimensions of the cross section depend on the connecting layer [3] [7]. The shape of the connecting layer can be different, varying from rectangular to elliptic, V shaped, trapeze, etc. Their advantages include high specific strength and stiffness, corrosion resistance, tailorability, stability and very good impact resistance.

The survey of literature conducted presented no mention regarding the low velocity impact behaviour of knitted sandwich fabrics.

The optimization of mechanical properties of composite materials reinforced with 3D sandwich knitted

performs was carried out by classical method [1]. These one involves varying one parameter at a time and keeping the other ones constant. These procedures are time consuming, require a lot of experimental samples and do not provide information regarding the interactions between the parameters, costing too much time and money.

In order to solve these problems, Taguchi method was designed based on the concept of orthogonal arrays. Although Taguchi method was successfully applied in many fields, such as chemical engineering, electronics, genetic algorithm [4, 18, 20, 21], it is not widely used in textile areas [12-14].

The statistically based Taguchi method was used to identify the importance of factor designs and to suggest an optimized design that can produce the optimal impact resistance for composite materials reinforced with 3D sandwich knitted fabrics.

2. Materials and methods

2.1 Materials

In order to complete this research para-aramid (Steel Kevlar and Twaron) and technical natural yarns (Linen) were used.

Para-aramid fibres are the choice for any products used to improve impact behaviour, but they are rather expensive. Currently, the trend is to use Kevlar fibres in combination with other raw materials that are less costly. For this research Steel-Kevlar yarns were chosen for their multi-functionality (steel allows for conductivity/EM shielding). Linen is a technical fibre that is cheap and presents acceptable tensile characteristics.

Physical and mechanical properties characterisation was carried out by studying the tensile strength, according to ISO 2062/1993 test standard and using a Housenfield H10 KS testing machine with following configuration:

- force cell of 5 kN
- pretension of 0.18N for Steel – Kevlar yarns, 0.25N for Linen yarns and 0.85N for Twaron yarns.
- Testing speed: 250 mm/min.
- Clamping distance: 250 mm

The experimental data that were obtained are presented in Table 1. For all of them has been calculated tenacity, Young modulus, breaking force and extension according to ISO 2062/1993 standard specifications.

Fig. 1 presents the effort elongation curves for Steel-Kevlar, Twaron and Linen yarns that were tested in standard conditions. The Twaron yarns have a very high elasticity modulus, around 23 times higher than elasticity modulus of Steel-Kevlar and Linen yarns.

Twaron yarns are also characterised by a very small elongation at break and high breaking force. Their Young modulus is 46.48 N/tex, indicating high forces at low elongations, while, in comparison, the linen yarn's Young modulus is only 1.941 N/tex and the steel Kevlar is 1.693 N/tex. If the values for Young modulus are similar for the last two yarns, the corresponding elongations are extremely different – the linen yarn has a high elongation (at low forces), while the steel Kevlar yarn presents a low elongation at similar forces.

Table 1 Characteristic values for tensile.

Fir		Breaking force [N]	Tenacity [N/tex]	Young Modulus [N/tex]	Extension [%]
Linen	Mean	**9.16**	**0.183**	**1.941**	**23.62**
	Min	7.22	0.144	1.076	17.88
	Max	10.73	0.214	3.487	28.59
	C_v	11.15	11.15	38.93	11.29
Steel Kevlar	Mean	**11.67**	**0.324**	**1.693**	**5.77**
	Min	9.77	0.271	1.299	5.2
	Max	13.2	0.366	2.302	6.4
	C_v	8.61	8.61	18.13	7.16
Twaron	Mean	**293.6**	**1.747**	**46.48**	**3.6**
	Min	260.8	1.552	44.82	3.208
	Max	316	1.881	48.47	3.912
	C_v	5.84	5.84	2.68	5.6

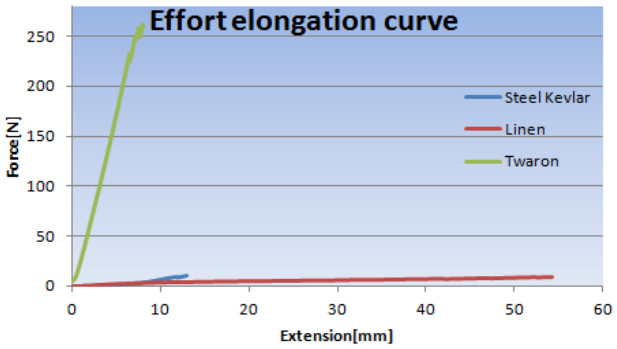

Fig. 1. Effort elongation curves.

All tests were made at University of Minho, Portugal

2.2. Development of knitted reinforcement

The experimental work focused on the production of U shaped sandwich knitted fabrics. The 3D knitted fabrics were produced on STOLL CMS 320 TC flat knitting machine, gauge 10E. The raw material for the outer and connecting layers was different, as presented in Table 2.

All fabric variants were produced at University of Minho, Portugal.

The fabric compactness, required to increase the volume fraction of the composites, was improved by introducing transversal Twaron yarns, as shown in Fig. 2.

Table 2 Raw materials used for producing sandwich fabrics

Fabric	Outer layers		Connecting layer	
	Yarn type	Linear density (tex)	Yarn type	Linear density (tex)
1	Kevlar 49®	28	Kevlar 49®	28
2	Kevlar 49®	28	Linen	20
3	Kevlar 49®	28	Kevlar 49®	28
	Twaron®	6		
4	Kevlar 49®	2	Linen®	20
	Twaron®	6		

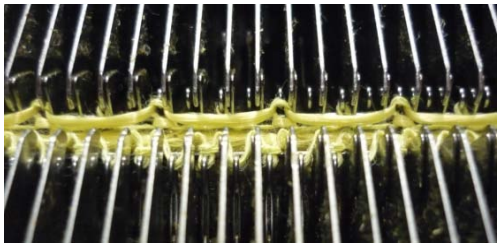

Fig. 2. Production of sandwich fabric (machine view).

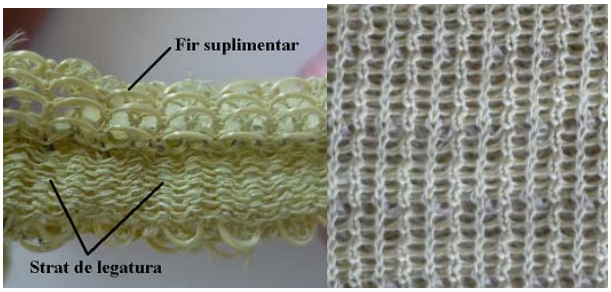

Fig. 3. Connecting and outer layer aspect

Fig. 4 presents the 3D sandwich knitted fabrics that were obtained using Kevlar® and linen yarns (fabric variant 1 and 2).

a) Fabric variant 1 b) Fabric variant 2

Fig. 4. U-shaped sandwich knitted fabrics

2.3 Development of composite materials

The 3D composite materials studied in this paper were produced using 3D knitted fabrics as performs and epoxy EPICURE 04908 and polyester DISTITRON 3501S as matrices. The composite materials were made using the Vacuum Assisted Resin Transfer Moulding (VARTM) technology. Table 3 presents the principal characteristics of the resins.

Table 3 Properties of epoxy and polyester resins.

Property	Unit	Epoxy Resin	Polyester resin
Viscosity at 25 °C	Mpa.s	10	150
Density	g/cm3	1.15	1.07
Tensile strength	MPa	74	65
Tensile strain	%	9.4	2.0
Tensile modulus	MPa	2900	4000
Flexural strength	MPa	112	110
Modulus in flexure	MPa	3100	4200
Water absorption after 24h, 23°C	pbw	0.18	-
Water absorption after 168h, 23°C	pbw	0.432	-

Both resins were cured at room temperature (23°C), the composite with epoxy for 46 hours and the one with polyester for 23 hours. The epoxy matrix had a mixing ratio of 30% EPIKURE Curing Agent 04908 and 5% Dearing agent BYK A535, while for the polyester resin the mixing contained 1.5% of initiator for unsaturated polyester resin NOROX MCP 75 and 0.08% polyester inhibitor NLC 10.

The final aspect of the composite materials that were obtained and the main steps that must be followed in order to obtain a composite material using VARTM technique is exemplified in Figure 4.

All fabric variants were produced at University of Minho, Portugal.

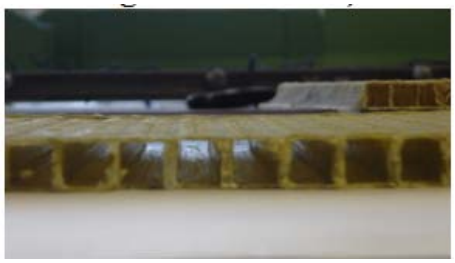

Fig. 5. Manufacturing of composite materials with 3D textile reinforcements.

Comparing the production of the composite material using the two matrix systems, the following observations can be made:

- The polyester resin is easier to work with due to its higher viscosity and lower density
- The composite processability was better in the case of the polyester resin during the insertion of the inner moulds and their subsequent removal

2.4 Impact testing of advanced composite materials

The low velocity impact behaviour of composite materials reinforced with knitted sandwich fabrics was

evaluated using a Ceast Fractovis Plus 2000 impact testing machine. The impactor (Ø 20 mm) had a hemispherical tip, and a 75x75 mm specimen plate was used. The Impact test was made according to ISO 6603 and ISO 7765.
The machine had the following settings:

- Impact height: 750 mm
- Carriage mass: 4.3 kg
- Support diameter: 20000 mm

All tests were made at University of Minho, Portugal.

3. Modelling of impact behaviour using Taguchi method

3.1 General aspects

In order to realize the experiments in an efficient an correct manner must be defined the input variables so that the studied process to achieve the expected performance and have a minimum sensitivity to noises.
The main differences reported between the classical DOE (design of experiments) method and Taguchi method are [6]:

- Classical DOE method does not consider the average values of the parameters that must be optimized, sometimes being completed with analysis of variance;
- Taguchi method unitary treats the average values and the variability of the parameters that must be optimized;
- Taguchi method use performance indicators, such the signal-noise (S/N) ratio, that simultaneously taking into consideration the desired response value (signal) and the variability thereof (noise).

In parallel with the S/N ratio Taguchi method use the quality loss function. It is recommended to maximize of performance indicator to correspond with minimize of quality loss function.

The way of determination for the quality loss function is given by relation:

$$L(y) = k(s^2 + (\bar{y} - y_N)^2) \quad (1)$$

Where:

- L(y) – average loss/unit;
- s – standard deviation;
- y_N – nominal value
- $\bar{y}$ - average of determined values;
- k – constant;

The S/N ration must be determined according to the system outputs.

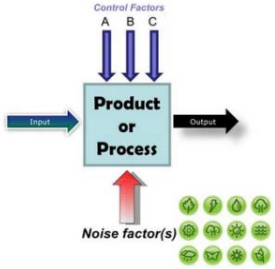

Fig. 6. Principle of application of the Taguchi method

General steps that must be followed in order to complete a Taguchi experiment are:

- Define the system objectives. This can be represented either by a parameter optimisation, either by reaching a minimum or maximum value. The deviation from optimum performance is used to define the quality loss function;
- The determination of parameters that influence the system and the specific levels of each. As the number of levels is higher for each parameter, the number of experiments to be conducted increases;
- Define the orthogonal array used in conducting the experiment, according to the number of parameters and their specific levels;
- Implementation of experiment and collect the experimental data;
- Statistically analysis and interpretation of obtained raw data;
- Results validation.

A well designed product should always respond in the same manner to the signals provided by the users. If the answer varies randomly when is applied the same stimulus the quality of the signal is not optimal. Taguchi method aims to minimize the parameters variability reported to the noise factors and to maximize the variability reported to the signal factors [19].

The main purpose followed by applying the S/N ratio is to find the optimal combination of signal parameters that influence the system in order to maximize their S/N ratio. In this way these parameters become system control factors.

The S/N ratio is determinate using the following relations:

- Smaller the better

$$\frac{S}{N} = -10\log(s^2 + \bar{y}^2) \quad (2)$$

- Nominal is the best

$$\frac{S}{N} = 10\log\left[\left(\frac{\bar{y}^2}{s^2}\right) - \frac{1}{n}\right] \quad (3)$$

- Larger the better

$$\frac{S}{N} = -10\log\left[\sqrt{y^2}\left(1 + 3s^2 * \sqrt{y^2}\right)\right] \quad (4)$$

Where:

- s – standard deviation;
- y – nominal value;
- $\bar{y}$ - average of determined values;
- n – number of runs.

After applying the S/N ratio test the generated loss will be lower as the calculated value will be higher. In this way will result a better optimisation of the studied system.

3.2. Selection of orthogonal array and signal factors

Using Taguchi plans one can study the effect of several parameters on the system performance using only a condensed set of experiments

After the analysis of orthogonal array models, the signal parameters and specific levels of each has been deemed adequate the L16 orthogonal array, presented in Table 4.

Table 4 Orthogonal array selection.

Experiment	Structure	Resin type	Cell Dimension
1	1	1	1
2	1	1	1
3	1	2	2
4	1	2	2
5	2	1	1
6	2	1	1
7	2	2	2
8	2	2	2
9	3	1	2
10	3	1	2
11	3	2	1
12	3	2	1
13	4	1	2
14	4	1	2
15	4	2	1
16	4	2	1

Table 5 Signal factors selection.

Parameters / Levels	Structure	Resin type	Cell dimension
1	Kevlar	Epoxy	1 cm
2	Kevlar Twaron	Polyester	1,5 cm
3	Kevlar Linen	-	-
4	Kevlar Twaron Linen	-	-
Symbol	A	B	C

The main purpose of this research is to find the optimal signal parameters for obtaining a higher low velocity impact resistance of composite materials that use three-dimensional sandwich knitted fabrics made of steel-Kevlar, Twaron and linen technical yarns as reinforcement and epoxy and polyester resins as matrix.

Selection of the noise factors takes into consideration the parameters considered significant for the dynamic behaviour of composite materials, as is shown in Table 5.

4. Results and discussions

The current study targeted the influence of signal parameters on the impact resistance of advanced composite materials. The first three columns of Table 6, noted A, B, and C, represent the signal factors (structure, resin type and cell dimension), while the following two, noted p1 and p2, are the noise factors (impact resistance of composite materials).

In order to complete the experiment, three different sets of eight runs, according to L16 orthogonal array were conducted. The definition of the signal and noise factors is followed by statistic analysis, as is shown in Table 6. The response resulting from Taguchi analysis revealed the significance of the signal factors reported to S/N ratio and the average. The classification of influence level, presented in Table 7, is:

- Maximum influence – the factor A (knitted structure);
- Average influence – the factor B (resin type);
- Minimum influence – the factor C (cell dimension)

Table 6 Experimental design using L16 array and experimental results

Experiment	A	B	C	p1	p2	S/N	LSTD	STDE	MEAN	CV
1	1	1	1	1198.7	1245.3	61.71	3.09	22.00	1217.36	0.02
2	1	1	1	1224.56	1200.87	*	*	*	*	*
3	1	2	2	1005.4	1009.25	60.03	1.45	4.28	1003.92	0.00
4	1	2	2	999.78	1001.25	*	*	*	*	*
5	2	1	1	2328.65	2430.59	67.56	3.79	44.40	2389.80	0.02
6	2	1	1	2412.3	2387.65	*	*	*	*	*
7	2	2	2	995.42	1086.27	60.17	4.04	57.09	1022.90	0.06
8	2	2	2	1051.65	958.24	*	*	*	*	*
9	3	1	2	1086.58	1161.28	60.75	4.20	66.84	1094.42	0.06
10	3	1	2	1005.2	1124.62	*	*	*	*	*
11	3	2	1	742.8	745.18	57.32	2.55	12.86	735.10	0.02
12	3	2	1	716.8	735.6	*	*	*	*	*
13	4	1	2	1120.98	1170.29	61.08	3.65	38.35	1133.77	0.03
14	4	1	2	1085.62	1158.2	*	*	*	*	*
15	4	2	1	1020.45	1063.01	60.25	3.54	34.49	1030.42	0.03
16	4	2	1	1051.9	986.3	*	*	*	*	*

Table 7 *Response table for S/N Ratios Larger is better*

Level	A	B	C
1	60.87	62.77	61.71
2	63.86	59.44	60.51
3	59.03		
4	60.66		
Delta	4.83	3.33	1.20
Rank	1	2	3

The values that were obtained for S/N ratio, average and standard deviation from Table 6 are graphically represented in Figs. 7, 8 and 9. The S/N ratio has been calculated using the formula defined for larger the better case. The optimal combination of signal parameters is A_2 B_1 C_1 meaning a composite materials made by steel Kevlar and Twaron yarns for reinforcement, epoxy resin as matrix and a cell dimension of 1 cm. As can be seen in Table 8, after applying the prediction method, the S/N ratio is maximal reported to the S/N ratio obtained from statistical processing of experimental data according to Taguchi experiment matrix.

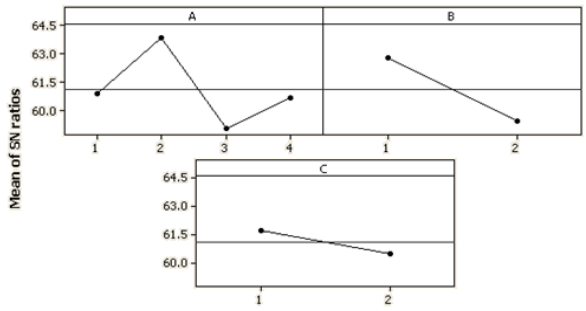

Fig. 7. Main effects plot for S/N ratio

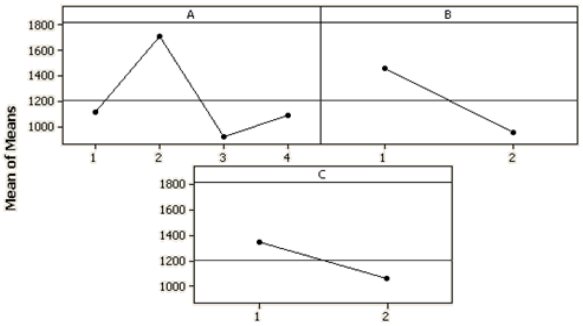

Fig. 8. Main effects plot for means

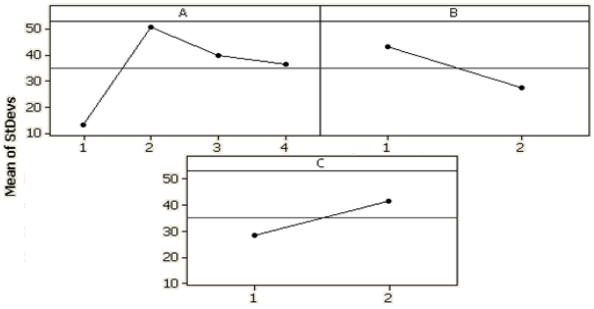

Fig. 9. Main effects for standard deviations

In order to do this the parameters levels must be set according to the results that were obtained from graphic analysis.

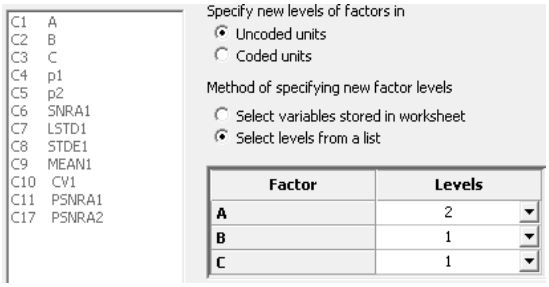

Fig. 10. Definition of the parameters levels for result prediction

Table 8. Predicted values.

S/N Ratio	Mean	St Dev	Ln (StDev)
66.13	2010.43	52	4.26

This method can be used for predicting results characterized by different combinations of the considered signal parameters.

5. Model validation

In order to determine the accuracy of Taguchi analysis, a model validation is required.

In this case, model validation was made by performing a number of tests, taking into account the intervals for the defined signal parameters.

Samples have been tested at low velocity impact according to the presented methodology. A part of experimental result is graphically exemplified in Figure 11.

From the graphical analysis of the experimental samples, Taguchi results correspond to the experimental results. The level of forces in the system determined through testing correspond to variant A_2 B_1 C_1 defined in the Taguchi analysis and present the maximum value – 2482 N.

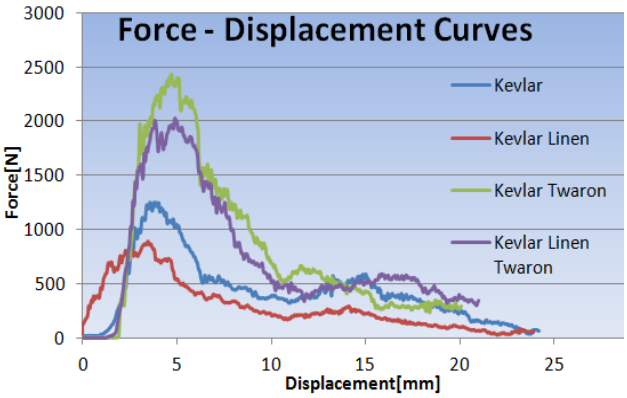

Fig. 11. Force displacement curves.

6. Conclusions

Advanced composite materials have known important developments in last decades. They require the use of 3D preforms that are produced in one stage through textile specific processes.

Impact behaviour is well documented throughout literature, but the bulk of it refers to 2D and 3D woven fabrics and high velocity loads. The paper targets the study of low velocity impact in the case of composites reinforced with 3D knitted sandwich fabrics with epoxy and polyester resins. The novelty of this study resides in the combination of production process, raw materials and type of impact (low velocity).

Taguchi method presents the advantage of generating accurate results based on a small number of runs in comparison to classical DOE methods. Currently, its use in textile modelling is somewhat limited. The orthogonal array was defined based on structure, resin type and cell dimension as signal parameters and impact resistance of advanced composite materials as noise factors.

The model was validated based on experimental results obtained by testing sandwich composites produced with similar parameters in similar technical conditions.

Acknowledgement

This paper is financially supported by EURODOC "Doctoral Scholarships for research performance at European level" project, financed by the European Social Found and Romanian Government.

References

[1] Md. Abounaim, G. Hoffmann, O. Diestel, C. Cherif, Composite Science and Technology **70**, 363 (2010).
[2] Md. Abounaim, G. Hoffmann, O. Diestel, C. Cherif, Proceedings of *A*UTEX 2009 World Textile Conference, pp 675-681 (2009)
[3] Md. Abounaim, G. Hoffmann, O. Diestel, C. Cherif, Composite Science and Technology **71**, 511 (2011).
[4] A. Adnani, M. Basri, A.E. Malek, A.B. Salleh, M. Rahman, N. Chaibakhsh, , R. Rahman, Industrial Crops and Products, pp 350-356, 2010.
[5] C. Akin, M. Senel, Fen Bilimeleri Enstitusu Dergisi, Nissan 2010, ISSN 1302 3055.
[6] J. Alexis, Taguchi Method in Industrial Practice, ISBN 973 31 1352 2, 1999
[7] M. D. Araujo, H. Hong, R. Fangueiro, O. Ciobanu, , L. Ciobanu, (2001). Developments in Weft – Knitting Technical Textiles, Proceedings of Technitex 2001 – Designing Textiles for technical applications, pp 253-261, ISBN 972-9468-3-9
[8] L. Ciobanu, (2003). Contributions to the development and production of technical knitted fabrics, Ph. D. thesis, Universitatea Tehnică "Gheorghe Asachi" Iaşi.
[9] J. Gustin, A. Joneson, M. Mahinfalah, J. Stone, Composite Srtucture, **69**, 396 (2005).
[10] M.V. Hosur, Composite Structures **67**, 253 (2005).
[11] B. Khan, R.M.V.G.K. Rao, N. Venkataraman, Journal of Reinforced Plastics and Composites, 14, 1995.
[12] E. Kilickap, Expert systems with Applications **37**, 6116 (2010).
[13] R.A. Kishore, R. Tiwari, A. Dvivedi, I. Singh Materials and Design, **30**, 2186 (2009).
[14] S.S. Mahapatra, A. Patnaik, A. Satapathy, WEAR, **265**, 214 (2008).
[15] N.R. Mathivanan, J. Jerald, Journal of Minerals and Materials Characterization and Energy **9**, 643 (2010), Wear **265**, 214 (2008).
[16] N. V. Padaki, R. Alagirusamy, B. I. Deopura, B. S. Sugun, R. Fangueiro, Indian Journal of Fibre and Textile Research, **33**, 189 (2008).
[17] A. Perez, L. Gil, S. Oller, Non destructive testing evaluation of low velocity impact damage in carbon fiber – reinforced laminated composites, ULTRAGRASAS, vol. 66, ISSN 1392 2114, 2011
[18] O. Peyronnard, M. Benzaazoua, Minerals and Engineering, **29**, 28 (2012).
[19] G. Taguchi, S. Chowdhury, S. Taguchi, Robust Engineering, McGraw Hill, New York, 2000
[20] W. C. Weng, F. Yang, A.Z. Elsherbeni, IEEE Transactions on antennas and propagation, vol. 55, 2007
[21] A. Yildiz, Computers in Industry, **60**, 613 (2009).

*Corresponding authors: dumitrascata@yahoo.com, lciobanu@tex.tuiasi.ro